2020-01-08

Identification and Verification of Differentially Methylated Regions in Cell-Free DNA as a Peripheral Biomarker for Bicuspid Aortic Valve Aortopathy

Maredia, Ashna Karimbhai

UNIVERSITY OF CALGARY

Identification and Verification of Differentially Methylated Regions in Cell-Free DNA as a Peripheral Biomarker for Bicuspid Aortic Valve Aortopathy

by

Ashna Karimbhai Maredia

A THESIS
SUBMITTED TO THE FACULTY OF GRADUATE STUDIES
IN PARTIAL FULFILMENT OF THE REQUIREMENTS FOR THE
DEGREE OF MASTER OF SCIENCE

GRADUATE PROGRAM IN MEDICAL SCIENCE

CALGARY, ALBERTA

JANUARY, 2020

Abstract

Bicuspid aortic valve (BAV) is a common congenital cardiac malformation associated with aortopathy for which the progression of aortic dilation is difficult to predict at present. BAV aortopathy has been linked to genetic factors and abnormal hemodynamic flow with regions of elevated wall shear stress (WSS) on the ascending aorta. The dying vascular smooth muscle cells release fragmented DNA into the circulation and this cell-free DNA (cfDNA) could be leveraged as a biomarker for aortopathy. Identification of tissue-specific differentially methylated regions (DMRs) in DNA provides a potential mechanism to identify cfDNA arising from the ascending aorta.

The **objective** is to identify aorta-specific DMRs in the cfDNA of BAV patients as a biomarker for the severity of the aortopathy. We **hypothesize** that BAV-associated aortopathy leads to increased cell death and increased release of aorta-specific cfDNA correlating with the severity of aortopathy as defined by aortic cell death, elastin degradation and dysregulation of ECM proteins.

BAV patient aortic wall samples corresponding to areas of elevated and normal WSS were collected and stained for cell death. Regions of elevated aortic WSS showed greater cell death when compared to regions of normal aortic WSS ($p=0.00006$). We established a bioinformatic pipeline for the identification of aorta-specific DMRs and they were verified with BAV patient cfDNA. The levels of aorta specific cfDNA of the DMRs on Chr 11, 18 and 22 of BAV patients had a significant correlation with levels of cell death in elevated aortic WSS regions. However, there was no correlation with elastin thickness, ECM concentrations of matrix metalloproteinases (MMP) types 1, 2 and 3, tissue inhibitor of metalloproteinases-1 and transforming growth factor-β1. Further work needs to be done in order to identify more specific aortic DMRs that have stronger correlation to the severity of BAV aortopathy markers with larger cohorts for biomarker validation.

The identification of a peripheral biomarker that correlates with tissue disease will be an important advance in the non-invasive diagnosis of BAV-associated aortopathy and potentially help guide clinical decision-making regarding the need for surgical intervention.

Preface

This thesis is original, unpublished, independent work by the author Ashna K. Maredia. Sections of Chapter One have been published as a review paper and copyright permission has been obtained from the co-author Steven C. Greenway.

The methods contained within this thesis were performed solely by the author, Ashna K Maredia, with assistance from the following individuals: David Guzzardi from Dr. Paul Fedak's lab provided histological data of aortic tissues including elastin thickness and concentrations of MMP types 1, 2 and 3, TIMPs-1 and TGF-β1in chapter four for BAV patients; Ms. Rasha Sabouny provided guidance on confocal microscopy and imaging of the paraffin embedded aortic tissue stained with TUNEL and DAPI; Ms. Fatima Iqbal, under my supervision, helped analyze the images taken of the aortic tissue stained with TUNEL and DAPI using ImageJ.

The experiments using patient materials were approved by the Conjoint Health Research Ethics Board (CHREB) at the University of Calgary (ethics certificate number REB17-0207_REN2) for the project "Role of Valve-Mediated Hemodynamics on Bicuspid Aortopathy".

Acknowledgements

I would first like to thank my supervisor, Dr. Steven Greenway, not only for giving me the opportunity for this incredible research experience but also for the constant and unwavering support, guidance and encouragement throughout my Master's experience. He ensured an accepting work environment which allowed me to grow and learn, make independent decisions, think critically and most of all gain confidence in my work. I am also thankful for the many opportunities he offered for me to present my research as it gave me the confidence for public speaking, connected me with the scientific community, and inspired me with my own project.

I would also like to thank my co-supervisor, Dr. Paul Fedak, for his guidance and expertise for the project. To my supervisory committee, thank you for your perspective and direction as it improved the quality of my research design. Your support was greatly appreciated.

To my friends and fellow Greenway laboratory members, Sabrina Pattar and Dimple Prasher, who welcomed me to Calgary and together we shared our graduate experience; we worked together and overcame all hurdles as we shared our findings, success and mistakes. Thank you for being by my side as we navigated bioinformatics, laboratory protocols, courses and all of our conference presentations. I cannot thank you enough for all the memories and support you have provided me in these two years and counting. Also, a great thank you to all of the members of the Greenway laboratory who I could rely on for support, help and advice.

Most importantly, I would like to thank my family who has always been my rock with their untiring support and encouragement for all the endeavors I undertake. You have always believed in me and my abilities and given me the strength I needed to overcome obstacles even though I was miles away. I know that I would not be where I am today without your love, care and guidance that each one of you shower upon me every day for which I am eternally grateful.

Table of Contents

List of Tables

List of Figures and Illustrations

List of Symbols, Abbreviations and Nomenclature

Symbol	Definition	Symbol	Definition
°C	Degrees Celsius	**ECM**	Extracellular matrix
µL	Microliter	**gDNA**	Genomic DNA
mL	Milliliter	**PCR**	Polymerase chain reaction
mM	Millimolar	**RL**	Right-left cusps
nm	Nanometer	**RN**	Right-noncoronary cusps
Q	Quality score	**miRNA**	Micro-ribonucleic acid
BAV	Bicuspid aortic valve	**MMP**	Matrix metalloproteinase
cfDNA	Cell-Free DNA	**NGS**	Next-generation sequencing
Chr	Chromosome	**PCR**	Polymerase chain reaction
Chr 11	Chromosome 11; **3,168,734 - 3,168,832**	**RL**	Right-left cusps
Chr 18	Chromosome 18: **74,171,459 - 74,171,505**	**RN**	Right-noncoronary cusps
Chr 20	Chromosome 20: **45,860,400 - 45,860,466**	**rTdT**	Recombinant terminal deoxynucleotidyl transferase
Chr 22	Chromosome 22: **27,999,645 - 27,999,717**	**RRBS**	Reduced-representation bisulfite sequencing
CHREB	Conjoint Health Research Ethics Board	**TIMP**	Tissue inhibitors of metalloproteinase
CpG	Cytosine-phosphate-guanine	**TGFβ-1**	Transforming growth factor β-1
DAPI	4′,6-diamidino-2-phenylindole	**Tm**	Melting temperature
DNMT	DNA methyltransferase	**TUNEL**	Terminal deoxynucleotidyl transferase dUTP nick end labeling
DMR	Differentially methylated region	**WGBS**	Whole-genome bisulfite sequencing
DNA	Deoxyribonucleic acid	**WSS**	Wall shear stress

CHAPTER ONE: GENERAL INTRODUCTION

1.1 Bicuspid Aortic Valve-Associated Aortopathy

Bicuspid aortic valve (BAV) is a common congenital cardiac malformation where the aortic valve has two leaflets or cusps instead of three due to abnormal fusion of the valve leaflets (1). The prevalence of BAV is 0.4–2.25% of the population worldwide making it the most common congenital cardiac defect in humans, with males more frequently affected at a ratio of 3:1 (2-4). The morphology of BAV is determined by where this fusion, or raphe, between the two cusps has occurred; the right-left cusps (RL), the right-noncoronary cusps (RN) or the left-noncoronary cusps (LN) (1). There can also be variation on the number of raphes: Type 0 indicated no raphes, Type 1 indicated one raphe and Type 2 indicates 2 raphes (5). As a result of the abnormal valve, one third of BAV patients develop complications over their lifetime (6). Patients may develop aortic stenosis (i.e. narrowing of the valve) or aortic regurgitation (i.e. leaking of the valve of blood back into the left ventricle). Many of the patients with BAV also have associated dilation of the ascending aorta (1). Progressive aortic dilation, also known as bicuspid aortopathy, is associated with development of an ascending aortic dissection or aneurysm with a risk of catastrophic rupture. There have been several attempts to classify BAV aortopathy with involvement of the aortic root, ascending aorta or aortic arch (1).

The cause of BAV appears to be multifactorial with inherent genetic defects combined with hemodynamic aortic wall shear stress (WSS) created by turbulent blood flow across the abnormal valve. Most commonly, the occurrence of BAV is sporadic but familial clustering has been identified indicating its potential heritability (7, 8). Genetic studies have been conducted to identify variants causing BAV and identify those individuals with an associated increased risk for aortopathy requiring intervention. Genetic studies have identified mutations specific to BAV with the *NOTCH1* gene being the most commonly affected (9-14). The NOTCH signalling pathway is a conserved pathway that

determines cell fate decisions (15, 16). It is also pertinent in development for the first vascular smooth muscle cells in the aorta as it coordinates neural crest cell migration for differentiation (16). Studies have also found other promising genetic variants that are specific to BAV patients such as *AXIN1*, *Nitric Oxide Sythase 3* (*NOS3*), *ELN*, *Fibrillin*-1 (*FBN*-1) and *Fibrnectin-1* (*FN1*) (10, 17-19). These genetic testing studies indicate a complex multigenic cause for BAV and the associated aortopathy (20).

Another mechanism is that of abnormal hemodynamic flow leading to an increase in WSS on the aortic wall and the aortic wall deteriorating over time. Due to the abnormal BAV, the hemodynamic flow through the aorta is non-laminar with helical and oscillatory characteristics causing increased stress on the aortic wall (21-25). Studies have also shown that this increased aortic WSS leads to the degradation of elastin and the dysregulation of extracellular matrix proteins leading to aortopathy. Aortopathy in BAV patients has been marked by several factors (25-29). The deterioration of the aortic wall is linked to degradation of elastin and collagen, cell death of smooth muscle cells and distinct expression levels of matrix metalloproteinases (MMPs), tissue inhibitors of metalloproteinases (TIMPs), transforming growth factor β-1 (TGFβ-1) and micro-RNAs (miRNAs) (25, 30-33). An increase in MMP expression can lead to the breakdown of elastin and collagen, detachment of smooth muscle cells and apoptosis (34-36). The TGFβ pathway has also attracted attention as it is involved in fibrosis, inflammation, cell proliferation and migration and extracellular matrix (ECM) remodeling (37-44). The loss of extracellular matrix integrity allows for cell detachment and apoptosis, accelerating aortopathy (34-36).

As aortopathy progress and the maximal aortic diameter increases beyond 4.5 cm, aortic valve replacement with prophylactic surgical resection of the aorta is recommended according to most contemporary clinical practice guidelines (45, 46). However, the threshold for surgical resection is unclear as some studies have shown a low risk of aortic complications after aortic valve replacement (47, 48). More recent studies also reveal that clinical outcomes for BAV patients as compared to patients with Marfan syndrome are different, suggesting that BAV patients could perhaps be treated more

conservatively than patients with a genetic connective tissue disorder (47, 48). Studies have also shown that aortic dimensions (absolute diameter and rate of progression) obtained using conventional imaging techniques may be insufficient for assessing BAV aortopathy and estimating the underlying risk for aortic rupture (6, 49-51). Due to the heterogeneity of BAV aortopathy, the selection of patients for prophylactic surgical intervention is controversial and highly dependent upon individual preference and institutional practice (51-55). The aortic threshold for intervention along with patient comorbidities and selection of the type and extent of aortic surgery is also varied among surgeons (54).

1.2 Biomarkers for Aortopathy

There is a need for a more accurate, specific and personalized method for defining the threshold for surgical intervention and for risk stratifying BAV aortopathy patients. A biomarker for BAV would ideally act as a tool for an accurate, objective and reproducible measurement for this pathogenic process (56). To design a biomarker for BAV aortopathy that is feasible in a clinical setting, it must mark a physiological state that determines when there is great risk for adverse cardiovascular events and what type of surgical intervention is necessary (56).

A few potential biomarkers have been studied. For instance, circulating markers linked to BAV aortopathy include serum MMPs, TGFβ-1/endoglin (ENG) and micro-RNAs (miRNAs) (38, 57-63). Higher ratios of TGFβ-1/ENG were found to be independently associated with higher expression of MMP-2 and a lower expression of superoxide dismutase 3 which leads to extracellular matrix degeneration and oxidative stress in the aorta (38). These markers stem from their differential expression in BAV aortopathy patients and still require further investigation. Additionally, aortopathy in BAV has also been found to be mediated by the presence of reactive oxygen species as there is a deficiency of an oxidative stress response (64). Studies have found superoxide anion accumulation and increased lipid peroxidation indicating the presence of oxidative stress in these patients (65). The absence of heightened superoxide dismutase activity in BAV patients indicates a deficiency in oxidative stress defense (65).

This suggests that cell damage in BAV aortopathy may be mediated by superoxide stress (65). With imaging methods being developed to detect oxidative stress *in vivo*, oxidative stress in the aortic regions may serve as a biomarker for BAV aortopathy (66, 67).

A promising imaging biomarker is the abnormal hemodynamic flow that has been shown to contribute to the development of aortopathy. Studies have used flow-sensitive cardiac magnetic resonance imaging (CMR) with full volumetric coverage of the ascending aorta to visualize abnormal blood flow patterns such as flow jets, vortices, and helical flow (21, 22, 68, 69). By using 4D flow CMR, the increase in WSS can be quantified in BAV patients who are known to show vessel wall remodeling related to abnormal blood flow (70). BAV morphology has also been associated with different patterns of flow and thus different patterns of ascending aorta dilation (71). There is substantial associative evidence that cusp fusion pattern corresponds with the extent of aortopathy (72, 73). Regions of elevated WSS of the aorta as compared to normal regions have been linked with histological parameters of elastin degradation and an increase in expression of the extracellular proteins MMP-1,2,3, TGFβ-1 and TIMP-1 (25). This association between flow and changes in the aorta wall shows that there is a key hemodynamic flow component that contributes to the progression of aortopathy. However, access to CMR is limited which restricts the utility of this imaging biomarker. A blood-based assay that provided reliable information about the state of the aorta would be an important medical advance.

1.3 Cell-free DNA as a Biomarker

Cell-free DNA (cfDNA) refers to the fragmented DNA released during cellular apoptosis and is found in the blood of all individuals (74, 75). The cfDNA molecules have an average length of 165 base pairs (bp), ranging from 70-200 bp, due to nucleosome-guided fragmentation (76). Most of the cfDNA in the bloodstream is released from the apoptosis of white blood cells but cfDNA can also be released from the healthy and diseased or damaged tissues. The concentration of cfDNA varies between 0-100 ng/mL (77) and can increase under certain circumstances, including trauma, surgery, stroke,

cardiovascular disease, sepsis and even exhaustive exercise (78, 79). It should be noted that elevated levels of cfDNA are temporary, especially if the cause of cfDNA release is short-lived, as cfDNA is rapidly cleared from the body. More specifically, the half-life of cfDNA ranges from 4-30 minutes and, although the exact mechanism of how it is cleared has not yet been determined, filtration by the kidneys and the liver play a role (80). Thus, the cfDNA that is present in the bloodstream provides a snapshot of the cellular apoptosis occurring throughout the body.

Initial research focused on sequence variants within cfDNA which had applications in cancer, transplant rejection and prenatal testing (81-85). This application of cfDNA is dependent on measuring the cfDNA sequence in the blood that differs from the normal host DNA such as arising from tumour DNA, donor DNA and fetal DNA, respectively. For example, the detection of fragments of fetal DNA in the circulation of the mother, could be used for next-generation sequencing (NGS) to detect aneuploidies or other genetic aberrations in the fetus, thereby replacing the invasive procedure of amniocentesis (74). Another major use of cfDNA has been seen in cancer biology where tumors release fragments of their DNA into the circulation (81). As such, “liquid biopsies” can be employed where cfDNA is isolated from serum or plasma and followed by NGS to identify tumour-related mutations and diagnose cancer (76, 77, 80, 81, 85, 86). In the case of organ transplantation, the cfDNA in the plasma of the organ recipient would be derived from both the donated organ as well as the recipient’s tissues and hematopoietic cells (82). Since cfDNA can be obtained via a simple blood draw and is increased in concentration of the DNA from damaged/diseased tissue (i.e. transplanted organs that are being attacked by the recipient immune system), this potentially makes cfDNA an excellent candidate for a non-invasive biomarker for the detection of rejection.

While sequencing cfDNA has led to great innovation, applications based on sequence differences in cfDNA are limited to those situations where there is a mixture of two different cfDNA populations arising from distinct sources. In contrast, measuring the methylation pattern of cfDNA would allow for a sequence-independent assay with its own important advantages. The cfDNA released into the

bloodstream has its epigenetic methylation pattern intact and this pattern is specific to its tissue of origin (78). Measuring the levels of cfDNA based on a tissue-specific methylation pattern can allow for the potential identification of tissue damage or disease (78). It has been demonstrated that tissue-specific differentially methylated regions (DMRs) can be identified from plasma cfDNA and quantified as a biomarker for tissue injury in human diseases such as diabetes and stroke (78).

1.4 DNA Methylation

DNA methylation is an epigenetic mechanism which acts to modify gene expression without a change in the DNA sequence (87, 88). Specifically, DNA methylation is where a methyl group is added onto the C5 position of cytosine (87). Most DNA methylation occurs where a cytosine is followed by a guanine forming a CpG site (88). When CpG islands, a clustering of the CpG sites, are present near the promoter of a gene, its hypomethylation is generally associated with increased gene expression (88). The methylation pattern of DNA is thus unique to each different cell type as it helps regulate gene expression and determine cell specificity. Since the methylation pattern of genomic DNA is preserved in cfDNA, these tissue-specific, differentially methylated regions (DMRs) can be detected in the blood. Based on the methylation pattern of the isolated cfDNA, the tissue that is undergoing increased apoptosis (i.e. due to injury) can be identified and the levels of cfDNA can be used as a biomarker to quantify the severity of tissue injury (78).

Several papers have shown that concentration levels of cfDNA with DMRs specific to the diseased tissue can act as a biomarker for the progression of the disease or injury (87, 89, 90). Lehmann-Werman and colleagues showed in a novel proof-of-concept paper that DMRs in cfDNA acted as a biomarker for the presence of type 1 diabetes, the progression and relapse of multiple sclerosis, the presence of traumatic brain injury and the presence of pancreatic cancer (78). Since then, others have used DMRs in cfDNA as a biomarker for various malignancies including breast cancer, colorectal

cancer, renal cancer and prostate cancer by identifying genes that are hypermethylated in patients compared to controls and using this knowledge to develop new biomarkers (91-94).

1.5 Cell Death in BAV

In order for cfDNA to be a potential biomarker for BAV-associated aortopathy, the severity of aortic dilation or damage should correlate with increased cellular apoptosis which should be reflected by increased levels of aorta-associated cfDNA. Work from others has suggested that BAV is associated with degeneration of the aortic media, the central layer of the aortic wall that regulates its biomechanics (34, 68, 95). It is also known that BAV aortopathy results in extracellular matrix (ECM) dysregulation specifically due to collagen and elastin and abnormal aortic biomechanics (25). Accumulating evidence suggests that abnormal aortic hemodynamic flow is related to the severity of medial wall degeneration (25). The presence of increased cellular apoptosis in areas of high WSS, as triggered by the altered hemodynamic flow, should lead to increased release of aorta-specific cfDNA. Previous work has shown apoptosis of vascular smooth muscle cells in Marfan Syndrome and BAV-related aortopathy but more recent work has shown differences in the histopathology of the aorta between these diseases (96-98). Therefore, there is a great variation between molecular and structural aortic components between patients and pathologies and the underlying cause remains poorly understood. Furthermore, there is also the debate of genetic variants of BAV patients allowing for increased apoptosis versus the hemodynamic flow causing the cell death of smooth muscle cells. However, as a biomarker, cfDNA is compelling since it is directly derived from the tissue of interest and represents a final common pathway, independent of mechanism. Here, the presence of apoptosis within the aortic media in tissue obtained from patients with BAV will be evaluated to confirm the mechanism of cfDNA release. Then, the correlation between blood levels of aorta-specific cfDNA (based on the quantity of newly-identified DMRs) and the severity of aortopathy will be tested.

1.6 Project Rationale

Due to the heterogeneity of BAV aortopathy, the threshold for surgical intervention is unclear and the current guidelines based only on aortic dilation are insufficient to identify high-risk patients. There is a pressing need for a minimally-invasive biomarker that addresses the integrity of the aortic wall and that could be used in combination with MRI imaging to aid in clinical decision making regarding the timing of surgical intervention. For this project, a novel biomarker based on a unique DNA methylation signature specific to the aorta and cfDNA will be identified and then applied to BAV patients who have undergone surgery for aortopathy.

1.7 Hypothesis

We hypothesize that the levels of aorta-specific cfDNA will be increased in patients with BAV-related aortopathy and that cfDNA levels will correlate with the severity of aortopathy as defined by anatomic and tissue factors including aortic apoptosis, elastin degradation and dysregulation of ECM proteins.

1.8 Experimental Objectives:

1) Demonstrate the mechanism of cfDNA release in BAV-associated aortopathy by measuring levels of apoptosis in regions of the aorta associated with and without increased WSS.

2) Identify and validate aorta-specific DMRs in cfDNA.

3) Correlate levels of the aorta-specific DMRs in cfDNA from BAV patients with aorta diameter and levels of cell death, elastin degradation and ECM proteins in explanted aorta obtained at the time of surgery.

CHAPTER TWO: CELL DEATH ASSAY OF BAV AORTIC TISSUE BETWEEN ELEVATED AND NORMAL WSS REGIONS

2.1 Introduction

Cell death is the irreversible degeneration of vital cellular functions resulting in the loss of cellular integrity (plasma membrane permeabilization or cellular fragmentation). BAV aortopathy has been shown to have cells that die through both mechanisms of apoptosis and necrosis. Cellular apoptosis, or programmed cell death, occurs through cell shrinkage, chromatin condensation and formation of apoptotic bodies (63). Cleavage of genomic DNA into oligonucleotide fragments is a biochemical hallmark of apoptosis but the cell undergoes extensive biochemical and morphological changes which can be monitored through a variety of apoptotic assays (63). Necrosis is a form of cell death that occurs due to external factors including physical trauma to the cell such as that caused by increased aortic WSS. Necrotic cells exhibit nuclear swelling, clumping of chromatin, loss of nuclear basophilia, breakdown of cytoplasmic structure and fragmentation of genomic DNA.

The terminal deoxynucleotidyl transferase (TdT) dUTP nick-end labeling (TUNEL) assay has been designed to detect the DNA fragmentation and degradation that occurs during late stages of apoptosis and necrosis (64). It is based on the ability of TdT to label blunt ends of double-stranded DNA breaks independent of a template (64).

In this chapter, paraffin-embedded sections of aortic tissue collected from BAV patients undergoing aortic surgery were stained for levels of cell death using the TUNEL assay. Levels of cell death were measured in an area of the aorta with elevated WSS region and compared to an area with normal WSS as determined using 4D-flow CMR. This study design allowed us to test the hypothesis that there would be increased levels of tissue cell death associated with areas of increased WSS.

The hemodynamic WSS is the tangential force exerted on the endothelium due to a blood velocity gradient (dV/dr) and blood viscosity (μ) (22). It can also be seen as the drag force of the blood

on the vessel wall. To calculate the WSS values, patients undergo a 4D flow magnetic resonance imaging (MRI). From this, a systolic WSS value can be calculated (22). For this study, WSS values were used to create a BAV patient specific 'heat map' which indicates the areas of significant elevation and depression of WSS of the BAV aorta from a cohort of 10-age matched controls (22). Areas of elevated and normal WSS in BAV patients in reference to control patients with healthy aortas were defined and samples from these areas were collected for cell death staining.

2.2 Hypothesis for Chapter Two

The cell death levels in BAV patient elevated and normal aortic WSS regions will be compared. We hypothesize that the levels of cell death will be significantly greater in the elevated aortic WSS regions compared to the normal aortic WSS regions of BAV patients.

2.3 Specific Aims:

1) Quantify and compare the proportion of cells undergoing apoptosis or necrosis in BAV aortic tissue from elevated WSS regions and normal WSS regions

2.4 Materials and Methods

2.4.1 Patient Data

BAV patient samples were obtained from the Bluhm Cardiovascular Institute of Northwestern University Feinberg School of Medicine in Chicago (Table 1). With the approval of the internal review board and informed consent, 15 Adult BAV patients undergoing aortic surgery were enrolled to allow aortic tissue to be obtained for the quantification cell death in that tissue (Table 1). WSS heat maps for BAV patients (n = 15) were created relative to the healthy age-matched controls (n = 10). All patients and healthy age-matched controls with tricuspid aortic valves (n=10) underwent flow cardiac magnetic resonance imaging (CMR) with a 4-D coverage to visualize 3-D blood flow patterns and calculate WSS

values. The healthy controls were recruited to create 95% confidence interval (CI) WSS values for the construction of a physiologically normal aortic heat map. The controls had no cardiovascular diseases and did not undergo surgery. BAV patient WSS heat maps were created relative to the healthy age-matched controls. Regions of depresses, normal and elevated WSS were determined on a 3-D heat map for each BAV patient. The regions with the highest and the lowest WSS were selected to be stained for quantification of cell death. This patient data was obtained from David Guzzardi in Dr. Paul Fedak's lab.

Table 1. BAV Study Population Characteristics for Blood and Plasma Samples for Chapter Two.
Characteristics of BAV patients that were recruited at the Bluhm Cardiovascular Institute of Northwestern University Feinberg School of Medicine in Chicago

Parameter	BAV Study Population (N = 23)
Age (Average years)	47.4 ±15.3
Male	13
Female	2
BAV Classification:	
Type 0, lateral	1
Type 1, RL	9
Type 2, RL/RN	3
Average Aortic Diameter (cm):	
Maximum Diameter	4.66 ±0.58
Diameter at Elevated WSS Region	4.59 ±0.65
Diameter at Normal WSS Region	4.63 ±0.60
Aortic Valve Function	
No AS, moderate/severe AR	5
Mild AS, moderate/severe AR	1
Moderate/severe AS, no AR	3
Moderate/severe AS, mild AR	
Moderate/severe AS, moderate/severe AR	3
Aortic Valve Surgical Procedure:	
Repair	3
Replacement	
AVR	8
Ross	4
Ascending Aorta Surgical Procedure:	
Ascending aorta replacement	12
Root replacement	2
Hemi-arch	1

Values are mean ± SD or n.
AR = aortic regurgitation; AS = aortic stenosis; AVR = aortic valve replacement; BAV = bicuspid aortic valve; RN = right coronary-non-coronary cusp fusion; RL = right-left coronary cusp fusion.

2.4.2 Tissue collection

Paraffin-embedded aortic wall tissue samples were obtained via the Fedak lab from the Northwestern Cardiovascular Tissue Biobank. These aortic wall samples were collected according to the extent of ascending aorta resection with the surgeons being blinded to the WSS heat maps. Samples were labeled based on pre-collection zonal designations. The tissue was sectioned circumferentially and paraffin embedded. Paired samples from each patient's aorta from regions of normal and elevated WSS were used for comparison.

2.4.3 TUNEL and DAPI Staining

The DeadEnd Fluorometric TUNEL System kit (Promega) was used to visualize apoptotic and necrotic smooth muscle cells within the aortic tissue sections (Procedure available in Appendix I). A crucial characteristic of apoptosis is the presence of fragmented genomic DNA (gDNA). The TUNEL assay uses a recombinant TdT which catalyzes the attachment of a dUTP nucleotide, labelled with a fluorescent marker, to the free 3'-OH group on the end of the fragmented DNA (Figure 1). Therefore, all cells that contained fragmented DNA, and were therefore, apoptotic or necrotic, stained positively for TUNEL.

In order for the tissue to be stained, slides created from the paraffin embedded biopsy samples were initially de-paraffinized using xylene substitute and then fixed using 4% paraformaldehyde in PBS. The samples were then rehydrated by immersing the slides in increasingly more dilute ethanol solutions followed by a dilute NaCl solution. The tissues were then permeabilized using a 20 μg/ml Proteinase K solution and fixed once more using 4% paraformaldehyde in PBS. The tissues were then allowed to equilibrate prior to the addition of the rTdT enzyme and the mixture of labelled dUTP nucleotides. During the addition of the enzyme and nucleotides, the slides were kept in a humidified chamber covered in aluminum foil to protect the slides from direct light and prevent photobleaching of the

fluorescent label. The reaction was then terminated using a 20X SSC (sodium chloride and sodium citrate) solution and the slides were washed several times using PBS to remove any unincorporated fluorescein-12-dUTP. Finally, in addition to the TUNEL staining, the tissues were stained with DAPI (NucBlue Fixed Cell Stain DAPI, Invitrogen) to visualize the total number of nucleated vascular cells within the sample. This ultimately allowed for the determination of the proportion of apoptotic and necrotic cells within the tissue samples. The slides were then covered using plastic coverslips provided by the Promega TUNEL kit and Calbiochem's Fluorosave as an adhesive agent.

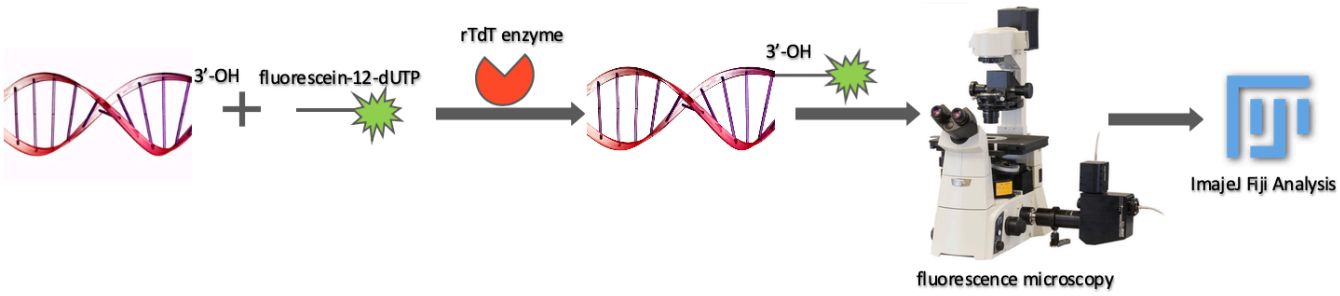

Figure 1. TUNEL staining and imaging process. The DeadEnd. Fluorometric TUNEL System kit uses a recombinant terminal deoxynucleotidyl transferase enzyme (rTdT) which catalyzes the attachment of a dUTP nucleotide, labelled with a 19-fluorescein-12 fluorescent marker, to the free 3'-OH group on the end of the fragmented DNA. This fragmented DNA was then viewed using fluorescence microscopy and the images were analyzed using the software ImageJ and its Fiji Analysis plug-in.

2.4.4 Fluroscence Microscopy

The stained aortic tissue slides were imaged using the spinning disk confocal super resolution microscope (SpinSR10, Olympus. The imaging was done using the widefield fluorescence microscopy where the whole specimen was exposed to the light. A green fluorescent signal was observed at 488 nm excitation in regions that contained apoptotic or necrotic smooth muscle cells, while DAPI-stained nuclei emitted a blue signal at 405nm excitation. The images were taken at 10X magnification to allow for the visualization of each of the 2 tissue sections on the slide within 5-20 images, depending on the size of each tissue section. Images were saved in a .TIFF format.

2.4.5 Analysis of Images of TUNEL-stained Tissue Sections Using ImageJ

The images taken at 488 nm and 405 nm excitation wavelengths for each tissue section were opened in the ImageJ plugin, Fiji. For each tissue sample, a brightness and contrast setting were established for the clearest visualization of the TUNEL and DAPI signal with the removal of all background noise. Then, using the selection tool, the image of the tissue section taken at 488 nm was traced whereby the edges and any areas of thin or torn tissue were omitted. This ensured that any cells that stained positively for TUNEL and DAPI due to physical damage of sample extraction did not skew the results. This traced outline was then pasted and aligned on the image taken at 405 nm, which contained all of the nucleated, DAPI-stained, cells. The traced outline was applied, which removed all areas of the image outside of the outline, leaving behind only the tissue section of interest. Next, both images taken at 488 and 405 nm were further enhanced by removing any residual noise using the “despeckle” option in Fiji. Following this, the cropped image taken at 405 nm was then used to create a mask, which functioned as a control for the expected number and location of all nucleated cells within the tissue sections when determining the colocalization of TUNEL and DAPI. Finally, the “coloc 2” test in Fiji was employed, whereby channel 1 was assigned as the image taken at 488 nm and displayed all TUNEL positive cells, channel 2

was assigned as the image taken at 405 nm and displayed all DAPI positive cells, and the mask created from the image taken at 405 nm was also plugged in. The test was allowed to run and resulted in the creation of a PDF, which listed the proportion of cells that displayed a colocalization of TUNEL and DAPI, and therefore, represented apoptotic or necrotic cells within the tissue.

2.4.6 Statistics

Statistical analysis was performed using GraphPad Prism 8.0. The percentage of cell death in the aortic tissue is presented as a mean ± standard deviation (SD) if normally distributed or as median with the interquartile range (IQR, 25^{th} quartile – 75^{th} quartile). The Shapiro –Wilk test was used to determine normality. A paired comparison was conducted for each patient's percentage of cell death in the aortic tissue in the normal WSS region and the elevated WSS region. For normally distributed paired comparisons, a paired Student t- test was used and for the non-normally distributed comparisons, a Wilcoxon signed rank test was used. Comparisons of mean percentage cell death between the two cohorts of normal WSS region and elevated WSS region for all patients was compared using the Student t-test when normally distributed or the Mann-Whitney test when not normally distributed. Tests were statistically significant when $p < 0.05$.

2.5 Results

2.5.1 Stained Images

The use of DAPI and TUNEL staining allowed for the visualization of the total number of cells (Figure 2A) and the number of those cells that had fragmented DNA (Figure 2B), respectively. Smooth muscle cells that displayed colocalization of DAPI and TUNEL (Figure 2C) were considered to have undergone apoptosis or necrosis. It should be noted that no cells displayed only TUNEL staining. If fragmented DNA was detected, which indicated the occurrence of cell death, a green (TUNEL) and blue (DAPI) signal was present at that cell. This indicated that there was no unwanted or off-target TUNEL staining within the tissues. Images were taken at 10X magnification using a spinning disc confocal microscope.

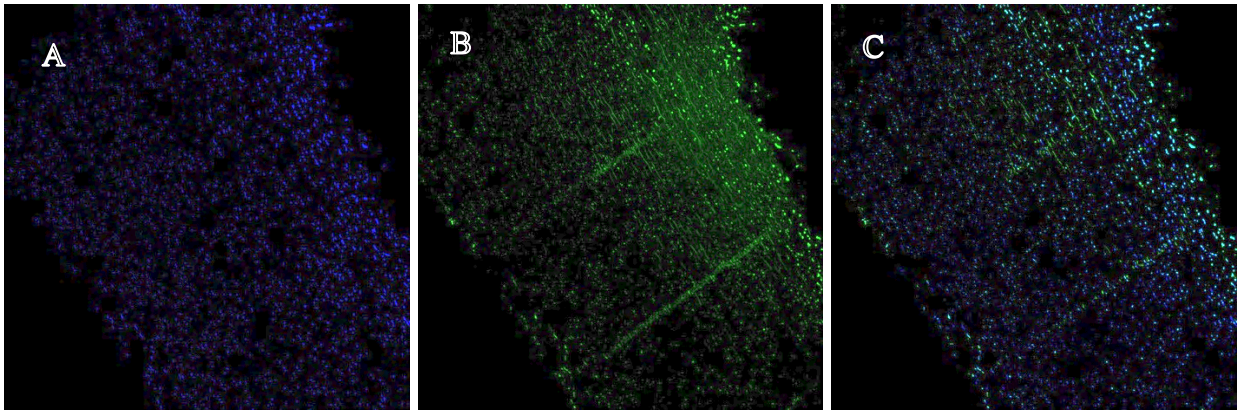

Figure 2. Examples of aorta tissue staining for DAPI and TUNEL.
Aortic tissue viewed under 10X magnification obtained from BAV patient 1237 undergoing surgery was stained with DAPI (A) and TUNEL (B) and the colocalization indicated the percentage of apoptotic or necrotic cells (C).

2.5.1 Individual Tissue Sample Data

Each image produced a percentage cell death detected by the TUNEL stain in comparison to the DAPI stain. The mean percentage of cell death for each tissue sample and the average percentage of cell death of each image for both tissue sections on the slide, was calculated. Each patient had two tissue samples: one from the normal WSS aortic region and one from the elevated WSS aortic region. For each BAV patient (n=15), the distribution of the percentage cell death was higher in elevated aortic WSS region compared to the distribution of the percentage cell death in normal aortic WSS region (Figure 3). In the normal WSS aortic regions, the range of cell death varied from 4.8 - 39.5% colocalization with a minimum value of 0.1% to a maximum of 40.6% and an average median of 6% colocalization of TUNEL with DAPI. Whereas in the elevated WSS aortic regions, the range of cell death varied from 12.8 - 56.7% colocalization with a minimum value of 0.46% to a maximum of 57.8% and an average median of 10.5% colocalization of TUNEL with DAPI colocalization. Tissue samples, especially the elevated aortic WSS regions, showed a larger range of mean percentage cell death as can be seen with long upper whiskers as some areas of the tissue sample were densely positive for cell death (Figure 3). Some patients had a greater difference in mean percentage cell death than others between their elevated and normal aortic WSS regions (Figure 4). The paired elevated WSS regions had a significantly higher percentage of TUNEL/DAPI colocalization than the normal WSS region for BAV patients ($P = 0.00006$, Figure 4).

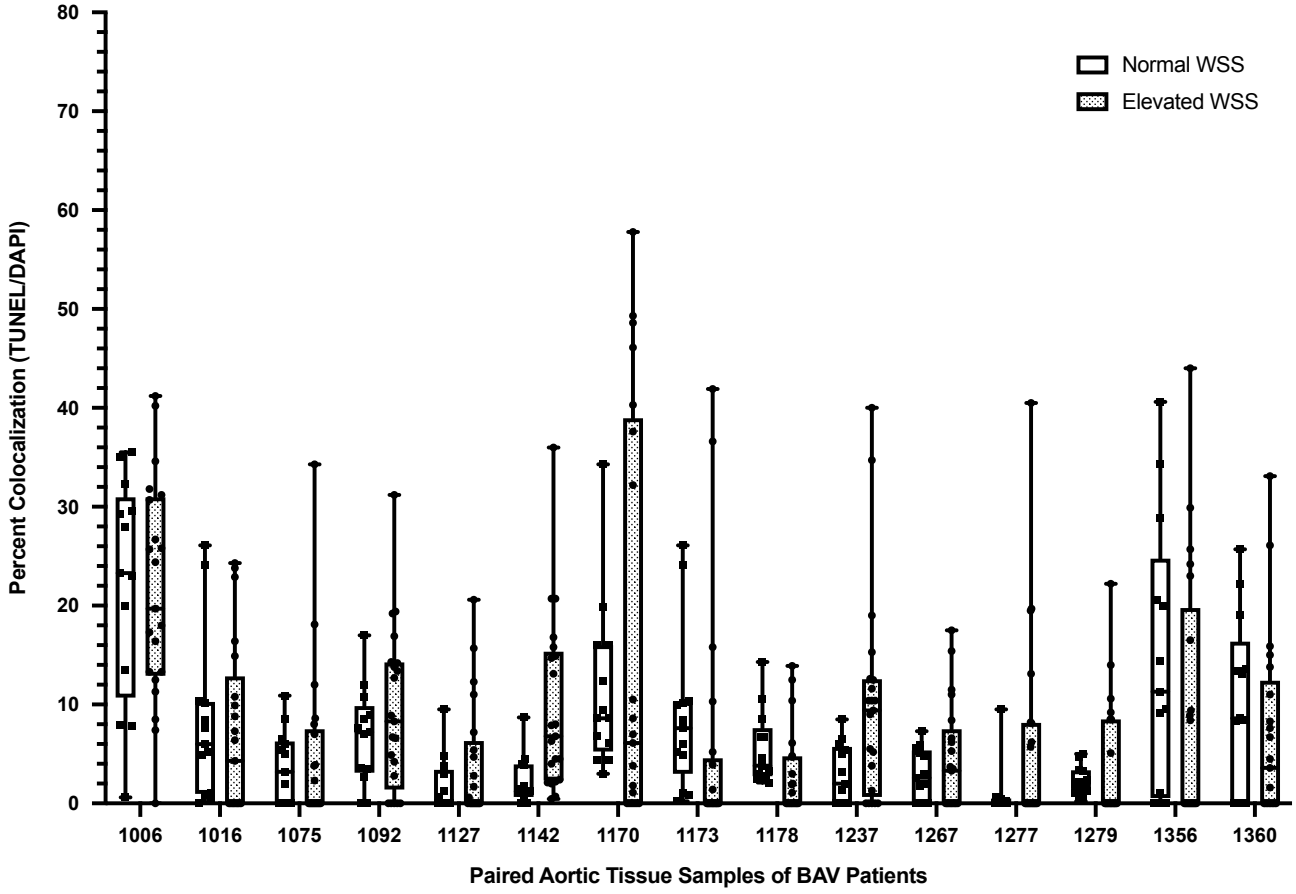

Figure 3. Distribution of percent colocalization of TUNEL/DAPI for aortic tissue samples of 15 BAV patients. The box-and-whisker plot shows the distribution of the percent colocalization data which represents the percentage of cell death for each image analyzed. There were 338 images analyzed in total, 4-20 images per each tissue sample and two tissue samples (normal and elevated WSS regions) for each of the 15 BAV patients. The distribution compared the paired elevated and normal aortic WSS regions for each BAV patients. The box represents the range from the second quartile to the third quartile with the horizontal line representing the median. The whiskers represent the minimum and maximum. In the normal WSS aortic regions, the range of cell death had a minimum of 0.1% to a maximum of 40.6% and an average median of 6% colocalization of TUNEL/DAPI. In the elevated WSS aortic regions, the range of cell death had a minimum of 0.46% and a maximum of 57.8% and an average median of 10.5% colocalization of TUNEL/DAPI.

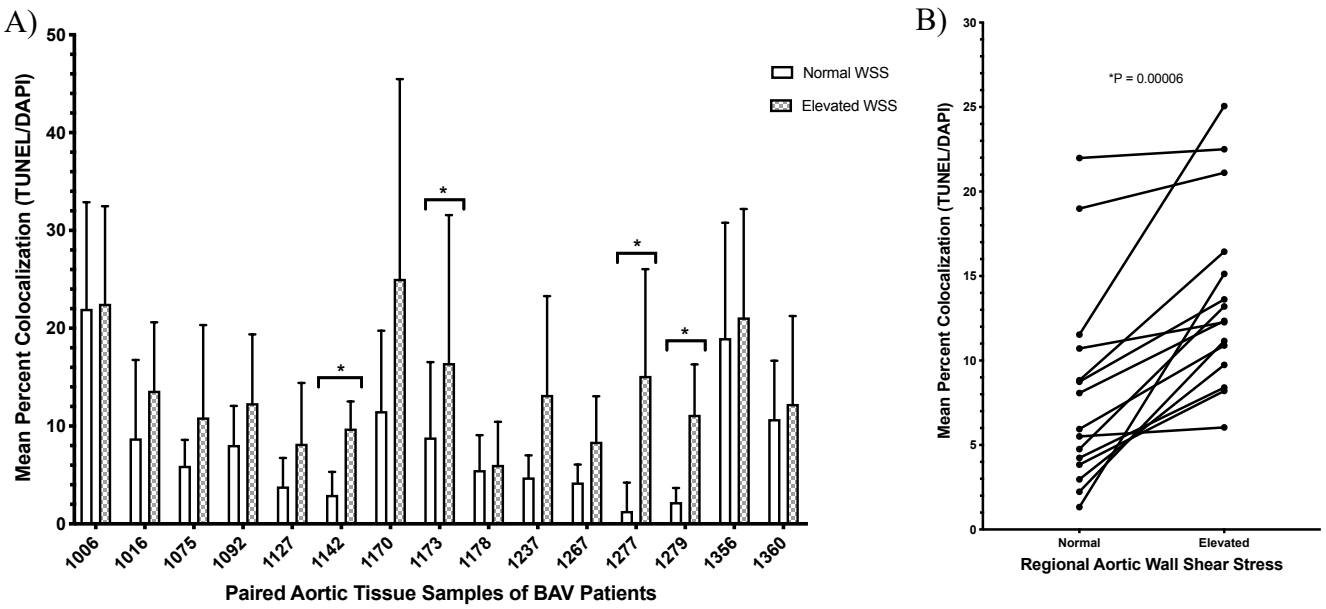

Figure 4. Difference between the mean TUNEL/DAPI ratio for normal and elevated aortic WSS regions for 15 BAV patients. A) The bar graph compares the mean percent colocalization which is the percent cell death between the normal and elevated WSS regions for each patient shown with standard deviation (n=15). * indicates a significant difference using the Mann-Whitney test between the means of elevated and normal WSS regions for percent colocalization of TUNEL/DAPI for the indicated BAV patients. B) The graph shows the difference between the elevated and normal WSS regions of the mean percent colocalization of TUNEL/DAPI. The paired data was found to be significantly different (P = 0.00006) using the Wilcoxon signed ranks test.

2.5.3 Cell Death for Elevated and Normal Aortic WSS Regions

The mean for all patient tissue samples from their elevated aortic WSS region was compared to the mean for all patient tissue samples from their normal aortic WSS region (Figure 5). There were 15 tissue samples (each with 5-20 images) for both elevated and normal aortic WSS regions. The mean percent colocalization of the normal WSS region was 7.98 ± 5.94% with a sample minimum of 1.32% and sample maximum of 21.98%. The mean percent colocalization of the elevated WSS region was 13.74 ± 5.49% with a sample minimum of 6.04% and a sample maximum of 25.06%. The median for the elevated aortic WSS region was 12.34% cell death and it was 5.94% cell death for the normal aortic WSS region. When normality was assessed using the Shapiro-Wilk normality test, the elevated WSS region data was normally distributed and the normal WSS region data was not normally distributed thus the Mann-Whitney test was utilized. The elevated aortic WSS regions had a significantly greater mean percentage of cell death than the normal aortic WSS regions ($P = 0.0027$, Figure 5).

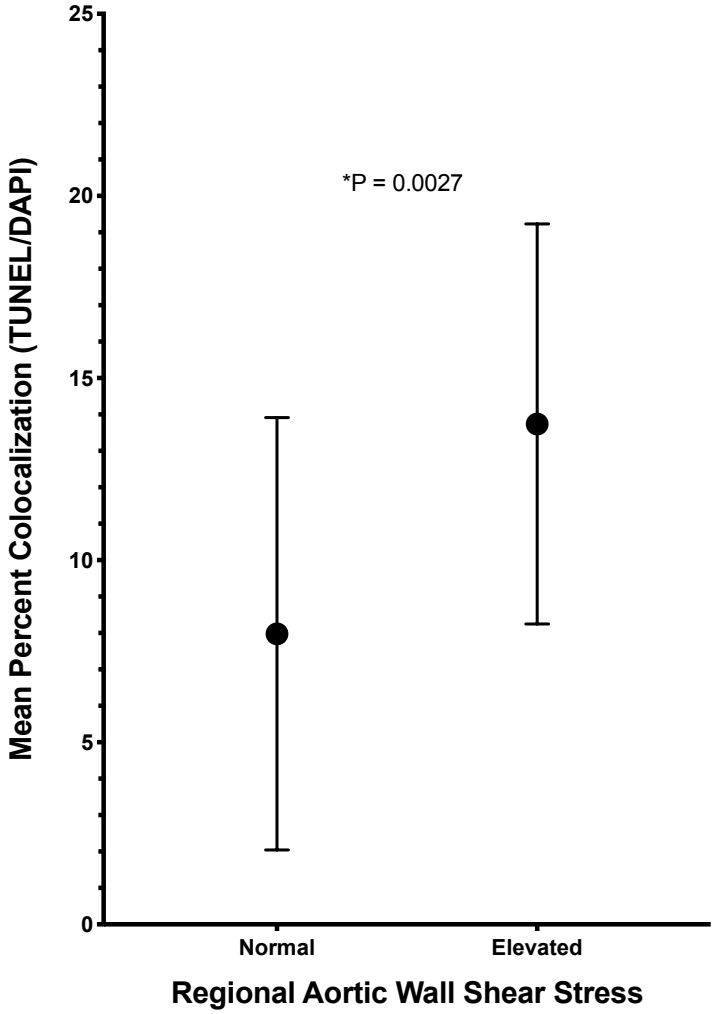

Figure 5. Mean percent colocalization of TUNEL/DAPI for normal and elevated WSS regions. The cohort means for each region (n=15 for each cohort) is shown. The mean percent colocalization shows the percent cell death in the aortic tissue for each region, normal and elevated WSS regions, for BAV patients. The Mann-Whitney U test was conducted to show that the elevated aortic WSS regions had a significantly greater mean percentage of cell death than the normal aortic WSS regions (P = 0.0027).

2.6 Discussion

BAV aortopathy has many factors that impact the integrity of the aortic wall with one of them being the apoptosis and depletion of vascular smooth muscle cells in the aortic wall. There are many factors that may lead to apoptosis. Nataatmadja et al., demonstrated defective fibrillin transport from VSMC to the ECM leading to intracellular accumulation of fibrillin in VSMC and decreased extracellular fibrillin (98). This defect in protein transport may play a role in the development of aortic aneurysms by resulting in improper maintenance of the extracellular matrix and VSMC apoptosis (98). Another possible mechanism for cell death is the physical force of the abnormal hemodynamic flow on the smooth muscle cells (99). Mohammad and colleagues published a paper in 2010, where inhibition of caspase-3 differentially affects vascular smooth muscle cell apoptosis in the concave versus convex aortic sites in ascending aneurysms with a bicuspid aortic valve (100). These studies indicate that there may be intrinsic genetic variation and/or differential hemodynamic flow that allows different levels of apoptotic response to external or internal stimuli. Regardless of the mechanism of the cell death, DNA fragmentation and its release into the circulation is a key common endstage. Thus, assessing the level of cell death in the aorta allows for the net degree of aortopathy to be determined regardless of the multiple factors that may be acting upon it.

The levels of cell death were measured for aortic tissue samples from the elevated WSS aortic region and the normal WSS aortic region for 15 BAV patients. The percent colocalization of TUNEL staining with the DAPI stain showed the percent cell death within each tissue sample as indicated by fragmented DNA. For each patient tissue sample, the TUNEL staining indicated certain areas of higher cell death which can be seen from the data points that are high in percent colocalization compared to the rest of the data sets (Figure 3). In Figure 3, for most elevated WSS aortic regions samples, the percent colocalization for some images, seen as individual data points, was much greater than the rest of the tissue sample which allowed for larger ranges of data (between 12.8 – 56.7%) and thus much longer data ranges. This is especially true for the elevated WSS regions of patients 1006, 1170, 1173, 1277 and 1356

where there were sections that were imaged that had >40% colocalization of TUNEL/DAPI (Figure 3). This larger range and variation in the elevated WSS regions may indicate that the levels of cell death are more localized in small clusters instead of being uniform across large regions of the tissue. For most BAV patients' normal WSS regions, the ranges of percent colocalization of TUNEL/DAPI was smaller than the elevated WSS regions, between 4.8 – 39.5% (Figure 3). This shows that there were lower levels of cell death in the quiescent regions and apoptosis was more uniform across the tissue sample.

Moreover, by analyzing the mean percent colocalization of TUNEL/DAPI of each tissue region for each patient, comparisons between the normal and elevated WSS regions can be done (Figure 4). BAV patients 1006, 1016, 1356 and 1360 all had high levels of mean percent colocalization of TUNEL/DAPI for both the normal and elevated WSS regions with the elevated WSS regions having a slightly higher mean value (Figure 4). This may indicate that large regions of their aortas were experiencing active cell death in both normal and elevated WSS regions with the elevated WSS regions having slightly more. Conversely, BAV patients 1178 and 1267 had lower levels of mean percent colocalization of TUNEL/DAPI for both the normal and elevated WSS regions with the elevated WSS regions having a slightly higher mean (Figure 4). This may indicate that intrinsic genetic variants or the integrity of the aortic wall based on other ECM or elastin factors influences the susceptibility of the smooth muscle cells to undergo cell death based on the levels of WSS.

Furthermore, some BAV patients had tissue samples with a large difference in the level of cell death between their normal and elevated WSS regions (Figure 4). Although all patients had greater levels of cell death or mean percent colocalization of TUNEL/DAPI in their elevated WSS region compared to their normal regions, the BAV patients 1142, 1173, 1277 and 1279 had a significant difference between their mean percent colocalization of TUNEL/DAPI in their elevated WSS region and their normal WSS region (Figure 4, $P < 0.05$). A larger difference may indicate cell death occurring from flow-mediated trauma to the cells in the elevated WSS region and a smaller difference may indicate that those patients may have intrinsic protection against flow-mediated cell trauma.

Nevertheless, there was a significantly greater mean percent colocalization of TUNEL/DAPI in the elevated WSS aortic regions compared to the normal WSS aortic regions for BAV patients (Figure 5, $P = 0.0027$). This indicates that the abnormal hemodynamic flow creating regions of elevated WSS leads to increased levels of cell death. As these BAV patients experience localized elevated WSS, over time the greater levels of cell death may lead to the depletion of vascular smooth muscle cells in certain regions and thereby impact the integrity of the aorta. This increased cell death due to hemodynamic forces should be detectable by aorta-specific DMRs in plasma cfDNA.

2.8 Conclusions

Through the TUNEL staining analysis, the state of active cell death was able to be measured for 15 BAV patients with aortopathy. This allowed us to quantify the net effect of all the various genetic, hemodynamic and structural aortic factors on the levels of cell death occurring in the vascular smooth muscle cells. When we compared the cell death levels between normal and elevated WSS regions for BAV patients, levels in the elevated WSS regions were generally significantly greater than the levels found in the normal regions. This suggests that aorta cell death is influenced by abnormal hemodynamic flow and that regions of the aorta with elevated WSS are more susceptible. It was also noted that some individual BAV patients demonstrated greater levels of cell death than others and some had a larger difference in the degree of cell death between their normal and elevated WSS regions. This suggests that there are other factors involved in determining active cell death in the aorta which may include genetic variants, structural aortic factors and levels of extracellular matrix proteins. The relationship between cell death and increased WSS in the aorta supports our rationale that the levels of aortic smooth muscle cell death as detected by aorta-specific cfDNA could represent a biomarker for aortopathy in BAV patients.

CHAPTER THREE: IDENTIFICATION AND VALIDATION OF AORTA-SPECIFIC DIFFERENTIALLY-METHYLATED REGIONS

3.1 Introduction

Epigenetics is the study of heritable DNA changes that are independent of nucleotide sequence and chromatin organization (101, 102). These heritable changes, including DNA methylation, influence gene expression across generations of cells (102). Epigenetic features have also been implicated in modulating chromatin to ensure that specific genes are expressed in a time-dependent manner to promote cellular specialization (103, 104). Some of the known epigenetic modifications include post-translational histone modifications, DNA methylation, and noncoding micro-RNAs (101). All of these mechanisms work synergistically to dictate the transcriptional activity of a genome.

DNA methylation is typically observed at CpG dinucleotide sites, where methyl groups are added to the C5 position of cytosine bases that are followed by a guanine residue. This process of methylation and the maintenance of methylation in mammals is carried out by three major DNA methyltransferases; DNMT1, DNMT3a, and DNMT3b (105, 106). DNMT1 was the first characterized DNA methyltransferase, and it has been noted that this enzyme preferentially catalyzes hemi-methylated DNA (106). Therefore, DNMT1 is believed to be the primary enzyme responsible for copying methylation patterns from the parental strand to the daughter strand following DNA replication, making it the "maintenance methyltransferase" (106). Moreover, DNMT1 is heavily involved during S-phase where the cell prepares itself for replication, as it is integral for the preservation of methylation patterns across generations of cells (106). DNMT3a and DNMT3b are responsible for the establishment of DNA methylation patterns early in mammalian development and are also involved in methylating the DNA of germ cells (103). Furthermore, DNMT3a and DNMT3b are regarded as *de novo* DNA methyltransferases, as they do not exhibit any significant preference between hemi-methylated and unmethylated DNA (103). It should be noted that 40% of genes are rich with CpG clusters, known as

CpG islands, and 70% of the CpG sites within an island are methylated (103). Upon investigating the role of methylated CpGs, it has been found that these islands act as docking sites for methyl-binding proteins (87). These bound proteins then come together in order to recruit chromatin remodeling complexes that promote chromatin condensation and therefore, gene inactivation (87). Given the role of methylation in the silencing of gene expression, which can be used to dictate the fate of a cell, differentially methylated regions specific to types of tissues can be exploited to indicate the origin of circulating cfDNA.

In order to analyze single-cytosine methylation levels and, therefore, differentially methylated regions within the human genome, the technique of whole genome bisulfite sequencing (WGBS) can be employed. This process begins with the bisulfite conversion of the DNA of interest whereby unmethylated cytosines are converted to uracil bases and then converted and read as thymine through PCR and sequencing, while methylated cytosines are protected and remain intact and are read as cytosine (107). Several algorithms are then employed to computationally map the bisulfite converted reads to the reference genome which allows for the methylated and unmethylated cytosines to be identified and create unique "methylomes" for various cell types (107). Since methylomes are specific to each tissue due to early cell differentiation, these methylomes can be used to indicate the tissue origin of the DNA. Using this principle, the tracking of a differentially methylated region (DMR) specific to a tissue can allow cfDNA to be mapped back to the cell or organ type that it originated from prior to its fragmentation and release into the circulation due to apoptosis (78). This theory has been demonstrated in practice for type-1 diabetes and islet-graft recipients whereby pancreatic β-cell cfDNA was identified and quantified in the circulation of these patients using the differentially hypomethylated insulin (INS) promoter region (78). In addition to this, DNA regions that were differentially methylated in oligodendrocytes were used to detect elevated levels of cfDNA derived from the increasing number of oligodendrocytes undergoing apoptosis in patients with relapsing multiple sclerosis (77). Glial-specific DMRs were also utilized to identify and quantify the increased concentration of cfDNA derived from

the brain within the circulation of patients who had suffered from a severe traumatic brain injury (77). Thus, this proof-of-concept study demonstrated that the organ from which cfDNA originated and the rate at which the given cell type undergoes apoptosis could be determined in humans. Furthermore, this approach could theoretically be adapted to identify cfDNA derived from any cell type in the body, on the basis of identifying DMRs specific to the organ of interest. This provides an alternative and minimally invasive method for diagnosing and monitoring a broad spectrum of human pathologies, such as cell death in the aortic wall due to constant elevated WSS for BAV patients.

3.2 Hypothesis and Specific Aims for Chapter Three

By identifying a unique methylation region specific to the aorta, the levels of aortic cell death could be measured using cfDNA isolated from the blood. This aorta-specific DMR could serve as the aortic "fingerprint", where the DMR is relatively hyper- or hypomethylated compared to all other cell types in the body. We hypothesize that levels of an aorta-specific DMR, which can be detected in cfDNA released from aortic cells undergoing cell death, will correlate with cell death and the severity of aortopathy in BAV patients.

Specific Aims:

1) Identify candidate aorta-specific DMRs *in silico*.

2) Evaluate the candidate aorta-specific DMRs *in vitro* using a tissue panel.

3) Retrospectively validate candidate aorta-specific DMRs *in vitro* using blood samples taken from BAV patients undergoing surgery.

3.3 Materials and Methods

3.3.1 Patient Data

There were 15 plasma samples from BAV patients obtained from the Bluhm Cardiovascular Institute of Northwestern University Feinberg School of Medicine in Chicago and 8 blood samples through the University of Calgary (Table 2). Adult BAV patients were recruited and 8-10 mL of blood was collected before the CMR imaging required for their surgery. Patients from the University of Calgary provided informed written consent for participation in this study which was approved by the Conjoint Health Research Ethics Board (study ID REB17-0207).

Table 2. BAV Study Population Characteristics for Blood and Plasma Samples for Chapter Three. Characteristics of BAV patients (n = 15) that were recruited at the the Bluhm Cardiovascular Institute of Northwestern University Feinberg School of Medicine in Chicago and of patients that were at recruited at the Libin Cardiovascular Institute at the University of Calgary (n = 8)

Parameter	BAV Study Population (N = 23)
Age (Average years)	49.3 ±14.9
Male	20
Female	3
BAV Classification:	
Type 0, lateral	1
Type 1, RL	15
Type 2, RL/RN	7
Average Maximum Diameter (cm)	4.67 ±0.52
Aortic Valve Surgical Procedure:	
Repair	3
Replacement	
AVR	15
Ross	4
Ascending Aorta Surgical Procedure:	
Ascending aorta replacement	19
Root replacement	2
Hemi-arch	1

Values are mean ± SD or n.

AR = aortic regurgitation; AS = aortic stenosis; AVR = aortic valve replacement; BAV = bicuspid aortic valve; RN = right coronary-non-coronary cusp fusion; RL = right-left coronary cusp fusion.

3.3.2 *In Silico* Identification of Candidate Aorta-Specific DMRs

Publicly-available whole genome bisulfite sequenced (WGBS) data from various tissues and cells within the human body were obtained from the NIH Roadmap Epigenomics and the Blueprint Epigenome projects (Procedure outlined in Appendix II). Data was stored and processed using the University of Calgary's computing cluster, Helix. The WGBS data was first mapped to the hg19 genome assembly then each file was converted from BigWig or Wig format to sorted bedgraph files (Appendix IV). After the files were in the correct format, the software program Metilene was used to identify DMRs specific to the aorta dataset (n = 1) in comparison to the non-aortic tissues (n = 21) and hematopoietic cells (n = 14). First, the input files were created for each of the two comparisons (Figure 6). The non-aortic tissue data sets were grouped together in one input file and were compared to the aortic tissue dataset. The two sets of methylomes were not pooled together for comparison as the DMR generated should be able to distinguish, for the large part, aortic DNA from hematopoietic DNA which is the primary contributor for the total cfDNA in the blood. Methylation percentage of each CpG site was taken into account for DMR calling. Metilene compared the assembled methylomes by removing all non-informative segments and identified regions within the genome that had significant differential methylation, and were therefore, potential DMRs (58). Essentially, DMRs were identified on the basis of a mean methylation level of all CpG sites within the given region, measured as a percentage (58). The parameters for the DMR were defined as a minimum of 4 CpG sites per DMR, a maximum of 25 bp between CpG sites, and a minimum of 10% mean methylation difference between the compared groups. An alpha level of 0.05 was chosen for the Mann-Whitney U test that Metilene uses to evaluate the statistical significance of the mean methylation difference between the two groups. A second set of DMRs were identified by comparing the same aortic tissue dataset with the input file of the hematopoietic cells.

The DMRs were then further constrained to a maximum length of a 100 bp, to only the autosomal chromosomes, to have at least 4 CpG sites and to a minimum of a 60% difference for the non-aortic

tissue group and a 90% difference for the hematopoietic cells group. The maximum size of 100 bp was chosen to allow for the product size (after the addition of primers) to be <165 bp, the average cfDNA length in the plasma.

Next, the DMR results for both groups (non-aorta and hematopoietic cells) were compared to identify the shared DMRs using the bedtools intersect command. From this, 23 DMRs were ultimately found and then 10 were chosen based on their mean methylation difference for validation *in vitro* (Table 3).

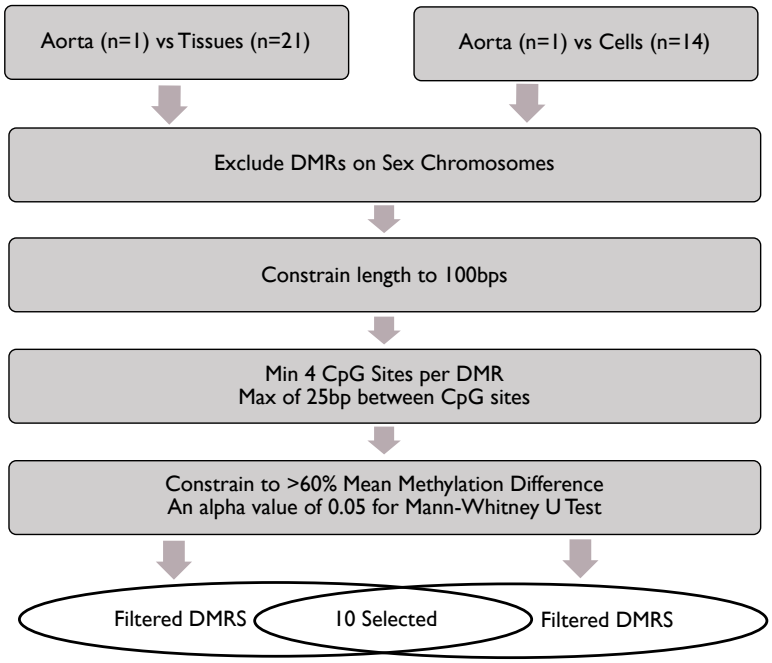

Figure 6. Bioinformatic Pipeline for in silico aorta-specific DMR identification. Using the publicly available methylomes of human non-aortic tissues and hematopoietic cells against the aorta methylome using the software Metilene for the identification of aorta-specific DMRs.

Table 3. Characteristics of the aorta-specific DMRs identified. Candidate DMRs chosen for further validation, including DMR position and length, number of CpG sites within each DMR, and mean methylation difference as a percentage.

	DMR				Mean Methylation Difference Level (%)	
Chromosome	**Start Position**	**End Position**	**DMR Length**	**#CpGs**	**Aorta vs Non-aortic Tissue**	**Aorta vs Hematopoietic cells**
1	3,192,823	3,192,903	80	7	71.28	90.77
2	128,431,046	128,431,099	53	6	72.51	92.80
8	6,398,313	6,398,394	81	7	77.97	92.64
9	134,550,721	134,550,791	70	7	73.42	91.12
11*	**3,168,734**	**3,168,832**	**73**	**6**	**70.60**	**92.75**
15	28,355,445	28,355,503	58	7	81.67	91.53
18*	**74,171,459**	**74,171,505**	**46**	**8**	**74.26**	**91.27**
19	3,603,393	3,603,454	61	7	62.70	92.31
20*	**45,860,400**	**45,860,466**	**65**	**6**	**86.88**	**81.01**
22*	**27,999,645**	**27,999,717**	**72**	**7**	**75.36**	**91.28**

* These DMRs are the four regions that were selected for complete validation.

3.3.3 Primer Design

In order to detect our DMRs in cfDNA and test tissue specificity, primers to amplify each DMR were designed using the online program MethPrimer. The sequences of the candidate DMRs as well as DNA sequence 100 bp upstream and downstream of these regions were taken from the aortic tissue methylome (accession number GSM983648) found in the NIH Roadmap Epigenomics project. MethPrimer (59), then generated primers for the amplification of the candidate DMRs from bisulfite-converted DNA (both genomic and cfDNA). Primers were generated for DMRs on chromosomes 1, 2, 9, 11, 15, 18, 19, 20 and 22 (Table 4). The target sequence for the primers was the DMR sequence containing a minimum of 4 CpG sites. Table 12 in Appendix I shows the parameters for the primer design. Specific parameters were used to ensure that the primers did not contain CpG islands so that no preferential amplification would occur between methylated and unmethylated regions of template DNA. Furthermore, each primer contained at least two non-CpG cytosines, which allowed for correct binding with greater stability to the template DNA. Target melting temperatures of the primers were within 55 - 65°C and total product size was constrained to <150 bp, but ideally <120 bp, to allow for the amplification of these regions within the small cfDNA fragments, which average 140-165 bp in length. The resulting primer sequences obtained from the online MethPrimer software (108) were then submitted to the University of Calgary Core Oligonucleotide Synthesis Laboratory to be synthesized.

3.3.4 Determining Primer Melting Temperatures

In order to determine the appropriate temperature that would allow for optimal primer annealing, a temperature gradient experiment was conducted (Procedure outlined in Appendix I). Each 200 µL PCR tube contained a total of 25 µL of reaction mixture. This mixture was comprised of 5 µL of 5X EpiMark. Hot Start Taq Reaction Buffer (New England BioLabs), 0.5 µL of 10 mM dNTP mix (Invitrogen), 0.5 µL of 10 µM forward primer, 0.5 µL of 10 µM reverse primer, 1.0 uL of 10 ng/µL bisulfite converted control human DNA (Qiagen), 0.125 µL of 5.00 U/mL EpiMark. Hot Start Taq DNA

Polymerase (New England BioLabs) and 17.38 µL of RNAse-free water to ensure the total volume was 25 uL. It should be noted that a master mix for each set of primers for a given DMR was created to reduce errors associated with pipetting volumes into each individual tube. Furthermore, the reagents were added in the order mentioned above. The tubes were then placed in the thermocycler and the PCR reaction was allowed to take place as follows: 3 minutes at 94°C, 45 seconds at 94°C, 45 seconds at one of eight temperatures between 55 - 65°C, 1.5 minutes at 68°C, steps 2-4 were repeated 40X, 10 minutes at 68°C, followed by an infinite hold at 4°C (Appendix I).

3.3.5 Production, Running, and Imaging of the 3% Agarose Gel

Small agarose gels with a 3% concentration were created by dissolving 1.50 g of UltraPure. Agarose (ThermoFisher Scientific) into 50 mL of 1X TAE buffer. For the purpose of imaging, 5 µL of SYBR Green dye (10,000X in DMSO) (Invitrogen) was mixed into the dissolved agarose solution prior to pouring the gel into the casting tray. Then, 2 µL of 6X DNA loading dye was added to 10 µL of the PCR products and 7 µL of the dyed products were loaded into the wells of the gel while immersed in 1X TAE buffer within the chamber. The gels were allowed to run for 45 minutes at 105 V. The gels were then imaged immediately after using the BioRad ChemiDoc Gel Imaging System under UV light (Appendix I).

3.3.6 Extraction of Cell-Free DNA from Whole Blood

Starting from whole blood, the process of determining DMR levels in cfDNA was begun (Figure 7). Prior to their CMR imaging each consented BAV patient provided 8-10 mL of whole blood collected into a Streck BCT tube. These tubes contain a preservative that limits cell lysis, thereby minimizing contamination of the plasma with genomic DNA from hematopoietic cells. Whole blood was centrifuged at 1900 *g* at room temperature for 10 minutes to fractionate the blood then the plasma supernatant was transferred into 2.0 mL Eppendorf tubes which were then centrifuged at maximum

speed (13,000 rpm) for 16 minutes at 4°C (Appendix I). The resulting supernatant was then transferred into new 2.0 mL Eppendorf tubes and stored at -80°C until the cfDNA was ready for isolation. Isolation was performed using the semi-automated MagNA Pure 24 System (Roche) (Appendix I). These served as samples for testing the utility of aorta-specific differentially methylated regions for the detection and quantification of cfDNA released from the aortic wall undergoing cell death.

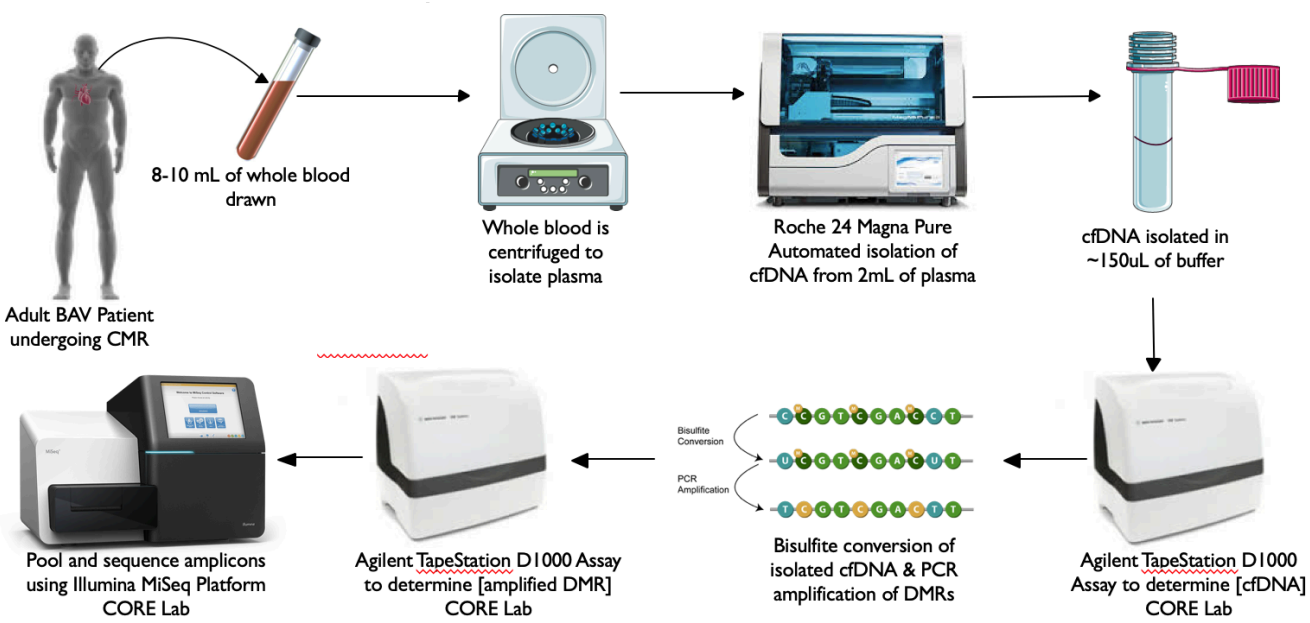

Figure 7. The workflow for DMR verification from cfDNA. A schematic of the process of obtaining cfDNA from whole blood of BAV patients in order to identify and quantify the amount of cfDNA from the aorta using candidate DMRs.

3.3.7 Bisulfite Conversion

This process began with the bisulfite conversion of the DNA of interest, whereby unmethylated cytosines were converted to uracil bases and then to thymine bases after PCR, while methylated cytosines were protected and remained intact (Appendix I). The protocol outlined in the Epitect Bisulfite Kit (Qiagen) was for bisulfite conversion of the extracted cfDNA samples. However, modifications to the manufacturer's procedure were made to improve the final yield. As such, the buffer EB was warmed to 56°C prior to elution at step 17. In addition to this, elution was carried out twice using 20 µL of the warmed EB buffer each time.

3.3.8 Genomic DNA Panel

Commercially-available gDNA isolated from various human tissues (Zyagen), each of which was derived from one of the three germ layers, was purchased in order to create a panel to evaluate the specificity of our putative aorta-specific DMRs. This panel acted as our negative control for methylation whereas the gDNA from the aorta was the positive control for aorta specific DMR verification. This panel was comprised of gDNA from the brain, colon, esophagus, intestine, kidney, liver, lung, pancreas, stomach, skin, spinal cord, skeletal muscle, spleen, and thymus. As such, we were able to compare the methylation levels of the DMR regions with other diverse tissues as well. This was done by bisulfite converting each gDNA sample, PCR amplifying the regions of interest, and sequencing the resulting amplicons. This ultimately allowed us to determine whether the methylation patterns within the regions of chromosomes 11, 18, 20 and 22 were in fact specific to the aorta.

3.3.9 PCR Amplification of DMRs from Patient Samples

Following the extraction of cfDNA from patient plasma samples, the cfDNA was bisulfite converted and functioned as the template DNA for the PCR amplification of the three DMRs of interest (Appendix I). More specifically, a master mix that contained the general reagents for each PCR reaction

was created to ensure minimal pipetting errors associated with the use of small volumes. Overall, each 200 µL PCR tube contained 5 µL of 5X EpiMark. Hot Start Taq Reaction Buffer (New England BioLabs), 0.5 µL of 10 mM dNTP mix (Invitrogen), 0.5 µL of 10 µM forward primer, 0.5 µL of 10 µM reverse primer, 1.0 uL of 10 ng/µL bisulfite converted cfDNA from patient samples, 0.125 µL of 5.00 U/mL EpiMark. Hot Start Taq DNA Polymerase (New England BioLabs), and 17.38 µL of RNAse-free water to ensure the total volume was 25 uL. The tubes were then vortexed and centrifuged to ensure all reagents were sufficiently incorporated at the bottom of each tube. Finally, the tubes were then placed in the thermocycler and the PCR reaction was allowed to take place as follows: 3 minutes at 94°C – 3 minutes, 45 seconds at 94°C, 45 seconds at the determined Tm of the given primer, 1.5 minutes at 68°C, steps 2-4 were repeated 40X, 10 minutes at 68°C, followed by an infinite hold at 4°C.

3.3.10 Amplicon Pooling

In order to maximize the efficiency of the sequencing runs performed on the Illumina MiSeq sequencing platform, amplicons of each of the three DMRs amplified from the same template DNA were pooled together in equimolar amounts (Table 13-16 in Appendix V). The molarity of each PCR product was determined through a high sensitivity TapeStation performed in the Core Laboratory at the University of Calgary. Overall, 63 µL of total solution was submitted in each tube. Therefore, 15.8 µL from the amplicon with the lowest molarity was added to the pool while the remaining two amplicons were diluted with pure water to the same molarity within 15.8 µL of solution to produce an equimolar mixture. For example, when amplifying the Chr 11 DMR within the bisulfite converted cfDNA obtained from the plasma of patient 1006, the molarity was 33.1 nM (Appendix V, Table 25), while the amplicon of Chr 18 had a molarity of 5.07 nM (Appendix V, Table 24), the amplicon of Chr 20 had a molarity of 12.6 nM (Appendix V, Table 26) and the amplicon for Chr 22 had a molarity of 24 nM. Therefore, 2.68 µL of the Chr 11 amplicon solution, 17.5 µL of the Chr 18 amplicon solution, 7.04 µL of the Chr 20 amplicon solution and 3.81 µL of the Chr 22 amplicon solution was added to the pool. Then 32 µL of

pure water was added to the pool to result in a 63 µL solution with a molarity of 5.07 nM. The volume of each amplicon required to obtain the desired molarity within 15.75 µL of solution was determined using the $C_1V_1=C_2V_2$ equation.

3.3.11 Amplicon Sequencing Using Illumina MiSeq

The Illumina MiSeq sequencing platform was implemented as it had the capacity to perform deep sequencing of PCR amplicons and allowed for cost-effective analysis of several genomic regions in a single run. The pooled samples were given to the University of Calgary Core Laboratory where sequencing libraries were prepared using the Illumina MiSeq library preparation kit. Libraries were then sequenced using the v3 MiSeq reagent kit v3 (150 cycles) to produce 2x75 bp paired end reads. The results of the run, provided in fastq format, were then accessed through the BaseSpace Sequencing Hub. The quality of each sequenced pool was assessed by generating a FastQC (109) report for each file, where a Q score 0.30 was used as a threshold.

3.3.12 Analysis of Bisulfite-Sequenced Runs

The bisulfite sequencing plugin for the CLC genomics workbench (Qiagen) was utilized to analyze the bisulfite sequenced reads. Reads were mapped such that the entire length of the read aligned with no less than 80% similarity to the hg19 reference genome. Therefore, all non-specific reads and broken pairs were discarded. Methylation levels were determined for each individual CpG site within each of the DMRs on chromosomes 11, 18, 20 and 22 using the methylation caller of the bisulfite sequencing plugin. Mean methylation levels were then calculated based on the methylation levels of the individual CpG sites within each of the four DMRs of interest.

3.3.13 Determination of Concentration of Total cfDNA & DMRs within Patients' Plasma

The total concentration of cfDNA, in copies/mL, within BAV patient plasma was determined by multiplying the concentration of total cfDNA extracted from 2 mL of patient plasma in ng/μL, as determined by a high sensitivity TapeStation, by 1000 μL/mL to obtain the concentration of cfDNA in ng/mL. This concentration was then divided by 0.00330ng, which is the approximate mass of a single human base and provided the total copies of cfDNA/ mL of plasma (110). In order to determine the absolute concentration of each DMR within the recipients' plasma in copies/mL, the fraction of unmethylated molecules within the given pool of amplicons, as determined from the analysis of the bisulfite sequenced reads, was multiplied by the total concentration of cfDNA extracted from the initial plasma sample in ng/mL, then divided by 0.00330 ng. Sample calculations are provided in Appendix IV.

3.4 Results

3.4.1 DMR Identification

Publicly available methylomes were obtained from both the NIH Roadmap Epigenomics (56) and the Blueprint Epigenome (57) projects. This included methylomes from hematopoietic cells (n=14), non-aortic tissues (n=21), as well as the aorta (n=1) (Appendix III). After comparing the aortic methylome to the 19 tissue methylomes, with a minimum mean methylation difference of 60%, 446 DMRs were identified, majority of which were hypomethylated in the aorta relative to the other tissues. The comparison of the aorta methylome to the 14 methylomes of hematopoietic cells, with a minimum mean methylation difference of 90%, 181 DMRs were identified, with a more even distribution between hypomethylated and hypermethylated regions. Of these datasets, 24 DMRs were common to both and located on autosomal chromosomes. From these 24 aorta-specific DMRs, 10 with the highest mean methylation differences were selected for further interrogation (Table 3).

3.4.2 Primer Verification for Amplification of Aorta-Specific DMRs

Using the software MethPrimer, and the sequences of regions that included the candidate DMRs, potential primer sets were identified for each DMR (Table 4). The specificity and optimal melting temperature of the generated primers was determined by PCR using a temperature gradient; the resulting products were visualized on a 3% agarose gel. As such, the primers generated for the amplification of the DMRs on chromosome 1, 2, 8, 9 were not successful as no bands were visible on the agarose gel (data not shown). DMRs on Chr 15 and 19 had significant contamination at around 60-75 bp length and thus were non-specific for the target DMR. This was most likely cause by primer dimerization. The forward and reverse primers generated by MethPrimer for the DMRs on Chr 11, 18, 20 and 22 successfully resulted in the amplification of a single strong band with no off-target amplification observed. The expected product sizes for Chr 11, 18, 20 and 22 were 127 bp, 119 bp, 139 bp and 122 bp respectively. When the primers for the mentioned DMRs were tested with control human gDNA, the product sizes were observed for all four DMRs as 135-145 bp. The temperature gradient with control human gDNA yielded optimal primer annealing temperatures for future PCR reactions: 55.7°C for Chr 11, 55°C for Chr 18, 58.5°C for Chr 20 and 56.9°C for Chr 22 (Figure 8). These primers were further tested with methylated control human gDNA, unmethylated control human gDNA, aortic gDNA and cfDNA from a control sample without any congenital cardiac disease (Figure 9). The presence of the band indicated that the DMRs identified *in silico* were able to be detected in gDNA and cfDNA with the primers synthesized.

Table 4: Primers synthesized for the testing of aorta-specific DMRs. Forward and reverse bisulfite PCR primer sequences designed using MethPrimer for each DMR of interest, and the associated melting temperature of the primer sets. Dashes denote an inability to determine a successful melting temperature for the amplification of the given DMR without off-target amplification.

DMR (Chr)	DMR Start Position	Expected Product Size	Forward Primer	Reverse Primer	Tm (°C)
1	3,192,823 – 3,192,903	135	GGTTTGATTTATTTTGTTTTGGGTA	ACAAAACCCCTCAAAAAACCTA	-
2	128,431,046 – 128,431,099	105	TAGTAAGGGAAGGTTGATTTTTGTT	TAAATCCCTTAAACCTTTCCCTAAA	-
8	6,398,313 – 6,398,394	150	TTATATTAGGAAATGGATTGGGTGT	CCCTCCAAAAAAACAAAATACTCTAC	-
9	134,550,721 – 134,550,791	128	TTGATTTAGGGAGGGTAAGAGTTAG	AAAAACACATAATAAACCCTATAA	-
11	3,168,734 – 3,168,832	127	GGGTATTTAGTTATGAGGGAATAATG	CAAACCTATCTTTAATTTCCACCC	55.7
15	28,355,445 – 28,355,503	121	GAGATGTGAAGTTTGATATTTTTTAAT	CATAACAAAATTACCCCTAAAATCAATA	-
18	74,171,459 – 74,171,505	120	AGTTTAGGATTTGTGTTATTTAGGA	TAAAAAATATTACTATTAACATCATAACAA	55
19	3,603,393 – 3,603,454	121	GAAATTGAGGTTTGGAGAGTAGATG	GAAATTGAGGTTTGGAGAGTAGATG	-
20	45,860,400 – 45,860,466	139	GGAGTAAAATGAATAAAATTTTTGTTGAGA	AAAAAACAAATACAAAAAAACTACAAAACC	58.5
22	27,999,645 – 27,999,717	122	GTTGAGGAATTGGAGGAAAATTAA	ACAAACTACTAAACAAAAAACACAA	56.9

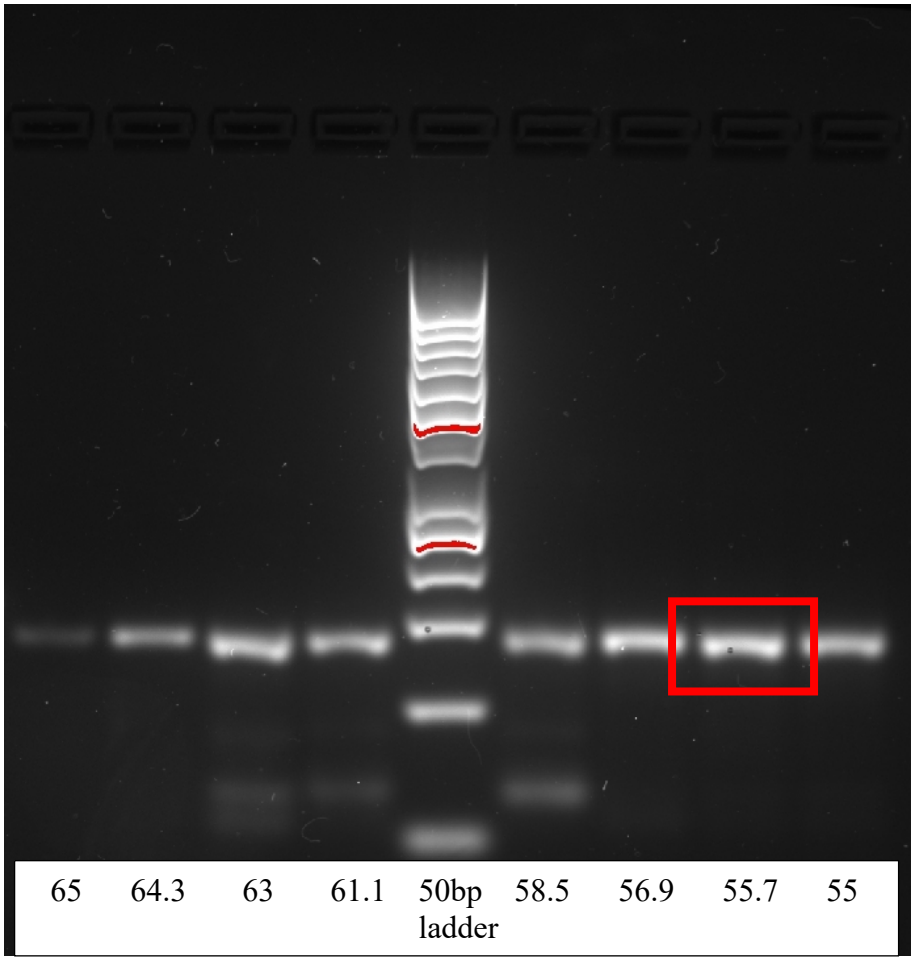

Figure 8: Gel showing a temperature gradient run for candidate Chr 11 DMR. The The temperature 55.7 °C is has the strongest band at the target size of 127 bps with the least amount of off-target amplification. Thus, 55.7 °C was chosen as the optimal temperature for primer annealing for Chr 11 DMR PCR amplification for all further PCR runs.

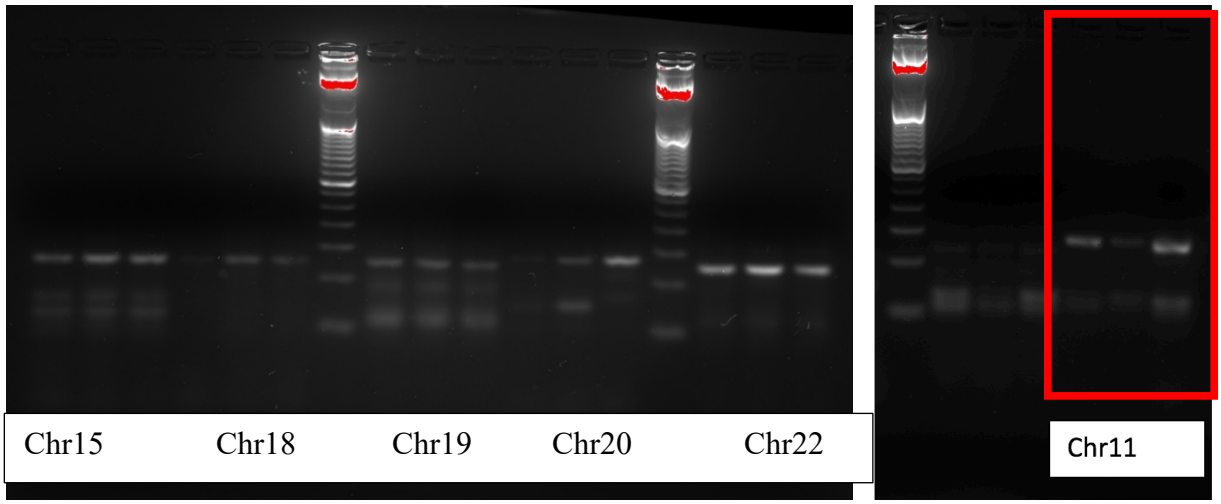

Figure 9: Gel showing candidate DMRs on chromosomes 11, 15, 18, 19, 20 and 22 run with 3 control cfDNA samples from 0 and 1 rejection grade heart transplant patients. The gel shows large amounts of off-target amplification for Chr 15 and 19 candidate DMRs in the control cfDNA. Thus, Chr 15 and 19 DMRs were not selected for further testing. The DMRs on Chr 11, 18, 20 and 22 were selected for further testing due to their strong bands and on-target amplification.

3.4.3 Methylation Levels of Each DMR in Aortic gDNA

Through amplification from bisulfite-converted genomic DNA from the aorta and sequencing of the Chr 11 DMR amplicons, the six individual CpG sites were methylated in only 24-28% of the sequence amplicons with an average overall methylation level of 25.8% for the entire DMR (Table 5). Through amplification from bisulfite converted genomic DNA from the aorta and sequencing of the Chr 18 DMR amplicons, the eight individual CpG sites were methylated in only 13-14% of the sequence amplicons with an average overall methylation level of 13.3% for the entire DMR. Through amplification from bisulfite converted genomic DNA from the aorta and sequencing of the Chr 20 DMR amplicons, the six individual CpG sites were methylated in only 12-14% of the sequence amplicons with an average overall methylation level of 13.2% for the entire DMR. Through amplification from bisulfite converted genomic DNA from the aorta and sequencing of the Chr 22 DMR amplicons, the seven individual CpG sites were methylated in only 16-21% of the sequence amplicons with an average overall methylation level of 19.6% for the entire DMR.

Table 5. Methylation levels for Aorta gDNA for each DMR tested. Total sequencing coverage, methylation levels at each CpG site, and the overall methylation level within the DMRs in gDNA extracted from human aorta tissue.

DMR	CpG Position	Total Coverage	Methylation Level (%)	Overall Methylation (%)
11	80,410,508	20,484	0.91	**25.8**
	80410526	20,497	0.96	
	80410542	20493	0.97	
	80410547	20489	0.96	
	80410573	20442	0.88	
	80410579	20419	0.87	
18	74171460	93012	0.13	**13.3**
	74171465	93038	0.14	
	74171469	93057	0.13	
	74171483	93114	0.13	
	74171490	93117	0.14	
	74171492	93121	0.13	
	74171495	93194	0.13	
	74171504	93099	0.13	
20	45860401	85376	0.14	**13.2**
	45860407	85335	0.12	
	45860417	84957	0.14	
	45860434	84874	0.13	
	45860456	84819	0.13	
	45860465	84665	0.13	
22	27,999,646	47,155	0.16	**19.6**
	27,999,672	47,223	0.2	
	27,999,679	47,169	0.2	
	27,999,682	47,178	0.21	
	27,999,684	47,144	0.21	
	27,999,708	44,800	0.2	
	27,999,716	44,739	0.19	

3.4.5 *In Vitro* Verification of Aorta-Specific DMRs - Genomic DNA Panel

In order to confirm that the three selected DMRs were in fact aorta-specific, we obtained genomic DNA from a variety of tissues within the human body, which encompassed all three developmental germ layers. All of the DMRs were the most unmethylated within the gDNA of the aorta: at the Chr 11 DMR 74.2% of the reads were unmethylated, at the Chr 18 DMR 86.8% of the reads were unmethylated, at the Chr 20 DMR 86.8% of the reads were unmethylated, at the Chr 22 DMR, 80.4% were unmethylated (Figure 10). Compared to the tissue panel, the region at Chr 11 was distinctly more unmethylated in the aorta and the difference between the aorta and the other tissues was on an average 56.8%. Compared to the tissue panel, the region at Chr 18 was distinctly more unmethylated in the aorta except for the gDNA from the brain and the difference between the aorta and the other tissues was on an average 59.8%. Compared to the tissue panel, the region at Chr 20 was distinctly more unmethylated in the aorta and the difference between the aorta and the other tissues was on an average 79.2%. The region at Chr 20 also had the largest difference in methylation when comparing the gDNA from the aorta and the tissue panel. Compared to the tissue panel, the region at Chr 22 was distinctly more unmethylated in the aorta, except for the gDNA from the brian and the skeletal muscle, and the difference between the aorta and the other tissues was on an average 53.1%.

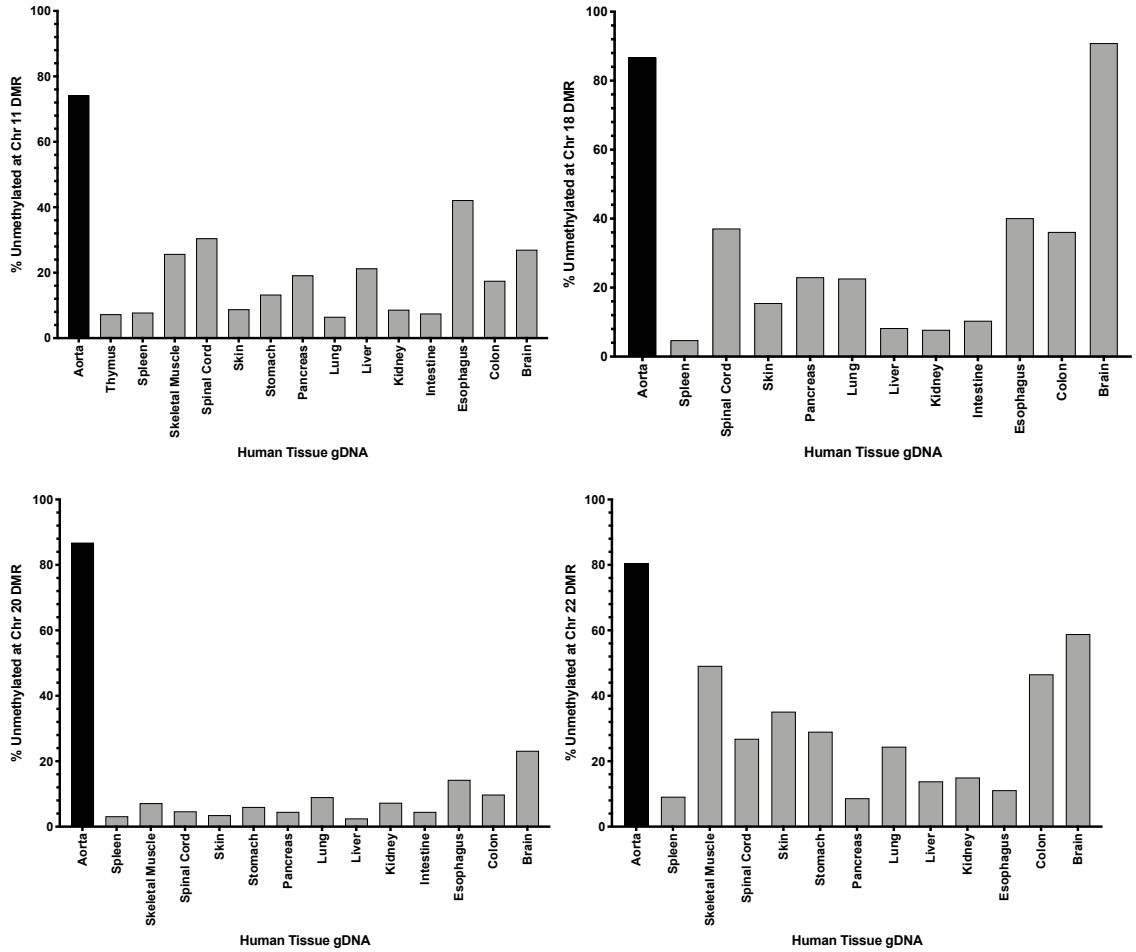

Figure 10. Unmethylation Levels of gDNA of the Aorta Compared to gDNA from a Tissue Panel. The percentage of unmethylated CpG sites within Chr 11, Chr 18, Chr 20 and Chr 22 in genomic DNA obtained from the aorta, highlighted in the black bar, and various other tissues in the human body, in the grey bars. Methylation levels were determined using bisulfite sequencing on the Illumina MiSeq sequencing platform.

3.4.5 Characteristics of Input Materials for Each Patient

The total cfDNA concentration, in ng/mL, from the plasma of 23 BAV patients ranged from 50.8 ng/mL to 2480 ng/mL. The mean concentration was 400 ng/mL while the median concentration was 193 ng/mL. This was due to two BAV patients having abnormally high cfDNA concentrations. When these outliers were omitted, the range was 50.8 ng/mL to 777 ng/mL with a mean of 213 ng/mL and a median of 171 ng/mL. Then, the cfDNA was used to amplify the four candidate DMRs at Chr 11, 18, 20 and 22 for each BAV patient. The average concentration of Chr 11 DMR after amplification was 3.13 ng/μL with a range of 0.853 ng/μL – 5.72 ng/μL. The average concentration of Chr 18 DMR after amplification was 0.733 ng/μL with a range of 0.324 ng/μL – 2.55 ng/μL. The average concentration of Chr 20 DMR after amplification was 1.25 ng/μL with a range of 0.377 ng/μL – 4.01 ng/μL. The average concentration of Chr 22 DMR after amplification was 2.53 ng/μL with a range of 0.426 ng/μL – 6.34 ng/μL. For Chr 11 DMR, there were 4 BAV patient samples from patient 1075, 1142, 1356 and 1 that did not amplify in sufficient concentration for sequencing and were not submitted. For Chr 18 DMR, there were 4 BAV patient samples from patient 1075, 1092, 1127, 1142 and 1173 that did not amplify in sufficient concentration for sequencing and were not submitted. The lowest peak molarity across all DMRs for each patient sample was used for sequencing for equal sequencing reads across all DMRs. The average peak molarity for each DMR for all cfDNA BAV patient samples was 8.70 nM and ranged from 4.14 nM – 24.7 nM.

3.4.6 Levels of candidate DMRs in cfDNA of BAV Patients with Maximal Aortic Diameter

The total cfDNA levels in the plasma of each patient and the cfDNA levels from the aorta as predicted by the candidate DMRs were correlated with the BAV patients' maximal aortic diameter (Figure 10). The maximal aortic diameter for the 23 patients undergoing aortic resection surgery ranged and whose blood samples were collected from 36-63 mm. The total levels of cfDNA of all the BAV

patient samples after sequencing varied between 16,764 – 35,310 copies/mL with a median of 56,430 copies/mL. The total cfDNA levels for BAV patients 1170 and 1360 were abnormally greater than the rest and were outliers for all DMRs. These two samples were omitted from analysis.

3.4.6.1 Chr 11 DMR

The sequencing of amplicons from BAV patients (n = 23) resulted in an average unmethylation perecentage of 9.61% with a small range of 7.00% – 14.3% (Table 6). This unmethylation percentage indicated the percent of Chr 11 DMR present in the total cfDNA in each sample. The concentration of the Chr 11 DMR for all BAV patients ranged from 1509 – 23504 copies/mL with a mean of 6735 copies/mL and a median of 5626 copies/mL. The cfDNA levels did not correlate with the maximal aoritc diameter for BAV patients (Figure 11).

Table 6. Methylation levels and cfDNA levels for each BAV patient sample for Chr 11 DMR
The overall methylation percent, the overall unmethylation percent within the DMR in cfDNA extracted from the plasma of each BAV patient by maximum aortic diameter.

Patient	Max. Aortic Diameter (mm)	Overall Methylation (%)	Overall Unmethylation (%)	Chr 11 DMR (copies/mL)	Total cfDNA (copies/mL)
1016	36	90.3	9.7	7050	72930
1092	41	91.2	8.8	5626	63690
1075	43	89.7	10.3	6649	64350
1173	43	88.1	11.9	14595	123090
7	43	91.0	9.0	1509	16764
1127	44	89.8	10.2	2573	25311
1178	45	90.8	9.2	23504	256410
2	45	91.5	8.5	3001	35310
1356	46	91.3	8.7	15930	183810
8	46	90.7	9.3	2193	23496
1142	47	90.0	10.0	8382	83820
3	47	89.3	10.7	2855	26763
1267	48	91.2	8.8	1796	20328
4	49	90.2	9.8	1762	17919
6	49	88.8	11.2	2086	18678
1237	50	92.0	8.0	2878	35970
1279	50	93.0	7.0	6445	92070
5	50	91.2	8.8	1927	21813
1277	52	90.2	9.8	12136	123420
1	52	85.7	14.3	8061	56430
1006	63	91.0	9.0	10484	116490

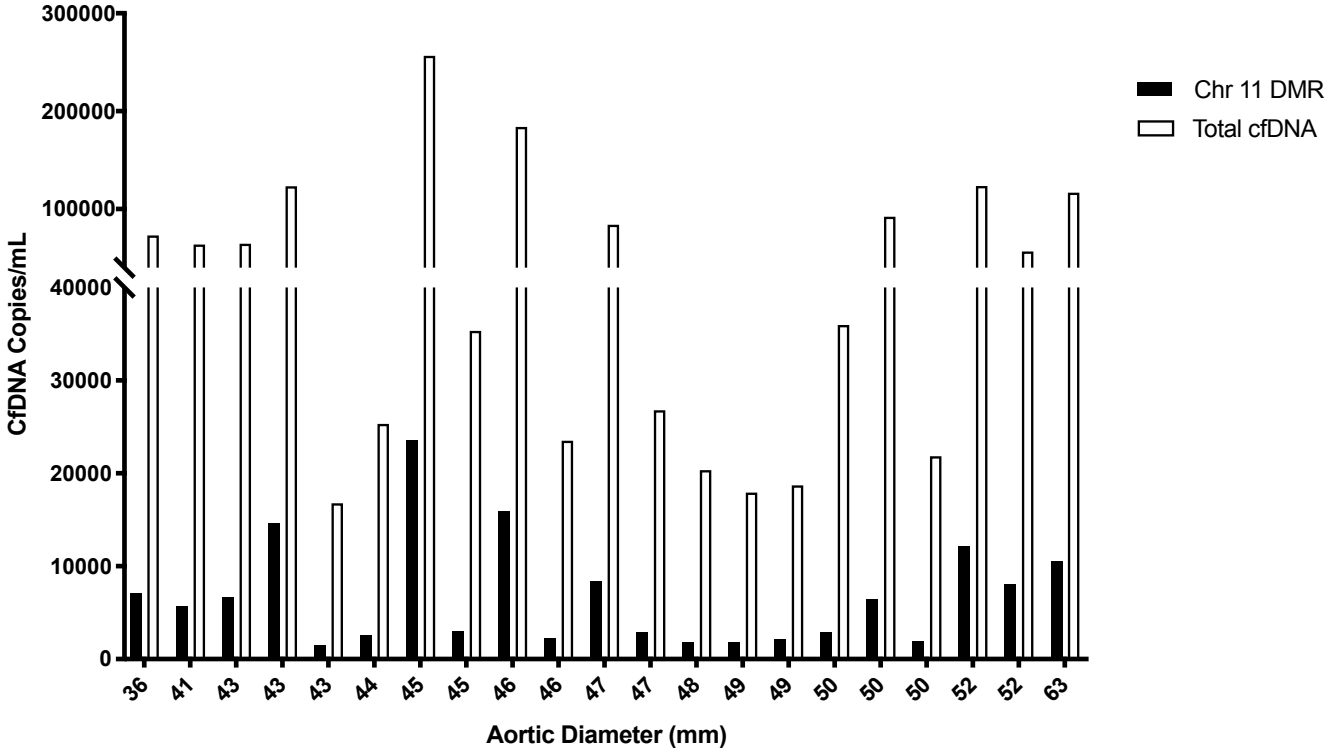

Figure 11. The concentration of the Chr 11 DMR and the total cfDNA plotted against the maximal aortic diameter of BAV patients. The concentration (copies/mL) of all cfDNA within the plasma of BAV patients (n = 23) along with the concentration (copies/mL) of the DMR at Chr 11 arranged according to patient maximal aortic diameter.

3.4.6.2 Chr 18 DMR

The sequencing of amplicons from BAV patients (n = 12) resulted in an average unmethylation perecentage of 70.7% with a range of 14.3% – 86.5% (Table 7). This unmethylation percentage indicated the percent of Chr 18 DMR present in the total cfDNA in each sample. The concentration of the Chr 18 DMR for all BAV patients ranged from 5126 – 157692 copies/mL with a mean of 54743 copies/mL and a median of 42242 copies/mL. The cfDNA levels did not correlate with the maximal aortic diameter for BAV patients (Figure 12).

Table 7: Methylation levels and cfDNA levels for each BAV patient sample for Chr 18 DMR
The overall methylation percent and the overall unmethylation percent within the DMR in cfDNA extracted from the plasma of each BAV patient by maximum aortic diameter. The values not listed show the samples that could not be amplified in sufficient amounts for sequencing and thus were not submitted for sequencing.

Patient	Max. Aortic Diameter (mm)	Overall Methylation (%)	Overall Unmethylation (%)	Chr 18 DMR (copies/mL)	Total cfDNA (copies/mL)
1016	36	16.3	83.8	61079	72930
1092	41	-	-	-	-
1075	43	-	-	-	-
1173	43	15.9	84.1	103549	123090
7	43	-	-	-	-
1127	44	24.8	75.3	19047	25311
1178	45	38.5	61.5	157692	256410
2	45	23.4	76.6	27056	35310
1356	46	-	-	-	183810
8	46	20.5	79.5	18679	23496
1142	47	-	-	-	-
3	47	-	-	-	-
1267	48	17.3	82.8	16821	20328
4	49	-	-	-	-
6	49	39.3	60.8	11347	18678
1237	50	85.8	14.3	5126	35970
1279	50	37.6	62.4	57429	92070
5	50	23.3	76.8	16741	21813
1277	52	34.7	65.3	80634	123420
1	52	-	-	-	-
1006	63	13.5	86.5	100764	116490

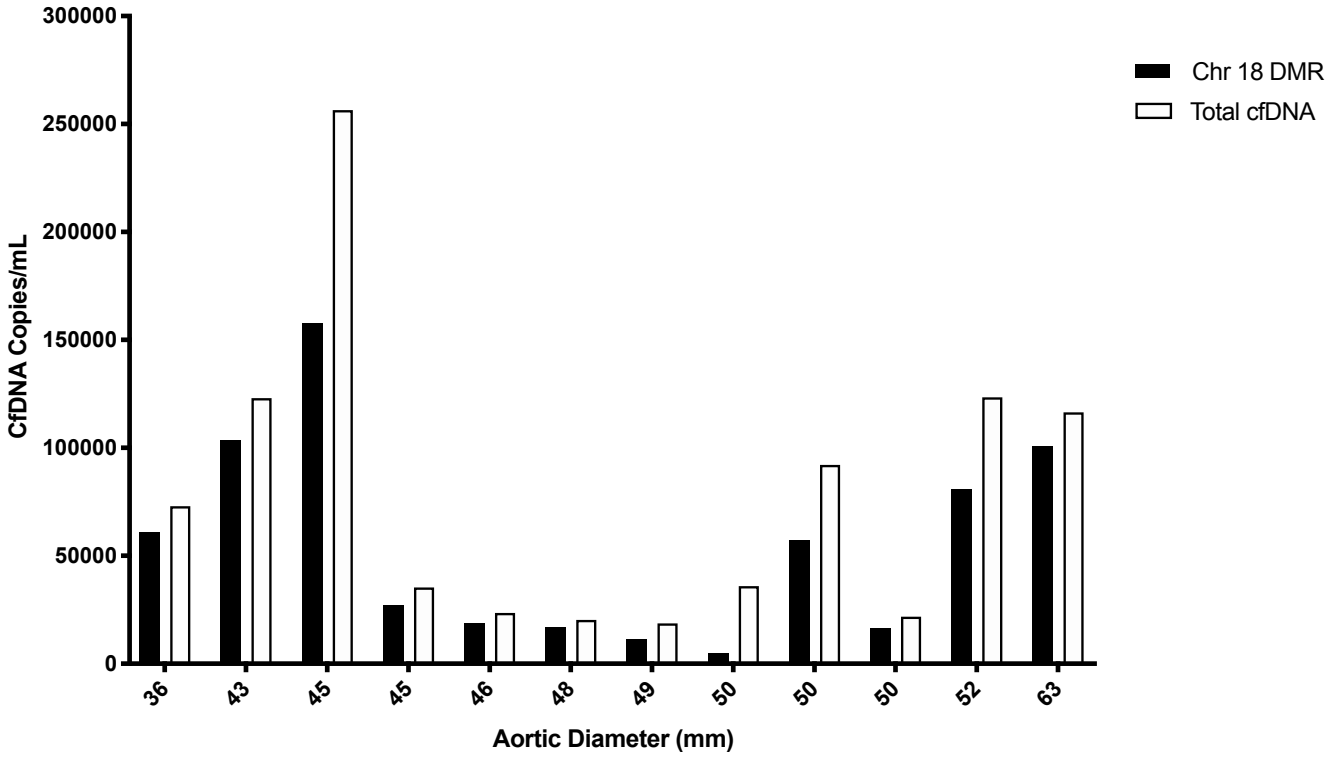

Figure 12. The concentration of the Chr 18 DMR and the total cfDNA plotted against the maximal aortic diameter of BAV patients. The concentration (copies/mL) of all cfDNA within the plasma of BAV patients (n = 12) along with the concentration (copies/mL) of the DMR at Chr 18 arranged according to patient maximal aortic diameter.

3.4.6.3 Chr 20 DMR

The sequencing of amplicons from BAV patients (n = 14) resulted in an average unmethylation perecentage of 22.9% with a range of 7.0% – 53.0% (Table 8). This unmethylation percentage indicated the percent of Chr 20 DMR present in the total cfDNA in each sample. The concentration of the Chr 20 DMR for all BAV patients ranged from 2518 – 46259 copies/mL with a mean of 14404 copies/mL and a median of 7065 copies/mL. The cfDNA levels did not correlate with the maximal aoritc diameter for BAV patients (Figure 13).

Table 8: Methylation levels and cfDNA levels for each BAV patient sample for Chr 20 DMR
The overall methylation percent and the overall unmethylation percent within the DMR in cfDNA extracted from the plasma of each BAV patient by maximum aortic diameter. The values not listed show the samples that could not be amplified in sufficient amounts for sequencing and thus were not submitted for sequencing.

Patient	Max. Aortic Diameter (mm)	Overall Methylation (%)	Overall Unmethylation (%)	Chr 20 DMR (copies/mL)	Total cfDNA (copies/mL)
1016	36	76.3	23.7	17260	72930
1092	41	-	-	-	-
1075	43	-	-	-	-
1173	43	-	-	-	-
7	43	-	-	-	-
1127	44	-	-	-	-
1178	45	-	-	-	-
2	45	47.0	53.0	18714	35310
1356	46	74.8	25.2	46259	183810
8	46	80.8	19.2	4503	23496
1142	47	-	-	-	-
3	47	81.7	18.3	4907	26763
1267	48	80.3	19.7	3998	20328
4	49	73.5	26.5	4749	17919
6	49	70.2	29.8	5572	18678
1237	50	93.0	7.0	2518	35970
1279	50	77.8	22.2	20409	92070
5	50	82.0	18.0	3926	21813
1277	52	73.3	26.7	32912	123420
1	52	84.8	15.2	8559	56430
1006	63	76.5	23.5	27375	116490

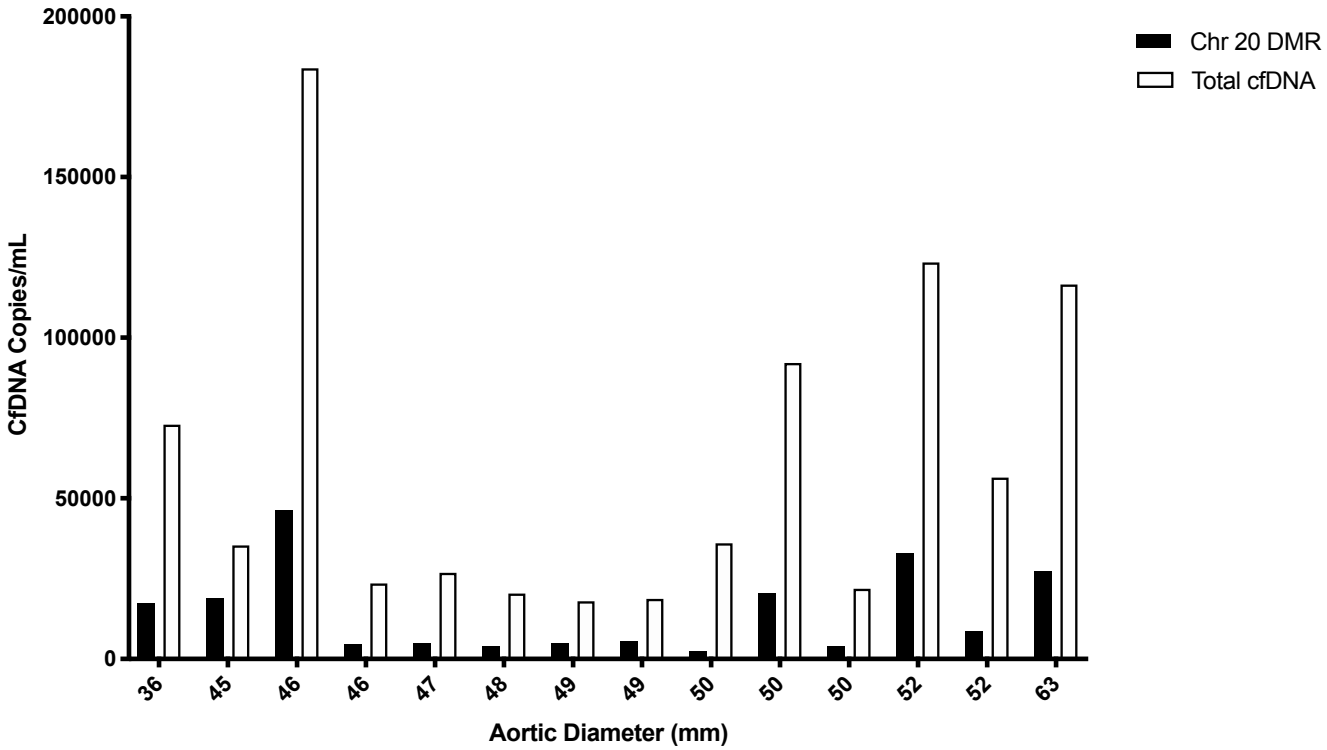

Figure 13. The concentration of the Chr 20 DMR and the total cfDNA plotted against the maximal aortic diameter of BAV patients. The concentration (copies/mL) of all cfDNA within the plasma of BAV patients (n = 14) along with the concentration (copies/mL) of the DMR at Chr 20 arranged according to patient maximal aortic diameter.

3.4.6.4 Chr 22 DMR

The sequencing of amplicons from BAV patients (n = 23) resulted in an average unmethylation perecentage of 54.4% with a range of 16.9% – 71.6% (Table 9). This unmethylation percentage indicated the percent of Chr 22 DMR present in the total cfDNA in each sample. The concentration of the Chr 22 DMR for all BAV patients ranged from 6063 – 136630 copies/mL with a mean of 39266 copies/mL and a median of 31845 copies/mL. The cfDNA levels did not correlate with the maximal aoritc diameter for BAV patients (Figure 14).

Table 9: Methylation levels and cfDNA levles for each BAV patient sample for Chr 22 DMR
The overall methylation percent and the overall unmethylation percent within the DMR in cfDNA extracted from the plasma of each BAV patient by maximum aortic diameter.

Patient	Max. Aortic Diameter (mm)	Overall Methylation (%)	Overall Unmethylation (%)	Chr 22 DMR (copies/mL)	Total cfDNA (copies/mL)
1016	36	43.4	56.6	41258	72930
1092	41	50.0	50.0	31845	63690
1075	43	42.4	57.6	37047	64350
1173	43	39.7	60.3	74206	123090
7	43	43.9	56.1	9412	16764
1127	44	43.6	56.4	14283	25311
1178	45	46.7	53.3	136630	256410
2	45	45.7	54.3	19168	35310
1356	46	46.4	53.6	98470	183810
8	46	47.0	53.0	12453	23496
1142	47	28.4	71.6	60036	83820
3	47	42.7	57.3	15331	26763
1267	48	50.6	49.4	10037	20328
4	49	44.3	55.7	9983	17919
6	49	46.6	53.4	9979	18678
1237	50	83.1	16.9	6063	35970
1279	50	38.1	61.9	56952	92070
5	50	45.1	54.9	11966	21813
1277	52	44.6	55.4	68410	123420
1	52	43.3	56.7	32004	56430
1006	63	40.7	59.3	69062	116490

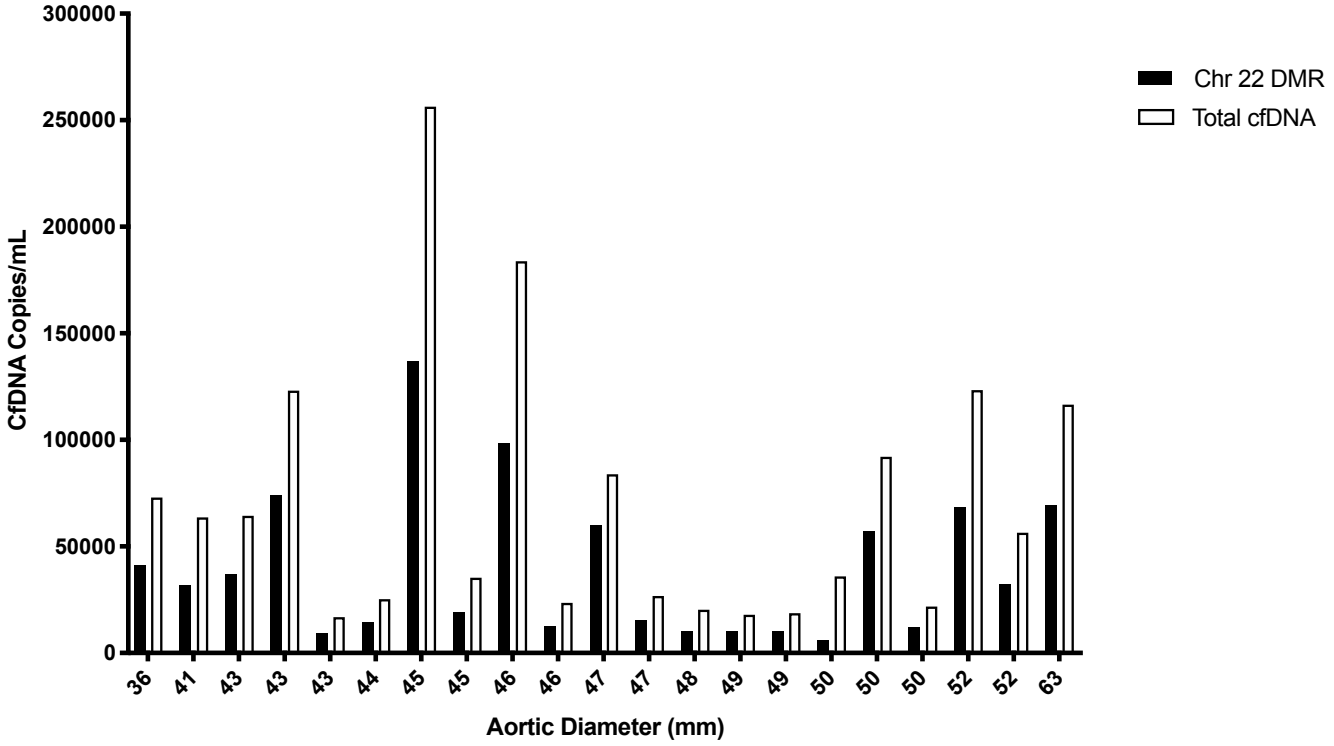

Figure 14. The concentration of the Chr 22 DMR and the total cfDNA plotted against the maximal aortic diameter of BAV patients. The concentration (copies/mL) of all cfDNA within the plasma of BAV patients (n = 23) along with the concentration (copies/mL) of the DMR at Chr 22 arranged according to patient maximal aortic diameter.

3.5 Discussion

DNA methylation plays a critical role in differentiation of a cell into a particular cell type due to its role in regulating gene expression. This allows for the DNA methylation pattern to act as a methylation 'fingerprint' for each tissue or organ with unique methylation patterns distinguishing between tissue types (101). Tissue-specific methylation patterns are conserved within a tissue type and, to a large degree, across individuals (101). This consistency was critical for the development of this universal minimally-invasive cfDNA-based assay using the limited number of publicly available methylomes (78). The use of all publicly available whole genome bisulfite-converted methylomes of tissues and hematopoietic cells within the human body and the software package Metilene allowed for an unbiased approach in the identification of potential aorta-specific DMRs. Metilene was chosen due to its ability to analyze the WGBS data, its sensitivity and accuracy for each methylated cytosine and lower computing time requirements (111).

For the comparison of the aortic methylome to the 19 non-aortic tissue methylomes, with a minimum mean methylation difference of 60%, 446 DMRs were identified, whereas for the comparison of the aortic methylome to the 14 methylomes of hematopoietic cells, with a minimum mean methylation difference of 90%, 181 DMRs were identified. This suggests that the methylation patterns of the hematopoietic cells were very similar as a group and more epigenetically different than the aorta compared to the non-aortic tissues which had more epigenetic variation as a cohort and had less epigenetic difference with the aorta. It should be noted that these comparisons were made separately due to the fact that the natural turnover of hematopoietic cells within the circulation accounted for a majority of the background noise when extracting cfDNA from the plasma of BAV patients. It should also be noted that there was only one publicly available methylome of the aorta that was used for DMR identification. This represents a potential limitation in the generalizability of the DMRs generated and also the specificity of the DMRs for the aorta. As more methylomes are generated for the aorta, non-

aortic tissues and hematopoietic cells, they can be added to the DMR identification pipeline to produce potentially more robust aorta-specific DMRs.

From the 24 aorta-specific DMRs identified, 10 were selected for further interrogation based upon having the greatest mean methylation differences, a varied number of CpG sites and a range of DMR lengths (Table 3). These criteria ensured that there was room for optimization of the DMR characteristics for amplification from cfDNA. Next, the DMR primers were synthesized for DMR amplification and optimization. From the 10 DMRs tested, four DMRs were selected for further analysis; they were located on Chr 11, Chr 18, Chr 20 and Chr 22. This selection was based on appropriate target amplification with minimal off-target amplification in both control genomic DNA and control cfDNA extracted from the plasma of heart transplant recipients. Based on *in silico* predictions, these DMRs were expected to have at least 70% difference in methylation levels between the aortic DNA compared to the non-aortic DNA. Since this was an *in silico* prediction, we then tested the DMRs *in vitro* against a tissue panel of genomic DNA of non-aortic tissues with the genomic DNA of the aorta.

The methylation differences between the aorta and the tissue panel were not the same as the *in silico* prediction. The observed *in vitro* methylation difference between the aorta and the tissue panel for Chr 11 DMR was 57%, for Chr 18 DMR was 60%, for Chr 20 was 80% and for Chr 22 was 53%. For Chr 11, 18 and 22, the *in silico* mean methylation difference was more optimistic than the *in vitro* methylation differences (Figure 10). This tissue panel testing depicted a lower specificity of the candidate DMRs to the aorta than originally predicted.

The candidate DMRs were also evaluated using cfDNA obtained from patients with severe BAV aortopathy undergoing aortic surgery. Based on the methylation levels of the DMRs, levels of cfDNA derived from the aorta were determined. The levels of aorta-specific cfDNA (as based on each DMR) were compared to the total cfDNA present in plasma obtained from BAV patients and were correlated with the maximal aortic diameter of these patients. There was no significant correlation between the levels of aorta-specific cfDNA and the maximal aortic diameter of BAV patients for all four candidate

DMRs (Figure 11 – 14). However, the maximal aortic diameter may not be a sufficient marker for the degree of aortopathy to verify the DMRs as a biomarker. Studies have shown that aortic dimensions (absolute diameter and rate of progression) obtained using conventional imaging techniques may be insufficient for assessing BAV aortopathy and estimating the underlying risk for aortic rupture (6, 49-51). Furthermore, although all of these BAV patients had been selected to undergo aortic surgery and thus all had severe, end-stage aortopathy, many of them have a maximal diameter lower than 45 mm which is a suggested threshold for surgery as per published guidelines. These patients may also represent those individuals with longstanding or burnt out disease with little ongoing apoptosis and therefore little cfDNA arising from the aorta specifically in the circulation. Thus, maximal diameter was not an indicator of the severity of aortopathy for these patients and we needed to consider other histological markers of aortic integrity for DMR verification. These findings are presented in the next chapter.

3.6 Conclusions

A novel bioinformatics pipeline has been established for the identification of organ-specific DMRs for the non-invasive detection of tissue injury. We used this pipeline and publicly-available data for the identification of aorta-specific DMRs. More specifically, we introduced the potential use of aorta-specific DMRs as a non-invasive biomarker for the identification and quantification of cfDNA derived from the aorta in the circulation due to cellular processes and hemodynamic forces. The four DMRs specific to the aorta that were identified *in silico* as being the most promising biomarkers were on Chr 11, Chr 18, Chr 20 and Chr 22. A tissue panel for evaluating DMRs testing has also been established for *in vitro* verification. We noted that the *in silico* methylation predictions for the DMRs differed from *in vitro* values and this may be due to the low number of publicly available aorta methylomes (n=1) for the initial DMR identification which may have resulted in low generalizability and specificity. Finally, the DMR-based aorta-specific cfDNA levels from BAV patients did not

correlate with maximal aortic diameter but further correlation with histological markers may provide better correlation for our biomarkers with the severity of aortopathy. Having a greater number of methylomes for DMR identification and a more comprehensive tissue panel for *in vitro* DMR validation (i.e. including genomic DNA from peripheral blood mononuclear cells) would potentially allow for the selection of DMRs that are more generalizable for all BAV patients and more specific to the aortic tissue.

CHAPTER FOUR: CORRELATION OF AORTA-SPECIFIC DIFFERENTIALLY-METHYLATED REGIONS IN CELL-FREE DNA FROM BAV PATIENTS WITH MARKERS OF AORTA INTEGRITY

4.1 Introduction

As the severity of aortopathy increases, the levels of aorta-specific cfDNA levels are expected to rise. In this chapter, our DMR-based biomarkers will be correlated with the levels of cell death of aortic smooth muscle cells, elastin degradation and ECM protein levels.

A key assessment of the degree of aortopathy is elastin degradation and the dysregulation of ECM proteins. In areas of elevated aortic WSS, the elastin fragments are thinner, there is less total elastin and that there is greater distance between elastin fibers (25). A recent study showed BAV aortic aneurysmal regions having less elastin closer to the intima and adventitia layers of the aorta compared to controls. It also observed greater elastin compaction in the media of the aorta possibly due to elevated hemodynamic WSS (112). This degeneration and altered structural formation of elastin results in decreased elasticity of the aorta and compromises its structural integrity and contributes to the dysregulation of ECM proteins, notably MMP types 1, 2, 3, TIMP-1 and TGFß-1 (25). MMPs are zinc dependent endopeptidases that are secreted by vascular smooth muscle cells (113). These MMPs can be activated to degrade various extracellular proteins such as collagen, elastin, ECM glycoprotein, and proteoglycans and can affect vascular smooth muscle cells migration and proliferation (29). This degradation leads to dilation of the aorta. Additionally, lowering levels of TIMPs, which inhibit the MMPs, leads to greater MMP activity (113). Lastly, the TGFß pathway has been intensely studied with regards to its role in aneurysm formation (37, 40). It plays an active role in fibrosis, inflammation, cell proliferation and migration and ECM remodeling and is involved in the development of aortopathy in the Loeys-Dietz and Marfan syndromes (37). Thus, these markers indicate the presence of aortopathy in BAV patients and indicate the activity of cellular processes leading to BAV aortopathy and dilation.

In the study by Guzzardi et al., the impact of abnormal hemodynamics on ECM dysregulation and elastin degradation was explored (25). It was found that regions of elevated WSS showed greater medial elastin degradation compared to regions of normal WSS with significantly decreased total elastin, thinner fibers and elastin fibers that were farther apart. There was also increased expression of TGFβ-1, MMP types 1, 2, 3 and TIMP-1 in regions of elevated WSS. These findings showed that hemodynamics have an important part to play in the cellular and structural progression of aortopathy. Studies are still needed to validate the appropriate use of 4-D imaging or other biomarkers in assessing WSS as there is currently no reasonable and safe method to access and evaluate the ECM dysregulation in aortopathy (114). Additionally, changes in the ECM proteins and elastin degeneration do not predict aortic dilation and dissection but rather are markers of severe aortopathy.

Another key marker for assessing severity of aortopathy is the cell death of vascular smooth muscle cells in the aorta. In BAV patients, there is a significant plurifocal apoptosis of vascular smooth muscle cells compared to controls (115). This increased cell death may be linked to genetic factors such as mutations in *fibrillin-1* which lead to a detachment of vascular smooth muscle cells from the elastic laminae, resulting in accelerated cell death (116). Increased cell death can also result from structural alterations within the ECM itself due to hemodynamic stresses (117). This depletion of cells in the aorta allows for fibrotic tissue replacement that leads to increased tissue stiffness and increased susceptibility for aortic dissection.

With the increase in cell death due to cellular processes and mechanical stressors, there is theoretically an increase in aorta-specific cfDNA released into the circulation. Being able to quantify the aorta-specific cfDNA in the circulation could provide an alternative assessment of the severity of the aortic wall integrity, regardless of the underlying mechanism causing the increased cell death. As a biomarker, cfDNA represents a minimally-invasive technique to assess the integrity of the aortic wall that could be used concomitantly with imaging and current standards of practice to aid in surgical planning.

4.2 Hypothesis and Specific Aims for Chapter Four

The correlation of candidate aorta-specific DMRs with histological markers of aortopathy in BAV patients could reveal the utility and strength of our putative biomarkers. We hypothesized that aorta-specific cfDNA levels as determined by the candidate DMRs on Chrs 11, 18, 20 and 22 will correlate with the following histological markers of aortopathy as measured in elevated aortic WSS regions in BAV patients: levels of vascular smooth muscle cell death, elastin thickness and tissue expression of MMPs (types 1, 2, 3), TIMP-1 and TGFβ-1.

Specific Aims:

1) Correlate aorta-specific cfDNA levels with vascular smooth muscle cell death levels in regions of elevated WSS in the aorta of BAV patients as determined by TUNEL/DAPI colocalization.

2) Correlate aorta-specific cfDNA levels with elastin degradation as defined by elastin thickness in regions of elevated WSS in the aorta of BAV patients.

3) Correlate aorta-specific cfDNA levels with tissue expression of MMP types 1, 2, 3, TIMP-1 and TGFβ-1 in regions of increased WSS in the aorta of BAV patients.

4.3 Materials and Methods

4.3.1 Patient Data

There were 15 BAV patients whose aortic wall samples were obtained from the BAV study at the Bluhm Cardiovascular Institute of Northwestern University Feinberg School of Medicine in Chicago (Table 10). The data for each patient was obtained from the 2015 Guzzardi et al. paper published in J Am Coll Cardiol. from Dr. Fedak's lab. The following data was collected for each BAV patient: aortic wall regional WSS data, elastin thickness and concentration levels of MMP type 1, 2 and 3, TGFβ-1 and TIMP-1. This data was gathered to correlate the cfDNA levels of the BAV patients with their aortic histological parameters for DMR verification.

4.3.2 Correlation of DMRs with aortic markers

The statistical analysis was computed using GraphPad Prism 8.2.0. The levels of aorta-specific cfDNA as predicted by each candidate DMR was correlated with levels of cell death as assessed in chapter two, elastin thickness and concentration levels of MMP type 1, 2 and 3, TGFβ-1 and TIMP-1. Linear regression was calculated to determine the presence of correlation between variables and the coefficient of determination (R^2) was calculated. The Pearson correlation coefficient was calculated to assess the presence of a significant correlation.

Table 10. BAV Study Population Characteristics for Blood and Plasma Samples. Characteristics of BAV patients that were recruited at the the Bluhm Cardiovascular Institute of Northwestern University Feinberg School of Medicine in Chicago

Parameter	BAV Study Population (N = 15)
Age (Average years)	47.4 ±15.3
Male	13
Female	2
BAV Classification:	
Type 0, lateral	1
Type 1, RL	9
Type 2, RL/RN	3
Average Aortic Diameter (cm):	
Maximum Diameter	4.66 ±0.58
Diameter at Elevated WSS Region	4.59 ±0.65
Diameter at Normal WSS Region	4.63 ±0.60
Aortic Valve Function	
No AS, moderate/severe AR	5
Mild AS, moderate/severe AR	1
Moderate/severe AS, no AR	3
Moderate/severe AS, mild AR	
Moderate/severe AS, moderate/severe AR	3
Aortic Valve Surgical Procedure:	
Repair	3
Replacement	
AVR	8
Ross	4
Ascending Aorta Surgical Procedure:	
Ascending aorta replacement	12
Root replacement	2
Hemi-arch	1

Values are mean ± SD or n.

AR = aortic regurgitation; AS = aortic stenosis; AVR = aortic valve replacement; BAV = bicuspid aortic valve; RN = right coronary-non-coronary cusp fusion; RL = right-left coronary cusp fusion.

4.4 Results

4.4.1 Verification of Chr 11 DMR

Overall, the aorta-specific cfDNA levels as determined using the Chr 11 DMR only mildly positively correlated with the levels of cell death in the aortic tissue region with elevated WSS from 13 BAV patients and there was no correlation with elastin thickness or levels of the MMPs, TGFβ-1 and TIMP-1.

The cfDNA levels of the DMR at Chr 11 from BAV patients were positively correlated with their level of cell death present in their elevated aortic WSS region, as determined in chapter two from TUNEL/DAPI colocalization. There was a significant positive correlation with an R^2 value of 0.65 (Figure 15, P = 0.0026).

The cfDNA levels of the DMR at Chr 11 from BAV patients were correlated with elastin thickness in aortic tissue from their elevated WSS region. There was no correlation as the liner regression line had an R^2 value of 0.1806 (Figure 16).

The cfDNA levels of Chr 11 DMR of BAV patients were correlated with MMP types 1, 2 and 3, TIMP-1 and TGFβ-1 concentrations in aortic tissue from their elevated WSS region (Figure 17). There was no correlation with all MMPs as the liner regression line for MMP-1 had an R^2 value of 0.06447, for MMP-2 had an R^2 value of 0.04019 and for MMP-3 was had an R^2 value of 0.1269. The cfDNA levels of Chr 11 DMR of BAV patients was correlated with TIMP-1 concentrations from their elevated WSS region. There was no correlation as the linear regression line had an R^2 value of 0.1727. The cfDNA levels of Chr 11 DMR of BAV patients was correlated with TGFβ-1 concentrations from their elevated WSS region. There was low correlation as the liner regression line had an R^2 value of 0.0011.

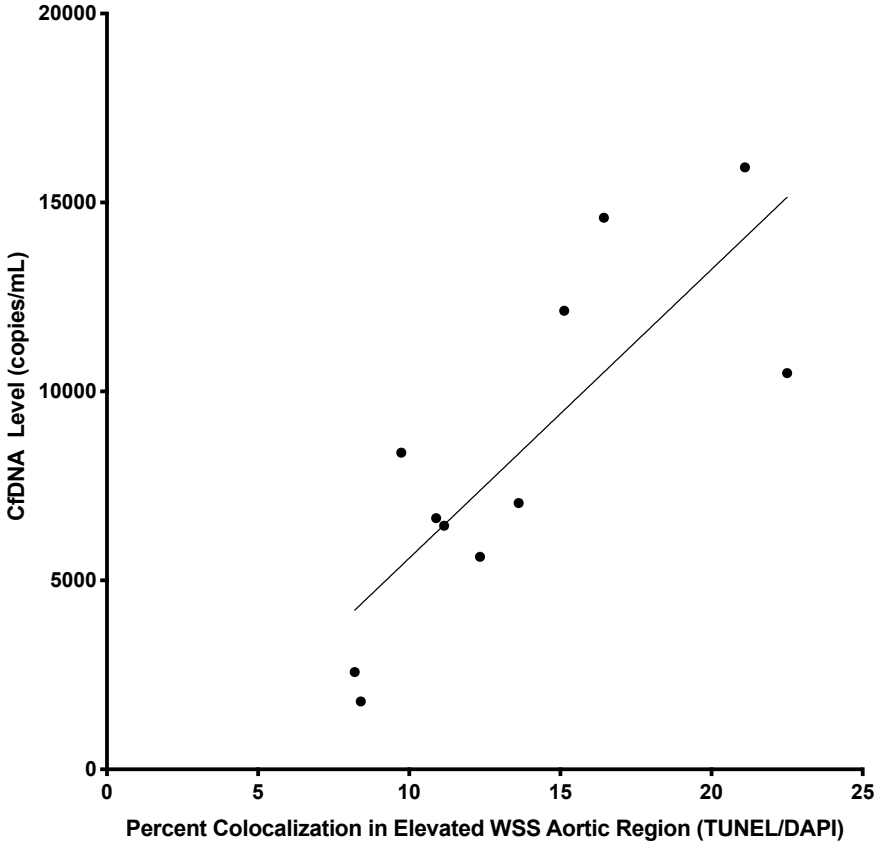

Figure 15. Chr 11 DMR cfDNA levels of BAV patients in correlation with percent cell death stained with TUNEL in elevated WSS aortic regions. The aorta-specific cfDNA levels in 12 BAV patients with severe aortopathy as determined by Chr 11 DMR in correlation with percent cell death in elevated aortic WSS regions determined by TUNEL/DAPI colocalized staining in chapter two. The linear regression line is $Y = 764X - 2052$ with an R^2 value of 0.6533. The correlation is significant with $p = 0.0026$ and Pearson $r = 0.8083$.

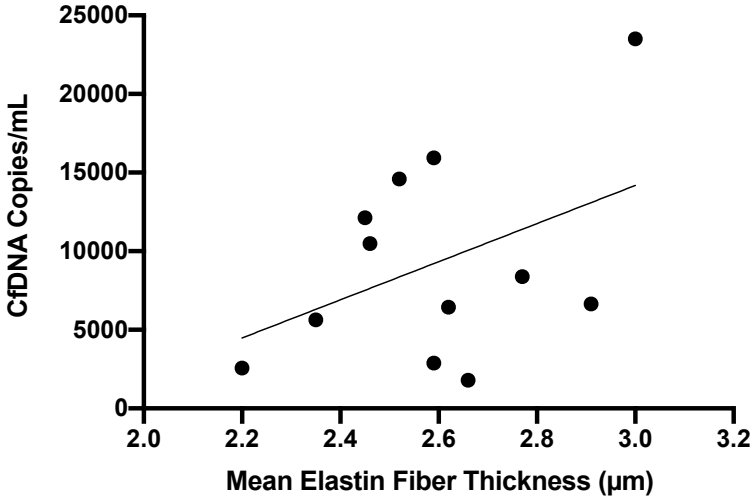

Figure 16. Chr 11 DMR cfDNA levels of BAV patients in correlation with mean elastin fiber thickness in elevated WSS aortic regions. The aorta-specific cfDNA levels in 12 BAV patients with severe aortopathy as determined by Chr 11 DMR in correlation with mean elastin fiber thickness in elevated aortic WSS regions determined by Verhoeff-Van Gieson staining and image analysis for the 2015 Guzzardi et al, study. The linear regression line is $Y = 12123X – 22190$ with an R^2 value of 0.1806.

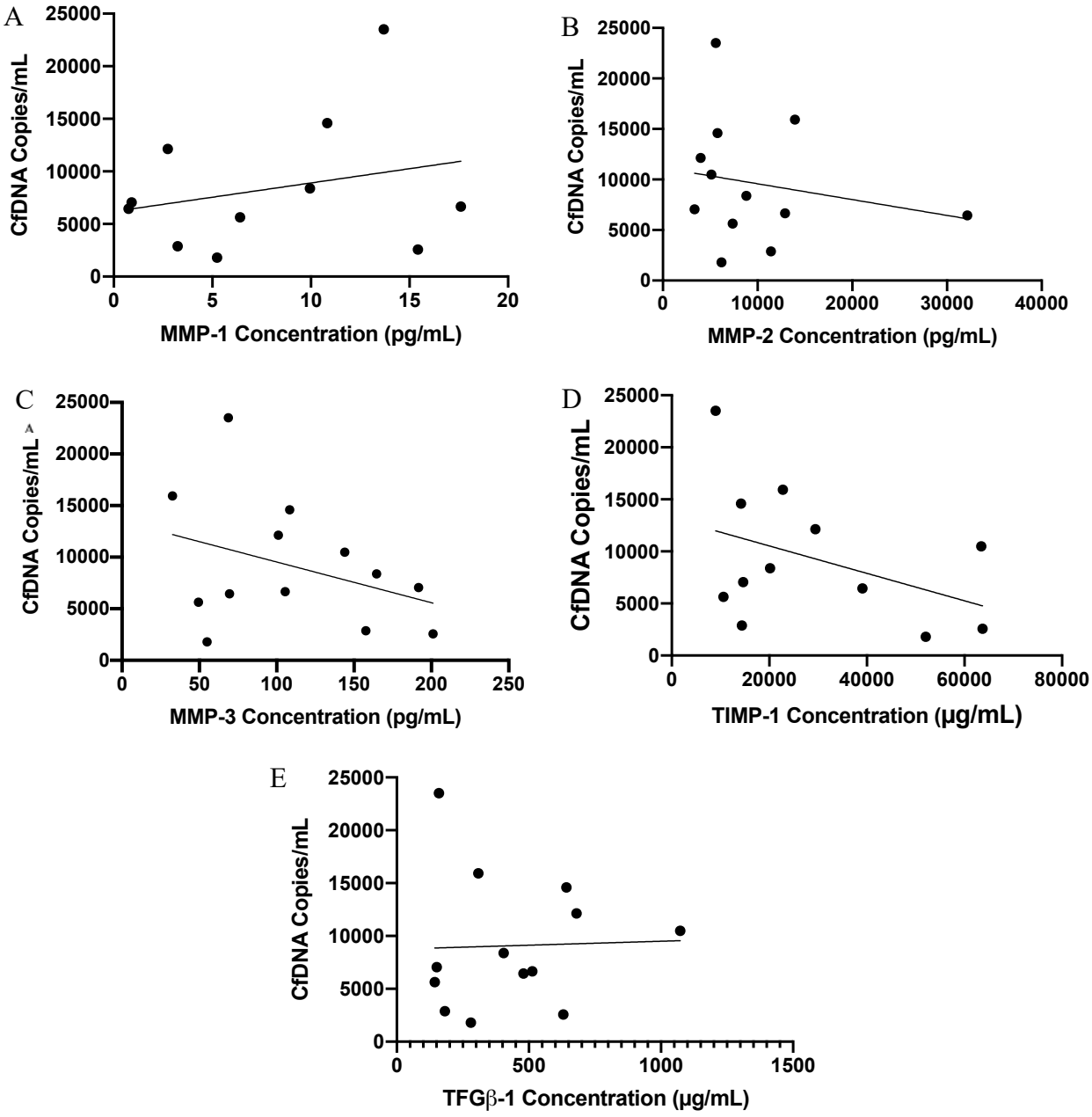

Figure 17. Chr 11 DMR cfDNA levels of BAV patients in correlation with ECM protein concentrations in elevated WSS aortic regions. A) The MMP-1 correlation had a linear regression line Y = 271.2X + 6191 with an R^2 value of 0.06447 (n = 11) B) The MMP-2 correlation with 12 BAV patients was Y = -0.1565X + 11144 with an R^2 value of 0.04019 (n = 12) C) The MMP-3 correlation had a linear regression Y = 39.48X + 13481 with an R^2 value of 0.1269 (n = 13) D) The TIMP-1 correlation had a linear regression Y = -0.1317X – 13163 with an R^2 value of 0.1727 (n = 12) E) The TGFβ-1 correlation had a liner regression line Y = 0.7472X + 8756 with an R^2 value of 0.0011.

4.4.2 Verification of Chr 18 DMR

Overall, the aorta-specific cfDNA levels as determined using the Chr 18 DMR only mildly positively correlated with the levels of cell death in the aortic tissue region with elevated WSS from 8 BAV patients and there was no correlation with elastin thickness or levels of the MMPs, TGFβ-1 and TIMP-1.

The cfDNA levels of the DMR at Chr 18 from BAV patients were positively correlated with their level of cell death present in their elevated aortic WSS region, as determined in chapter two from TUNEL/DAPI colocalization. There was a significant positive correlation with an R^2 value of 0. 8293 (Figure 18, P = 0.0017).

The cfDNA levels of the DMR at Chr 18 from BAV patients were correlated with elastin thickness in aortic tissue from their elevated WSS region. There was no correlation as the liner regression line had an R^2 value of 0. 2653 (Figure 19).

The cfDNA levels of Chr 18 DMR of BAV patients were correlated with MMP types 1, 2 and 3 concentrations in aortic tissue from their elevated WSS region (Figure 20). There was no correlation with all MMPs as the liner regression line for MMP-1 had an R^2 value of 0.1068, for MMP-2 was had an R^2 value of 0.1546 and for MMP-3 had an R^2 value of 0.001097. The cfDNA levels of Chr 18 DMR of BAV patients was correlated with TIMP-1 concentrations from their elevated WSS region. There was no correlation as the liner regression line had an R^2 value of 0.1263. The cfDNA levels of Chr 18 DMR of BAV patients was correlated with TGFβ-1 concentrations from their elevated WSS region. There was no correlation as the liner regression line had an R^2 value of 0.03398.

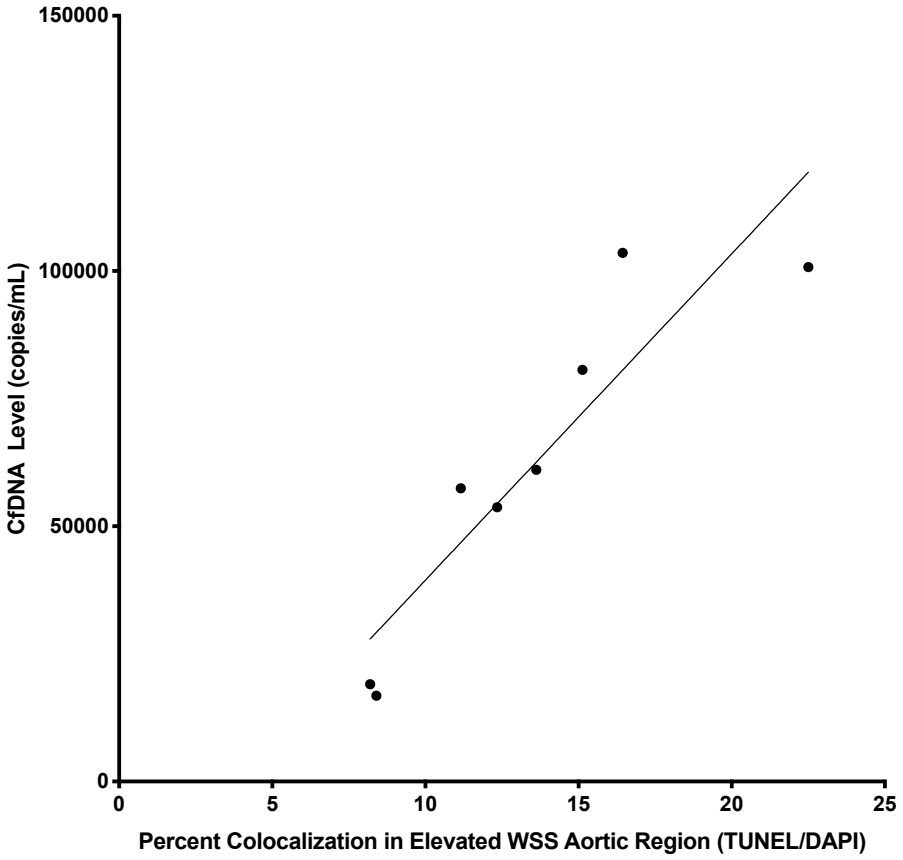

Figure 18. Chr 18 DMR cfDNA levels of BAV patients in correlation with percent cell death stained with TUNEL in elevated WSS aortic regions. The aorta-specific cfDNA levels in 8 BAV patients with severe aortopathy as determined by Chr 18 DMR in positive correlation with percent cell death in elevated aortic WSS regions determined by TUNEL/DAPI colocalized staining in chapter two. The linear regression line is $Y = 6393X - 24497$ with an R^2 value of 0.8293. The correlation is significant with $p = 0.0017$ and Pearson $r = 0.9106$.

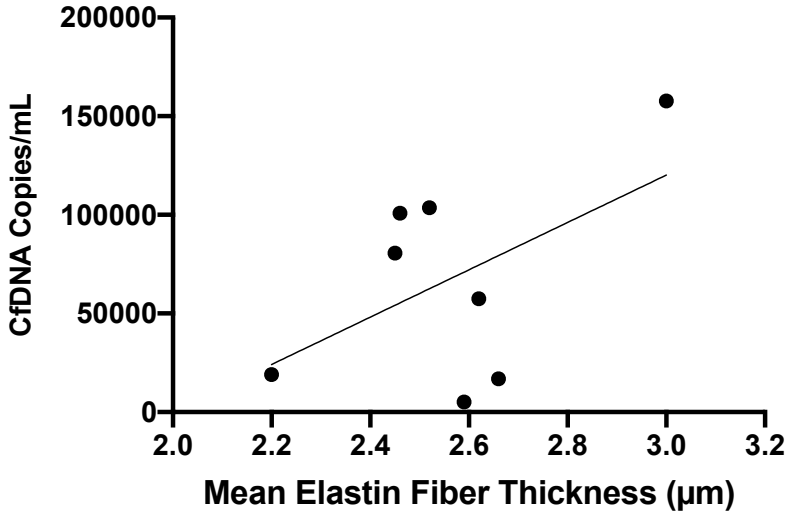

Figure 19. Chr 18 DMR cfDNA levels of BAV patients in correlation with mean elastin fiber thickness in elevated WSS aortic regions. The aorta-specific cfDNA levels in 8 BAV patients with severe aortopathy as determined by Chr 18 DMR in positive correlation with mean elastin fiber thickness in elevated aortic WSS regions determined by Verhoeff-Van Gieson staining and image analysis for the 2015 Guzzardi et al, study. The linear regression line is Y = 120018X - 239914 with an R^2 value of 0.2653.

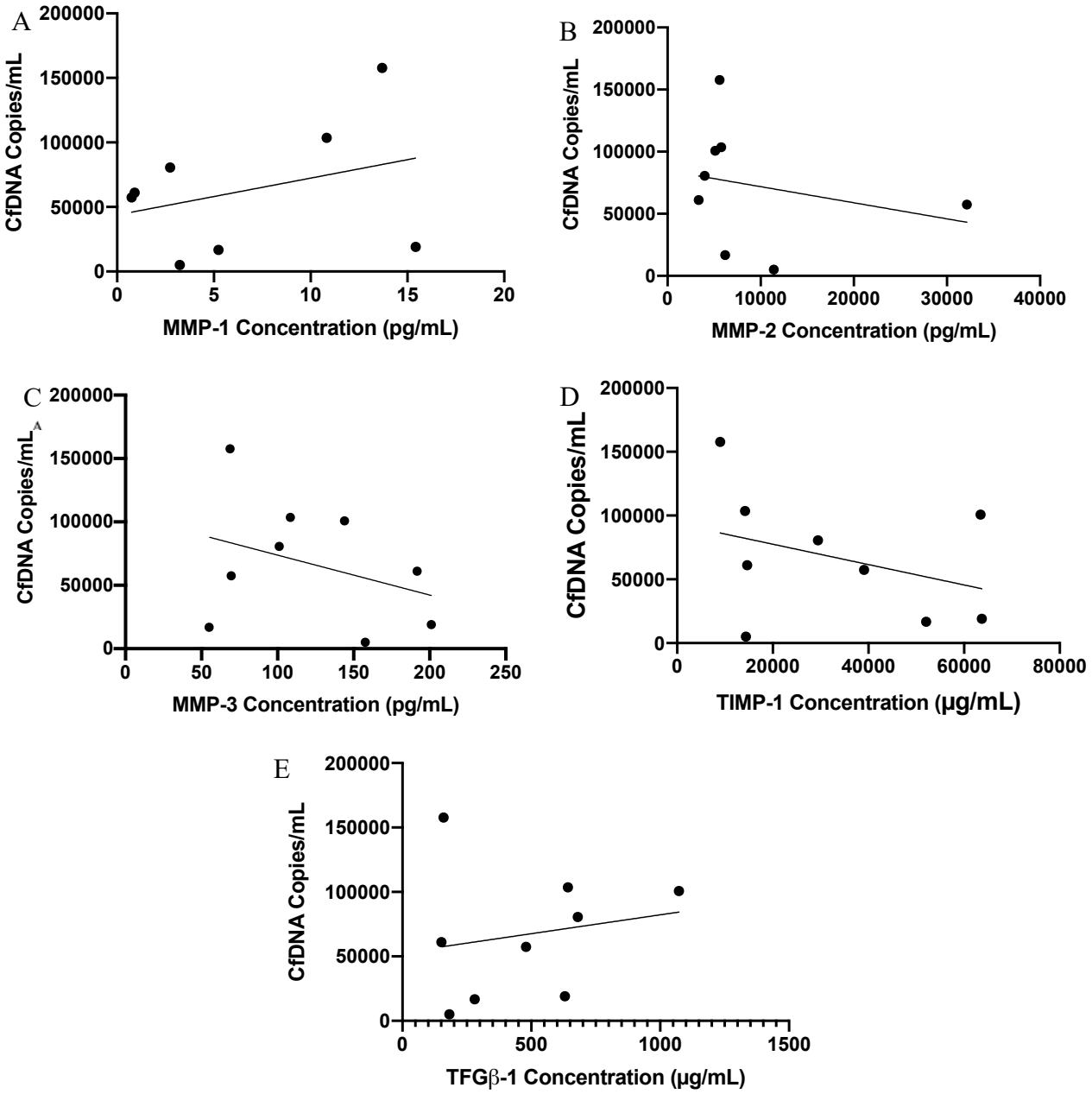

Figure 20. Chr 18 DMR cfDNA levels of BAV patients in correlation with ECM protein concentrations in elevated WSS aortic regions. There was no strong correlation between aorta-specific cfDNA levels of BAV patients with severe aortopathy as determined by Chr 18 DMR and the concentrations of MMP type 1, 2 and 3, TGFβ-1 and TIMP-1 in elevated aortic WSS regions determined by protein quantification for the 2015 Guzzardi et al, study. A) The MMP-1 correlation had a linear regression line Y = 2854X + 43827 with an R^2 value of 0.1068 (n = 8) B) The MMP-2 correlation with 12 BAV patients was Y = -0.3271X + 76335 with an R^2 value of 0.1546 (n = 8) C) The MMP-3 correlation had a linear regression Y = -30.65X + 49735 with an R^2 value of 0.001097 (n = 8) D) The TIMP-1 correlation had a linear regression Y = -0.7985X + 93518 with an R^2 value of 0.1263 (n = 9) E) The TGFβ-1 correlation had a liner regression line Y = 29.28X + 52985 with an R^2 value of 0.03398.

4.4.3 Verification of Chr 20 DMR

Overall, the aorta-specific cfDNA levels as determined using the Chr 20 DMR only mildly positively correlated with the levels of cell death in the aortic tissue region with elevated WSS from 8 BAV patients and there was no correlation with elastin thickness or levels of the MMPs, TGFβ-1 and TIMP-1.

The cfDNA levels of the DMR at Chr 20 from BAV patients were correlated with their level of cell death present in their elevated aortic WSS region, as determined in chapter two from TUNEL/DAPI colocalization. There was a mild correlation (not significant) as the liner regression line was had an R^2 value of 0.6265 (Figure 21, P = 0.0607).

The cfDNA levels of the DMR Chr 20 from BAV patients were correlated with elastin thickness in aortic tissue from their elevated WSS region. There was no correlation as the liner regression line had an R^2 value of 0.2256 (Figure 22).

The cfDNA levels of Chr 20 DMR of BAV patients were correlated with MMP types 1, 2 and 3 concentrations in aortic tissue from their elevated WSS region (Figure 23). There was no correlation with all MMPs as the liner regression line for MMP-1 had an R^2 value of 0.2699, for MMP-2 had an R^2 value of 0.002154 and for MMP-3 had an R^2 value of 0.06493. The cfDNA levels of Chr 20 DMR of BAV patients was correlated with TIMP-1 concentrations from their elevated WSS region. There was no correlation as the liner regression line had an R^2 value of 0.0001787. The cfDNA levels of Chr 20 DMR of BAV patients was correlated with TGFβ-1 concentrations from their elevated WSS region. There was low correlation as the liner regression line had with an R^2 value of 0.1530.

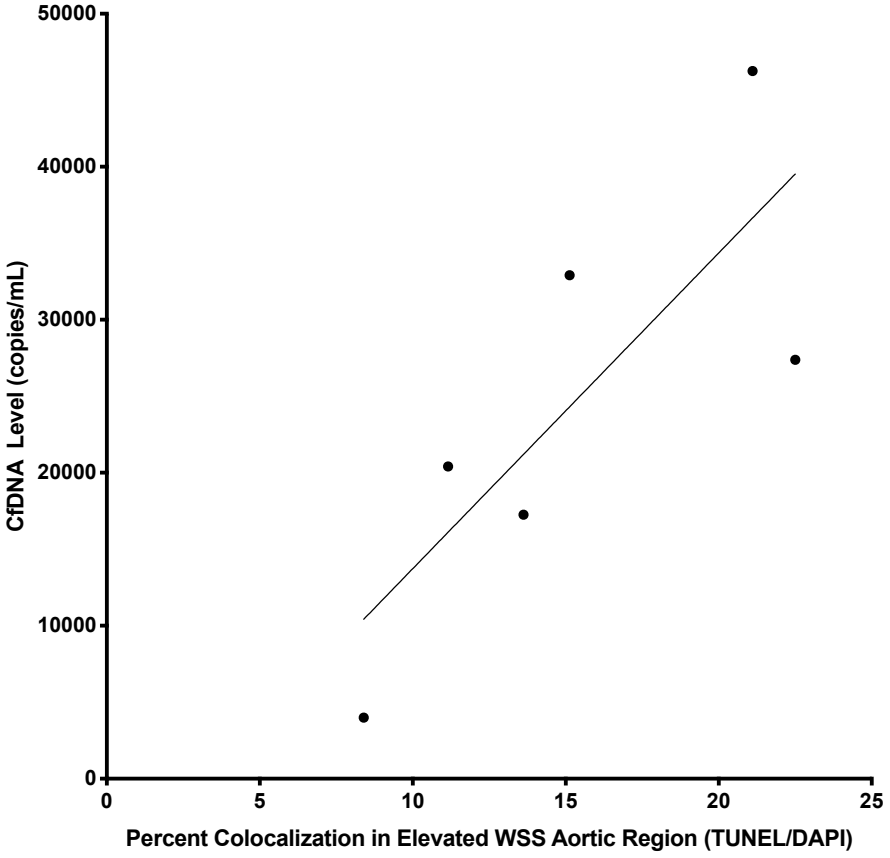

Figure 21. Chr 20 DMR cfDNA levels of BAV patients in correlation with percent cell death stained with TUNEL in elevated WSS aortic regions. The aorta-specific cfDNA levels in 6 BAV patients with severe aortopathy as determined by Chr 20 DMR in correlation with percent cell death in elevated aortic WSS regions determined by TUNEL/DAPI colocalized staining in chapter two. The linear regression line is $Y = 2064X - 6911$ with an R^2 value of 0.6265. The correlation is not significant with $p = 0.0607$ and Pearson $r = 0.9715$.

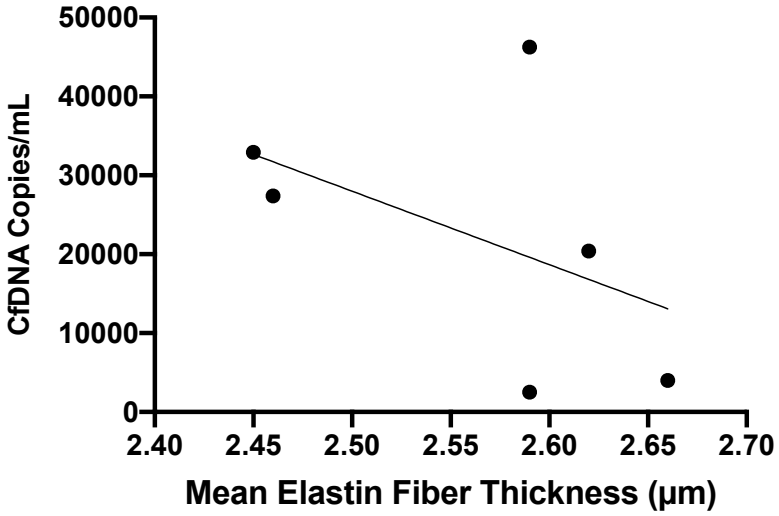

Figure 22. Chr 20 DMR cfDNA levels of BAV patients in correlation with mean elastin fiber thickness in elevated WSS aortic regions. The aorta-specific cfDNA levels in 6 BAV patients with severe aortopathy as determined by Chr 20 DMR in correlation with mean elastin fiber thickness in elevated aortic WSS regions determined by Verhoeff-Van Gieson staining and image analysis for the 2015 Guzzardi et al, study. The linear regression line is $Y = -93179X + 260939$ with an R^2 value of 0.2256.

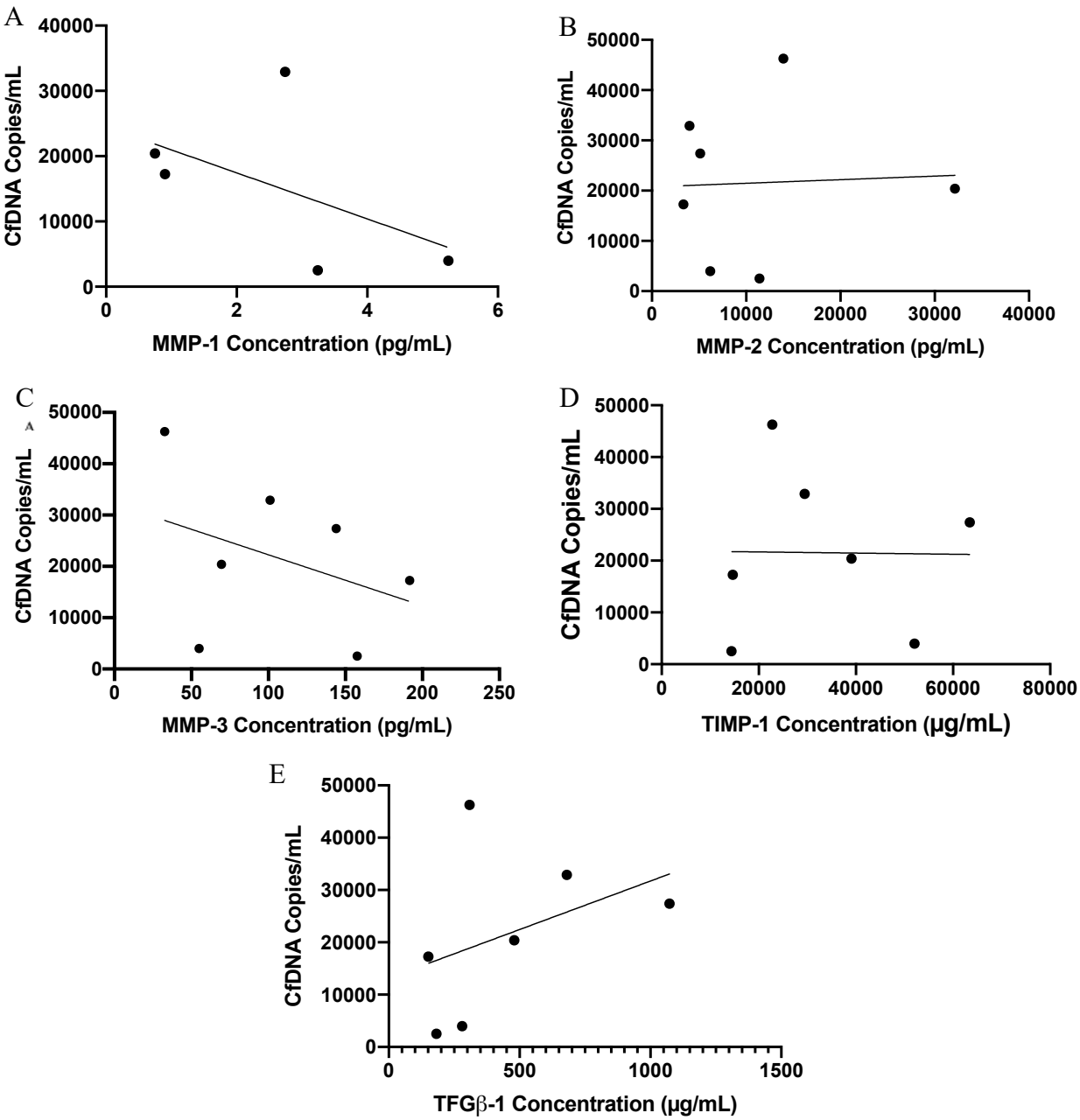

Figure 23. Chr 20 DMR cfDNA levels of BAV patients in correlation with ECM protein concentrations in elevated WSS aortic regions. There was no strong correlation between aorta-specific cfDNA levels of BAV patients with severe aortopathy as determined by Chr 20 DMR and the concentrations of MMP type 1, 2 and 3, TGFβ-1 and TIMP-1 in elevated aortic WSS regions determined by protein quantification for the 2015 Guzzardi et al, study. A) The MMP-1 correlation had a linear regression line Y = -3525X + 24493 with an R^2 value of 0.2699 (n = 5) B) The MMP-2 correlation with 12 BAV patients was Y = 0.07126X + 20758 with an R^2 value of 0.002154 (n = 7) C) The MMP-3 correlation had a linear regression Y = -71.66X + 19583 with an R^2 value of 0.06493 (n = 7) D) The TIMP-1 correlation had a linear regression Y = -0.01110X + 21907 with an R^2 value of 0.0001787 (n = 7) E) The TGFβ-1 correlation had a liner regression line Y = 18.54X + 13174 with an R^2 value of 0.1530.

4.4.4 Verification of Chr 22 DMR

Overall, the aorta-specific cfDNA levels as determined using the Chr 22 DMR only mildly positively correlated with the levels of cell death in the aortic tissue region with elevated WSS from 6 BAV patients and there was no correlation with elastin thickness or levels of the MMPs, TGFβ-1 and TIMP-1.

The cfDNA levels of the DMR at Chr 22 from BAV patients were correlated with their level of cell death present in their elevated aortic WSS region, as determined in chapter two from TUNEL/DAPI colocalization. There was a significant positive correlation as the liner regression line had an R^2 value of 0.6374 (Figure 24, P = 0.0032).

The cfDNA levels of the DMR at Chr 22 from BAV patients were positively correlated with elastin thickness in aortic tissue from their elevated WSS region. There was no correlation as the liner regression line had an R^2 value of 0.1931 (Figure 25).

The cfDNA levels of Chr 22 DMR of BAV patients were correlated with MMP types 1, 2 and 3 concentrations in aortic tissue from their elevated WSS region (Figure 26). There was no correlation with all MMPs as the liner regression line for MMP-1 had an R^2 value of 0.04143, for MMP-2 had an R^2 value of 0.1075 and for MMP-3 had an R^2 value of 0.1435. The cfDNA levels of Chr 22 DMR of BAV patients was correlated with TIMP-1 concentrations from their elevated WSS region. There was no correlation as the liner regression line had an R^2 value of 0.1104. The cfDNA levels of Chr 20 DMR of BAV patients was correlated with TGFβ-1 concentrations from their elevated WSS region. There was low correlation as the liner regression line had an R^2 value of 0.005245.

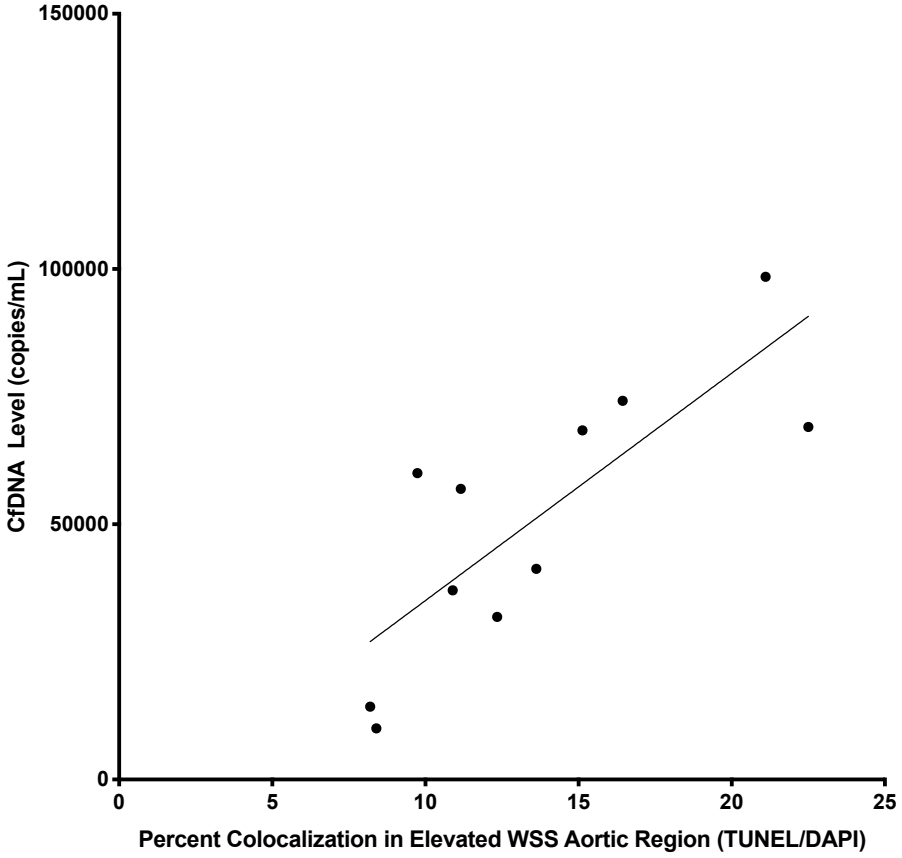

Figure 24. Chr 22 DMR cfDNA levels of BAV patients in correlation with percent cell death stained with TUNEL in elevated WSS aortic regions. The aorta-specific cfDNA levels in 11 BAV patients with severe aortopathy as determined by Chr 22 DMR in correlation with percent cell death in elevated aortic WSS regions determined by TUNEL/DAPI colocalized staining in chapter two. The linear regression line is $Y = 4454X - 9489$ with an R^2 value of 0.6374. The correlation is significant with $p = 0.0026$ and Pearson $r = 0.8083$. The correlation is significant with $p = 0.0032$ and Pearson $r = 0.7984$.

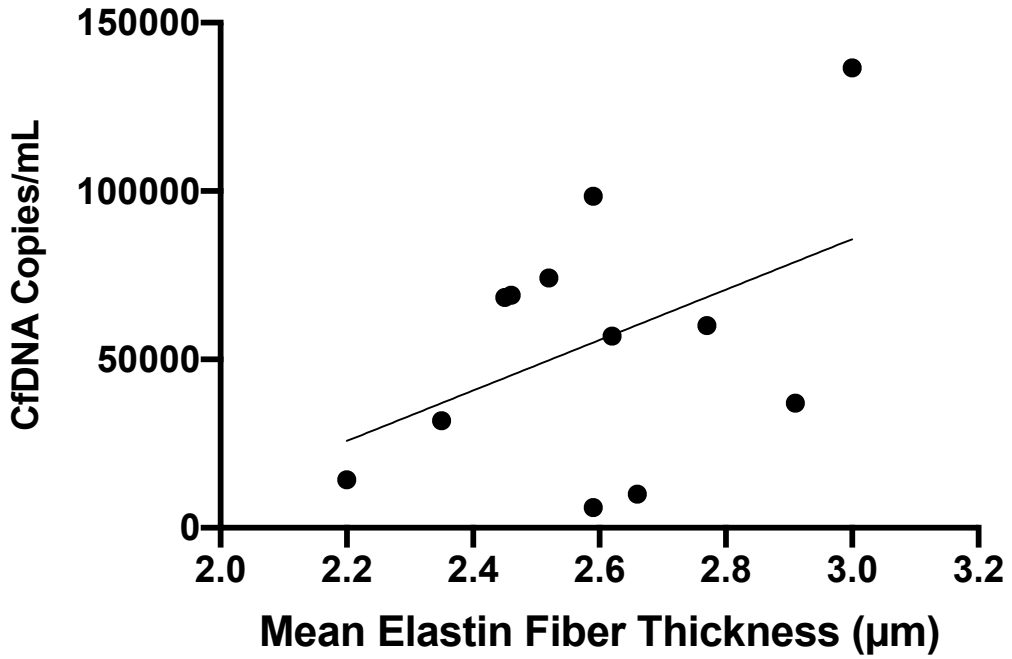

Figure 25. Chr 22 DMR cfDNA levels of BAV patients in correlation with mean elastin fiber thickness in elevated WSS aortic regions. The aorta-specific cfDNA levels in 12 BAV patients with severe aortopathy as determined by Chr 22 DMR in correlation with mean elastin fiber thickness in elevated aortic WSS regions determined by Verhoeff-Van Gieson staining and image analysis for the 2015 Guzzardi et al, study. The linear regression line is Y = 74898X – 138982 with an R^2 value of 0.1931.

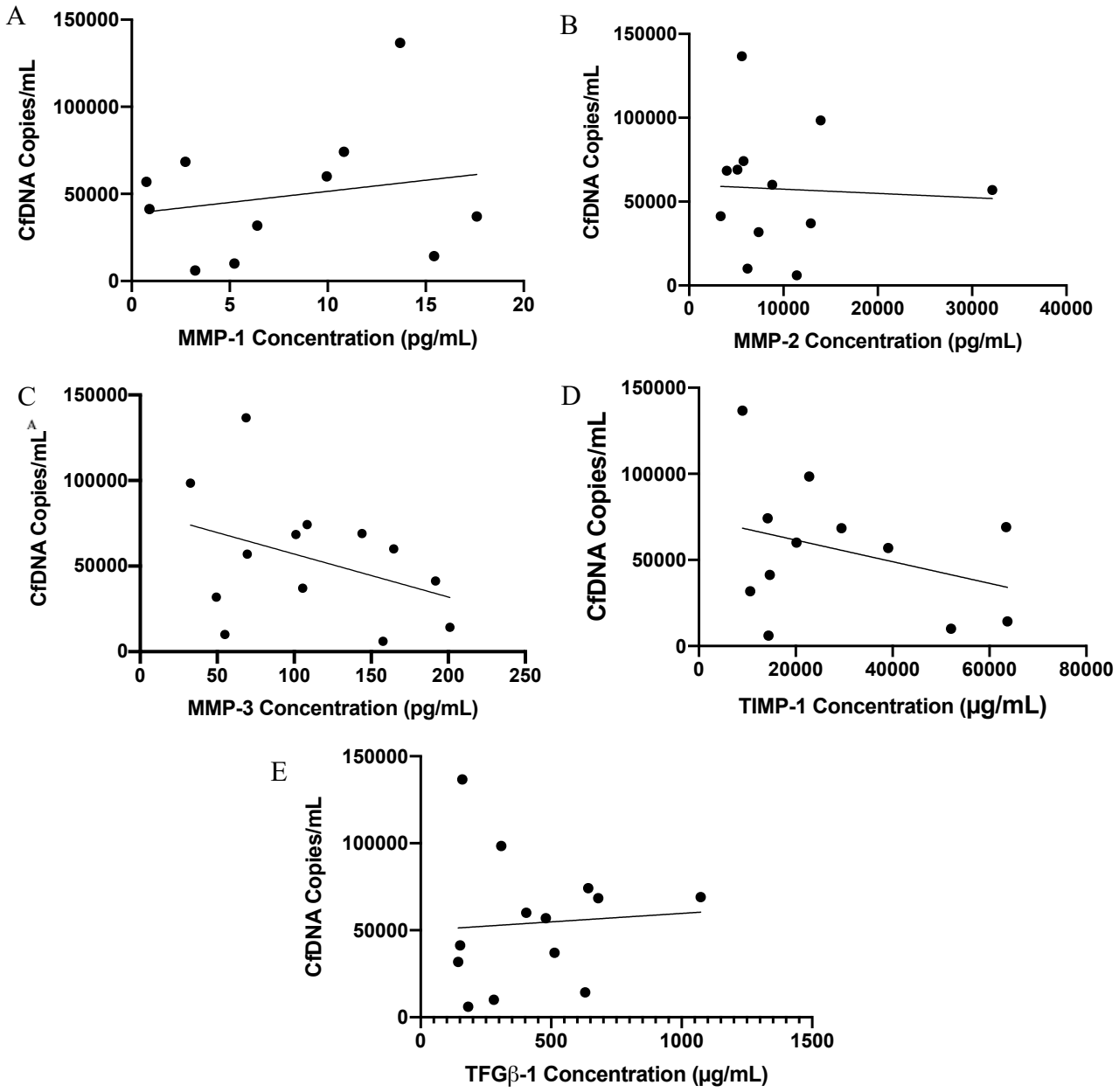

Figure 26. Chr 22 DMR cfDNA levels of BAV patients in correlation with ECM protein concentrations in elevated WSS aortic regions. There was no strong correlation between aorta-specific cfDNA levels of BAV patients with severe aortopathy as determined by Chr 22 DMR and the concentrations of MMP type 1, 2 and 3, TGFβ-1 and TIMP-1 in elevated aortic WSS regions determined by protein quantification for the 2015 Guzzardi et al, study. A) The MMP-1 correlation had a linear regression line Y = 1275X + 38734 with an R^2 value of 0.04143 (n = 11) B) The MMP-2 correlation with 12 BAV patients was Y = -0.2455X + 59889 with an R^2 value of 0.1075 (n = 12) C) The MMP-3 correlation had a linear regression Y = -251.0X + 82157 with an R^2 value of 0.1435 (n = 12) D) The TIMP-1 correlation had a linear regression Y = -0.6279X + 74100 with an R^2 value of 0.1104 (n = 12) E) The TGFβ-1 correlation had a liner regression line Y = 9.779X + 49928 with an R^2 value of 0.005245 (n = 13).

4.5 Discussion

In order to assess our candidate biomarkers, the levels of DMR-specific cfDNA in the plasma from BAV patients were correlated with histological markers of their aortopathy. For all DMRs on Chr 11, 18 and 22, there was a significant correlation between their cfDNA levels of the DMRs from BAV patients and the levels of cell death in their elevated aortic WSS regions. The correlation for Chr 11 DMR had an $R^2 = 0.653$ ($p = 0.0023$), Chr 18 had an $R^2 = 0.829$ ($p = 0.0017$), Chr 20 DMR had an $R^2 = 0.627$ ($p = 0.0607$) and Chr 22 DMR had an $R^2 = 0.637$ ($p = 0.0032$). This indicates that the levels of cell death in the aorta correlate with the levels of cfDNA in their plasma and this increased level of aorta-specific DNA is what is being identified with the DMRs. This is promising as this provides a rationale for cfDNA as a biomarker for aortic vascular smooth muscle cell death. However, these preliminary findings need to be replicated in another cohort of patients. Patients with BAV-associated aortopathy are currently being recruited in Calgary and could be enrolled as a validation cohort for our novel biomarkers.

Our candidate DMRs showed no significant correlation with multiple histological markers associated with the elastin degradation and dysregulation of ECM proteins known to occur in aortopathy. For all candidate DMRs, we attempted to correlate the levels of cfDNA for the aorta-specific DMRs with histological markers of the patients' elevated aortic WSS region. Unfortunately, the DMR cfDNA levels of BAV patients did not show a significant correlation with elastin thickness and the concentrations of MMP type 1, 2 and 3, TGFβ-1 and TIMP-1 as each had an $R^2 < 0.27$ for its linear regression line. Thus, all of the DMRs tested were not obviously associated with the molecular changes underlying aortopathy. This is potentially related to apoptosis and the release of cfDNA being end-stage markers of aortopathy.

Another potential concern is that active vascular smooth muscle cell death may not be in complete correlation with all of the histological markers tested. Some BAV patients with highly fibrous aortic tissue may have already depleted many of its vascular smooth muscle cells and show severe

aortopathy with degraded elastin and dysregulated ECM proteins; but since the vascular smooth muscle cells have already been depleted and there is minimal active cell death, the aorta-specific cfDNA levels would be quite low and not be indicative of severe aortopathy.

4.6 Conclusions

The verification of DMRs on Chr 11, 18, 20 and 22 with histological markers of BAV aortopathy revealed significant correlation of DMRs on Chr 11, 18 and 22 with percent cell death in the elevated aortic WSS regions of BAV patients but no strong correlations with ECM protein concentrations including: elastin thickness and concentration levels of MMP type 1, 2 and 3, TGFβ-1 and TIMP-1. The correlation of cfDNA with histological markers revealed that the candidate DMRs were not specific enough to the aorta to function as an aortopathy marker but it created a strong framework for testing new DMRs with greater specificity for the aorta.

CHAPTER FIVE: SUMMARY

5.1 Conclusions

The current guidelines for surgical intervention for BAV aortopathy patients are based on aortic diameter which is not sufficient to address the aortic integrity. The abnormal hemodynamic flow through the aorta has been linked to regions of elevated WSS and the progression of aortopathy. Using TUNEL staining, we were able to compare the mean percentage of apoptotic or necrotic cells between aortic regions of elevated WSS and normal WSS in BAV patients. We found that the elevated WSS regions had significantly higher levels of cell death than the normal WSS regions for the same patients. This led us to believe that the hemodynamic forces do play a role in cell death and that this continuous hemodynamic force provided the rationale for the release of cfDNA from the aorta.

We leveraged this release of cfDNA from the aorta to serve as a minimally invasive biomarker for aortopathy. We established a pipeline for the identification for organ-specific DMRs to quantify the level of cell death based on the methylation levels of cfDNA in the circulation. We tested four identified DMRs on Chr 11, Chr 18, Chr 20 and Chr 22 with BAV patient cfDNA samples to verify its use as a biomarker to indicate the severity of aortopathy. The aorta-specific cfDNA levels of the DMRs on Chr 11, Chr 18 and Chr 22 correlated significantly with levels of cell death in the elevated WSS regions of the aorta. The aorta-specific cfDNA levels did not show any correlation with elastin degradation and the concentrations of MMP type 1, 2 and 3, TGFβ-1 and TIMP-1. Even though these DMRs show some potential, more work needs to be done to identify DMRs with even greater specificity to the aorta and clear correlation with severity of aortopathy with larger patient and control cohorts.

4.2 Future Directions

For the identification of aorta-specific DMRs *in silico*, we can increase the number of methylomes of that were used and thus increase the specificity and generalizability of the DMRs identified. Another technique that can be utilized is randomly resampling sets of methylomes to compare with the aortic methylome as this will increase the statistical power of the identification process. For example, randomly selected 5 tissue methylomes from a pool can be compared to the aorta methylome through the Metilene process 50 times. The DMRs that are consistently identified amongst these several output files could represent an even more robust list of candidate DMRs for this novel assay. Additionally, since we used an unbiased approach by interrogating whole bisulfite-sequenced genomes of the tissues and hematopoietic cells, we could instead take a more targeted approach by utilizing methylation patterns of genes that are known to be unique to the aorta, and therefore, highly differentially methylated relative to other cells and tissues.

In terms of the validation of these DMRs *in vitro*, the methylation patterns at these regions must be compared between the aorta and hematopoietic cells in order to confidently ascertain the specificity of these DMRs to the aorta. This will ultimately improve our ability to identify and quantify the fraction of cfDNA that is truly derived from the aorta. Finally, the verification of the DMRs with BAV patient cfDNA can be done with a larger range of aortopathy severity and larger cohorts to determine if a true correlation exists. Highly severe aortopathy patient samples can serve as positive controls and individuals with healthy aortas can serve as negative controls which could further ascertain the specificity of the DMRs to the aorta.

References

1. Verma S, Siu SC. Aortic dilatation in patients with bicuspid aortic valve. N Engl J Med. 2014;370(20):1920-9.
2. Hoffman JI. Incidence of congenital heart disease: II. Prenatal incidence. Pediatr Cardiol. 1995;16(4):155-65.
3. Tutar E, Ekici F, Atalay S, Nacar N. The prevalence of bicuspid aortic valve in newborns by echocardiographic screening. Am Heart J. 2005;150(3):513-5.
4. Basso C, Boschello M, Perrone C, Mecenero A, Cera A, Bicego D, et al. An echocardiographic survey of primary school children for bicuspid aortic valve. Am J Cardiol. 2004;93(5):661-3.
5. Sievers HH, Schmidtke C. A classification system for the bicuspid aortic valve from 304 surgical specimens. J Thorac Cardiovasc Surg. 2007;133(5):1226-33.
6. Michelena HI, Della Corte A, Prakash SK, Milewicz DM, Evangelista A, Enriquez-Sarano M. Bicuspid aortic valve aortopathy in adults: Incidence, etiology, and clinical significance. Int J Cardiol. 2015;201:400-7.
7. Glick BN, Roberts WC. Congenitally bicuspid aortic valve in multiple family members. Am J Cardiol. 1994;73(5):400-4.
8. Huntington K, Hunter AG, Chan KL. A prospective study to assess the frequency of familial clustering of congenital bicuspid aortic valve. J Am Coll Cardiol. 1997;30(7):1809-12.
9. Mohamed SA, Aherrahrou Z, Liptau H, Erasmi AW, Hagemann C, Wrobel S, et al. Novel missense mutations (p.T596M and p.P1797H) in NOTCH1 in patients with bicuspid aortic valve. Biochem Biophys Res Commun. 2006;345(4):1460-5.
10. Foffa I, Ait Ali L, Panesi P, Mariani M, Festa P, Botto N, et al. Sequencing of NOTCH1, GATA5, TGFBR1 and TGFBR2 genes in familial cases of bicuspid aortic valve. BMC Med Genet. 2013;14:44.
11. Freylikhman O, Tatarinova T, Smolina N, Zhuk S, Klyushina A, Kiselev A, et al. Variants in the NOTCH1 gene in patients with aortic coarctation. Congenit Heart Dis. 2014;9(5):391-6.
12. McBride KL, Riley MF, Zender GA, Fitzgerald-Butt SM, Towbin JA, Belmont JW, et al. NOTCH1 mutations in individuals with left ventricular outflow tract malformations reduce ligand-induced signaling. Hum Mol Genet. 2008;17(18):2886-93.
13. McKellar SH, Tester DJ, Yagubyan M, Majumdar R, Ackerman MJ, Sundt TM, 3rd. Novel NOTCH1 mutations in patients with bicuspid aortic valve disease and thoracic aortic aneurysms. J Thorac Cardiovasc Surg. 2007;134(2):290-6.
14. Theis JL, Hrstka SC, Evans JM, O'Byrne MM, de Andrade M, O'Leary PW, et al. Compound heterozygous NOTCH1 mutations underlie impaired cardiogenesis in a patient with hypoplastic left heart syndrome. Hum Genet. 2015;134(9):1003-11.
15. Artavanis-Tsakonas S, Rand MD, Lake RJ. Notch signaling: cell fate control and signal integration in development. Science. 1999;284(5415):770-6.
16. Niessen K, Karsan A. Notch signaling in cardiac development. Circ Res. 2008;102(10):1169-81.
17. Girdauskas E, Disha K, Borger MA, Kuntze T. Relation of bicuspid aortic valve morphology to the dilatation pattern of the proximal aorta: focus on the transvalvular flow. Cardiol Res Pract. 2012;2012:478259.
18. Yang B, Zhou W, Jiao J, Nielsen JB, Mathis MR, Heydarpour M, et al. Protein-altering and regulatory genetic variants near GATA4 implicated in bicuspid aortic valve. Nat Commun. 2017;8:15481.
19. Gago-Diaz M, Brion M, Gallego P, Calvo F, Robledo-Carmona J, Saura D, et al. The genetic component of bicuspid aortic valve and aortic dilation. An exome-wide association study. J Mol Cell Cardiol. 2017;102:3-9.

20. Maredia AK, Greenway SC, Verma S, Fedak PWM. Bicuspid aortic valve-associated aortopathy: update on biomarkers. Curr Opin Cardiol. 2018;33(2):134-9.
21. Barker AJ, Lanning C, Shandas R. Quantification of hemodynamic wall shear stress in patients with bicuspid aortic valve using phase-contrast MRI. Ann Biomed Eng. 2010;38(3):788-800.
22. Barker AJ, Markl M, Burk J, Lorenz R, Bock J, Bauer S, et al. Bicuspid aortic valve is associated with altered wall shear stress in the ascending aorta. Circ Cardiovasc Imaging. 2012;5(4):457-66.
23. Barker AJ, Markl M, Fedak PWM. Assessing wall stresses in bicuspid aortic valve-associated aortopathy: Forecasting the perfect storm? J Thorac Cardiovasc Surg. 2018;156(2):471-2.
24. Barker AJ, Robinson JD, Markl M. Bicuspid aortic valve phenotype and aortopathy: nomenclature and role of aortic hemodynamics. JACC Cardiovasc Imaging. 2013;6(8):921.
25. Guzzardi DG, Barker AJ, van Ooij P, Malaisrie SC, Puthumana JJ, Belke DD, et al. Valve-Related Hemodynamics Mediate Human Bicuspid Aortopathy: Insights From Wall Shear Stress Mapping. J Am Coll Cardiol. 2015;66(8):892-900.
26. Atkins SK, Cao K, Rajamannan NM, Sucosky P. Bicuspid aortic valve hemodynamics induces abnormal medial remodeling in the convexity of porcine ascending aortas. Biomech Model Mechanobiol. 2014;13(6):1209-25.
27. Marom G, Kim HS, Rosenfeld M, Raanani E, Haj-Ali R. Effect of asymmetry on hemodynamics in fluid-structure interaction model of congenital bicuspid aortic valves. Conf Proc IEEE Eng Med Biol Soc. 2012;2012:637-40.
28. Pasipoularides A. Clinical-pathological correlations of BAV and the attendant thoracic aortopathies. Part 2: Pluridisciplinary perspective on their genetic and molecular origins. J Mol Cell Cardiol. 2019;133:233-46.
29. Wang Y, Wu B, Dong L, Wang C, Wang X, Shu X. Circulating matrix metalloproteinase patterns in association with aortic dilatation in bicuspid aortic valve patients with isolated severe aortic stenosis. Heart Vessels. 2016;31(2):189-97.
30. Borghini A, Foffa I, Pulignani S, Vecoli C, Ait-Ali L, Andreassi MG. miRNome Profiling in Bicuspid Aortic Valve-Associated Aortopathy by Next-Generation Sequencing. Int J Mol Sci. 2017;18(11).
31. Pulignani S, Borghini A, Andreassi MG. microRNAs in bicuspid aortic valve associated aortopathy: Recent advances and future perspectives. J Cardiol. 2019;74(4):297-303.
32. Xia W, Chen Q, Wang J, Mao Q, Dong G, Shi R, et al. DNA methylation mediated silencing of microRNA-145 is a potential prognostic marker in patients with lung adenocarcinoma. Sci Rep. 2015;5:16901.
33. Guzzardi DG, Verma S, Fedak PW. Bicuspid aortic valve aortopathy: mechanistic and clinical insights from recent studies. Curr Opin Cardiol. 2017;32(2):111-6.
34. Fedak PW, Verma S, David TE, Leask RL, Weisel RD, Butany J. Clinical and pathophysiological implications of a bicuspid aortic valve. Circulation. 2002;106(8):900-4.
35. Fedak PW, de Sa MP, Verma S, Nili N, Kazemian P, Butany J, et al. Vascular matrix remodeling in patients with bicuspid aortic valve malformations: implications for aortic dilatation. J Thorac Cardiovasc Surg. 2003;126(3):797-806.
36. Boyum J, Fellinger EK, Schmoker JD, Trombley L, McPartland K, Ittleman FP, et al. Matrix metalloproteinase activity in thoracic aortic aneurysms associated with bicuspid and tricuspid aortic valves. J Thorac Cardiovasc Surg. 2004;127(3):686-91.
37. Forte A, Della Corte A, Grossi M, Bancone C, Provenzano R, Finicelli M, et al. Early cell changes and TGFbeta pathway alterations in the aortopathy associated with bicuspid aortic valve stenosis. Clin Sci (Lond). 2013;124(2):97-108.

38. Forte A, Bancone C, Cobellis G, Buonocore M, Santarpino G, Fischlein TJM, et al. A Possible Early Biomarker for Bicuspid Aortopathy: Circulating Transforming Growth Factor beta-1 to Soluble Endoglin Ratio. Circ Res. 2017;120(11):1800-11.
39. Crivello A, Giacalone A, Scola L, Forte GI, Nuzzo D, Giacconi R, et al. Frequency of polymorphisms of signal peptide of TGF-beta1 and -1082G/A SNP at the promoter region of Il-10 gene in patients with carotid stenosis. Ann N Y Acad Sci. 2006;1067:288-93.
40. Forte A, Galderisi U, Cipollaro M, De Feo M, Della Corte A. Epigenetic regulation of TGF-beta1 signalling in dilative aortopathy of the thoracic ascending aorta. Clin Sci (Lond). 2016;130(16):1389-405.
41. Hagler MA, Hadley TM, Zhang H, Mehra K, Roos CM, Schaff HV, et al. TGF-beta signalling and reactive oxygen species drive fibrosis and matrix remodelling in myxomatous mitral valves. Cardiovasc Res. 2013;99(1):175-84.
42. Lindsay ME, Dietz HC. Lessons on the pathogenesis of aneurysm from heritable conditions. Nature. 2011;473(7347):308-16.
43. ten Dijke P, Arthur HM. Extracellular control of TGFbeta signalling in vascular development and disease. Nat Rev Mol Cell Biol. 2007;8(11):857-69.
44. Wheeler JB, Ikonomidis JS, Jones JA. Connective tissue disorders and cardiovascular complications: the indomitable role of transforming growth factor-beta signaling. Adv Exp Med Biol. 2014;802:107-27.
45. Borger MA, Fedak PWM, Stephens EH, Gleason TG, Girdauskas E, Ikonomidis JS, et al. The American Association for Thoracic Surgery consensus guidelines on bicuspid aortic valve-related aortopathy: Full online-only version. J Thorac Cardiovasc Surg. 2018;156(2):e41-e74.
46. Erbel R, Aboyans V, Boileau C, Bossone E, Bartolomeo RD, Eggebrecht H, et al. 2014 ESC Guidelines on the diagnosis and treatment of aortic diseases: Document covering acute and chronic aortic diseases of the thoracic and abdominal aorta of the adult. The Task Force for the Diagnosis and Treatment of Aortic Diseases of the European Society of Cardiology (ESC). Eur Heart J. 2014;35(41):2873-926.
47. Charitos EI, Stierle U, Petersen M, Mohamed SA, Hanke T, Schmidtke C, et al. The fate of the bicuspid valve aortopathy after aortic valve replacement. Eur J Cardiothorac Surg. 2014;45(5):e128-35.
48. Itagaki S, Chikwe JP, Chiang YP, Egorova NN, Adams DH. Long-Term Risk for Aortic Complications After Aortic Valve Replacement in Patients With Bicuspid Aortic Valve Versus Marfan Syndrome. J Am Coll Cardiol. 2015;65(22):2363-9.
49. Nakamura Y, Ryugo M, Shikata F, Okura M, Okamura T, Yasugi T, et al. The analysis of ascending aortic dilatation in patients with a bicuspid aortic valve using the ratio of the diameters of the ascending and descending aorta. J Cardiothorac Surg. 2014;9:108.
50. Adamo L, Braverman AC. Surgical threshold for bicuspid aortic valve aneurysm: a case for individual decision-making. Heart. 2015;101(17):1361-7.
51. Wasfy JH, Armstrong K, Milford CE, Sundt TM. Bicuspid aortic disease and decision making under uncertainty - The limitations of clinical guidelines. Int J Cardiol. 2015;181:169-71.
52. Della Corte A, Michelena HI, Citarella A, Votta E, Piatti F, Lo Presti F, et al. Risk Stratification in Bicuspid Aortic Valve Aortopathy: Emerging Evidence and Future Perspectives. Curr Probl Cardiol. 2019.
53. Della Corte A, Body SC, Booher AM, Schaefers HJ, Milewski RK, Michelena HI, et al. Surgical treatment of bicuspid aortic valve disease: knowledge gaps and research perspectives. J Thorac Cardiovasc Surg. 2014;147(6):1749-57, 57 e1.

54. Verma S, Yanagawa B, Kalra S, Ruel M, Peterson MD, Yamashita MH, et al. Knowledge, attitudes, and practice patterns in surgical management of bicuspid aortopathy: a survey of 100 cardiac surgeons. J Thorac Cardiovasc Surg. 2013;146(5):1033-40 e4.
55. Sundt TM. Aortic replacement in the setting of bicuspid aortic valve: how big? How much? J Thorac Cardiovasc Surg. 2015;149(2 Suppl):S6-9.
56. Strimbu K, Tavel JA. What are biomarkers? Curr Opin HIV AIDS. 2010;5(6):463-6.
57. Branchetti E, Bavaria JE, Grau JB, Shaw RE, Poggio P, Lai EK, et al. Circulating soluble receptor for advanced glycation end product identifies patients with bicuspid aortic valve and associated aortopathies. Arterioscler Thromb Vasc Biol. 2014;34(10):2349-57.
58. Ikonomidis JS, Ruddy JM, Benton SM, Jr., Arroyo J, Brinsa TA, Stroud RE, et al. Aortic dilatation with bicuspid aortic valves: cusp fusion correlates to matrix metalloproteinases and inhibitors. Ann Thorac Surg. 2012;93(2):457-63.
59. Kilickesmez KO, Abaci O, Kocas C, Yildiz A, Kaya A, Okcun B, et al. Dilatation of the ascending aorta and serum alpha 1-antitrypsin level in patients with bicuspid aortic valve. Heart Vessels. 2012;27(4):391-7.
60. McMillan WD, Pearce WH. Increased plasma levels of metalloproteinase-9 are associated with abdominal aortic aneurysms. J Vasc Surg. 1999;29(1):122-7; discussion 7-9.
61. Tzemos N, Lyseggen E, Silversides C, Jamorski M, Tong JH, Harvey P, et al. Endothelial function, carotid-femoral stiffness, and plasma matrix metalloproteinase-2 in men with bicuspid aortic valve and dilated aorta. J Am Coll Cardiol. 2010;55(7):660-8.
62. Boon RA, Dimmeler S. MicroRNAs and aneurysm formation. Trends Cardiovasc Med. 2011;21(6):172-7.
63. Albinsson S, Sward K. Targeting smooth muscle microRNAs for therapeutic benefit in vascular disease. Pharmacol Res. 2013;75:28-36.
64. Phillippi JA, Eskay MA, Kubala AA, Pitt BR, Gleason TG. Altered oxidative stress responses and increased type I collagen expression in bicuspid aortic valve patients. Ann Thorac Surg. 2010;90(6):1893-8.
65. Billaud M, Phillippi JA, Kotlarczyk MP, Hill JC, Ellis BW, St Croix CM, et al. Elevated oxidative stress in the aortic media of patients with bicuspid aortic valve. J Thorac Cardiovasc Surg. 2017;154(5):1756-62.
66. Khoo NK, Cantu-Medellin N, St Croix C, Kelley EE. In Vivo Immuno-Spin Trapping: Imaging the Footprints of Oxidative Stress. Curr Protoc Cytom. 2015;74:12 42 1-11.
67. Prunty MC, Aung MH, Hanif AM, Allen RS, Chrenek MA, Boatright JH, et al. In Vivo Imaging of Retinal Oxidative Stress Using a Reactive Oxygen Species-Activated Fluorescent Probe. Invest Ophthalmol Vis Sci. 2015;56(10):5862-70.
68. Bissell MM, Hess AT, Biasiolli L, Glaze SJ, Loudon M, Pitcher A, et al. Aortic dilation in bicuspid aortic valve disease: flow pattern is a major contributor and differs with valve fusion type. Circ Cardiovasc Imaging. 2013;6(4):499-507.
69. van Ooij P, Potters WV, Collins J, Carr M, Carr J, Malaisrie SC, et al. Characterization of abnormal wall shear stress using 4D flow MRI in human bicuspid aortopathy. Ann Biomed Eng. 2015;43(6):1385-97.
70. Lehoux S, Tedgui A. Cellular mechanics and gene expression in blood vessels. J Biomech. 2003;36(5):631-43.
71. Mahadevia R, Barker AJ, Schnell S, Entezari P, Kansal P, Fedak PW, et al. Bicuspid aortic cusp fusion morphology alters aortic three-dimensional outflow patterns, wall shear stress, and expression of aortopathy. Circulation. 2014;129(6):673-82.

72. Della Corte A, Bancone C, Dialetto G, Covino FE, Manduca S, D'Oria V, et al. Towards an individualized approach to bicuspid aortopathy: different valve types have unique determinants of aortic dilatation. Eur J Cardiothorac Surg. 2014;45(4):e118-24; discussion e24.
73. Kang JW, Song HG, Yang DH, Baek S, Kim DH, Song JM, et al. Association between bicuspid aortic valve phenotype and patterns of valvular dysfunction and bicuspid aortopathy: comprehensive evaluation using MDCT and echocardiography. JACC Cardiovasc Imaging. 2013;6(2):150-61.
74. Lo YM, Corbetta N, Chamberlain PF, Rai V, Sargent IL, Redman CW, et al. Presence of fetal DNA in maternal plasma and serum. Lancet. 1997;350(9076):485-7.
75. Lo YM, Tein MS, Pang CC, Yeung CK, Tong KL, Hjelm NM. Presence of donor-specific DNA in plasma of kidney and liver-transplant recipients. Lancet. 1998;351(9112):1329-30.
76. Schwarzenbach H, Hoon DS, Pantel K. Cell-free nucleic acids as biomarkers in cancer patients. Nat Rev Cancer. 2011;11(6):426-37.
77. Gedvilaite V, Schveigert D, Cicenas S. Cell-free DNA in non-small cell lung cancer. Acta Med Litu. 2017;24(2):138-44.
78. Lehmann-Werman R, Neiman D, Zemmour H, Moss J, Magenheim J, Vaknin-Dembinsky A, et al. Identification of tissue-specific cell death using methylation patterns of circulating DNA. Proc Natl Acad Sci U S A. 2016;113(13):E1826-34.
79. Atamaniuk J, Vidotto C, Tschan H, Bachl N, Stuhlmeier KM, Muller MM. Increased concentrations of cell-free plasma DNA after exhaustive exercise. Clin Chem. 2004;50(9):1668-70.
80. Fleischhacker M, Schmidt B. Circulating nucleic acids (CNAs) and cancer--a survey. Biochim Biophys Acta. 2007;1775(1):181-232.
81. Crowley E, Di Nicolantonio F, Loupakis F, Bardelli A. Liquid biopsy: monitoring cancer-genetics in the blood. Nat Rev Clin Oncol. 2013;10(8):472-84.
82. De Vlaminck I, Valantine HA, Snyder TM, Strehl C, Cohen G, Luikart H, et al. Circulating cell-free DNA enables noninvasive diagnosis of heart transplant rejection. Sci Transl Med. 2014;6(241):241ra77.
83. Kinnings SL, Geis JA, Almasri E, Wang H, Guan X, McCullough RM, et al. Factors affecting levels of circulating cell-free fetal DNA in maternal plasma and their implications for noninvasive prenatal testing. Prenat Diagn. 2015;35(8):816-22.
84. Norton ME, Wapner RJ. Cell-free DNA Analysis for Noninvasive Examination of Trisomy. N Engl J Med. 2015;373(26):2582.
85. Salvi S, Gurioli G, De Giorgi U, Conteduca V, Tedaldi G, Calistri D, et al. Cell-free DNA as a diagnostic marker for cancer: current insights. Onco Targets Ther. 2016;9:6549-59.
86. Barault L, Amatu A, Siravegna G, Ponzetti A, Moran S, Cassingena A, et al. Discovery of methylated circulating DNA biomarkers for comprehensive non-invasive monitoring of treatment response in metastatic colorectal cancer. Gut. 2018;67(11):1995-2005.
87. Bird A. DNA methylation patterns and epigenetic memory. Genes Dev. 2002;16(1):6-21.
88. Razin A, Cedar H. DNA methylation and gene expression. Microbiol Rev. 1991;55(3):451-8.
89. Galanopoulos M, Tsoukalas N, Papanikolaou IS, Tolia M, Gazouli M, Mantzaris GJ. Abnormal DNA methylation as a cell-free circulating DNA biomarker for colorectal cancer detection: A review of literature. World J Gastrointest Oncol. 2017;9(4):142-52.
90. Wang J, Han X, Sun Y. DNA methylation signatures in circulating cell-free DNA as biomarkers for the early detection of cancer. Sci China Life Sci. 2017;60(4):356-62.
91. Kang S, Li Q, Chen Q, Zhou Y, Park S, Lee G, et al. CancerLocator: non-invasive cancer diagnosis and tissue-of-origin prediction using methylation profiles of cell-free DNA. Genome Biol. 2017;18(1):53.

92. Kureshi N, Ghaffar S, Siddiqui S, Salahuddin I, Frossard PM. Head and neck cancer susceptibility: a genetic marker in the methylenetetrahydrofolate reductase gene. ORL J Otorhinolaryngol Relat Spec. 2004;66(5):241-5.
93. Li Z, Guo X, Tang L, Peng L, Chen M, Luo X, et al. Methylation analysis of plasma cell-free DNA for breast cancer early detection using bisulfite next-generation sequencing. Tumour Biol. 2016;37(10):13111-9.
94. Symonds EL, Pedersen SK, Murray DH, Jedi M, Byrne SE, Rabbitt P, et al. Circulating tumour DNA for monitoring colorectal cancer-a prospective cohort study to assess relationship to tissue methylation, cancer characteristics and surgical resection. Clin Epigenetics. 2018;10:63.
95. de Sa M, Moshkovitz Y, Butany J, David TE. Histologic abnormalities of the ascending aorta and pulmonary trunk in patients with bicuspid aortic valve disease: clinical relevance to the ross procedure. J Thorac Cardiovasc Surg. 1999;118(4):588-94.
96. Bonderman D, Gharehbaghi-Schnell E, Wollenek G, Maurer G, Baumgartner H, Lang IM. Mechanisms underlying aortic dilatation in congenital aortic valve malformation. Circulation. 1999;99(16):2138-43.
97. Grewal N, Franken R, Mulder BJ, Goumans MJ, Lindeman JH, Jongbloed MR, et al. Histopathology of aortic complications in bicuspid aortic valve versus Marfan syndrome: relevance for therapy? Heart Vessels. 2016;31(5):795-806.
98. Nataatmadja M, West M, West J, Summers K, Walker P, Nagata M, et al. Abnormal extracellular matrix protein transport associated with increased apoptosis of vascular smooth muscle cells in marfan syndrome and bicuspid aortic valve thoracic aortic aneurysm. Circulation. 2003;108 Suppl 1:II329-34.
99. Liu J, Shar JA, Sucosky P. Wall Shear Stress Directional Abnormalities in BAV Aortas: Toward a New Hemodynamic Predictor of Aortopathy? Front Physiol. 2018;9:993.
100. Mohamed SA, Misfeld M, Hanke T, Charitos EI, Bullerdiek J, Belge G, et al. Inhibition of caspase-3 differentially affects vascular smooth muscle cell apoptosis in the concave versus convex aortic sites in ascending aneurysms with a bicuspid aortic valve. Ann Anat. 2010;192(3):145-50.
101. Egger G, Liang G, Aparicio A, Jones PA. Epigenetics in human disease and prospects for epigenetic therapy. Nature. 2004;429(6990):457-63.
102. Kelsey G, Feil R. New insights into establishment and maintenance of DNA methylation imprints in mammals. Philos Trans R Soc Lond B Biol Sci. 2013;368(1609):20110336.
103. Ji H, Ehrlich LI, Seita J, Murakami P, Doi A, Lindau P, et al. Comprehensive methylome map of lineage commitment from haematopoietic progenitors. Nature. 2010;467(7313):338-42.
104. Miao F, Wu X, Zhang L, Riggs AD, Natarajan R. Histone methylation patterns are cell-type specific in human monocytes and lymphocytes and well maintained at core genes. J Immunol. 2008;180(4):2264-9.
105. Cheng X. Structure and function of DNA methyltransferases. Annu Rev Biophys Biomol Struct. 1995;24:293-318.
106. Jurkowska RZ, Jurkowski TP, Jeltsch A. Structure and function of mammalian DNA methyltransferases. Chembiochem. 2011;12(2):206-22.
107. Tsuji J, Weng Z. Evaluation of preprocessing, mapping and postprocessing algorithms for analyzing whole genome bisulfite sequencing data. Brief Bioinform. 2016;17(6):938-52.
108. Li LC, Dahiya R. MethPrimer: designing primers for methylation PCRs. Bioinformatics. 2002;18(11):1427-31.
109. Leggett RM, Ramirez-Gonzalez RH, Clavijo BJ, Waite D, Davey RP. Sequencing quality assessment tools to enable data-driven informatics for high throughput genomics. Front Genet. 2013;4:288.

110. Stephenson FH. Calculations for molecular biology and biotechnology. Third edition. ed. Amsterdam ; Boston: Elsevier/AP, Academic Press is an imprint of Elsevier; 2016. xiii, 481 pages p.
111. Juhling F, Kretzmer H, Bernhart SH, Otto C, Stadler PF, Hoffmann S. metilene: fast and sensitive calling of differentially methylated regions from bisulfite sequencing data. Genome Res. 2016;26(2):256-62.
112. Chim YH, Davies HA, Mason D, Nawaytou O, Field M, Madine J, et al. Bicuspid valve aortopathy is associated with distinct patterns of matrix degradation. J Thorac Cardiovasc Surg. 2019.
113. Wang X, Khalil RA. Matrix Metalloproteinases, Vascular Remodeling, and Vascular Disease. Adv Pharmacol. 2018;81:241-330.
114. Yassine NM, Shahram JT, Body SC. Pathogenic Mechanisms of Bicuspid Aortic Valve Aortopathy. Front Physiol. 2017;8:687.
115. Balistreri CR, Pisano C, Candore G, Maresi E, Codispoti M, Ruvolo G. Focus on the unique mechanisms involved in thoracic aortic aneurysm formation in bicuspid aortic valve versus tricuspid aortic valve patients: clinical implications of a pilot study. Eur J Cardiothorac Surg. 2013;43(6):e180-6.
116. Robertson E, Dilworth C, Lu Y, Hambly B, Jeremy R. Molecular mechanisms of inherited thoracic aortic disease - from gene variant to surgical aneurysm. Biophys Rev. 2015;7(1):105-15.
117. Sun L, Chandra S, Sucosky P. Ex vivo evidence for the contribution of hemodynamic shear stress abnormalities to the early pathogenesis of calcific bicuspid aortic valve disease. PLoS One. 2012;7(10):e48843.

Appendices

I. Laboratory Protocols

TUNEL Assay Protocol

Promega (DeadEnd TM Fluorometric TUNEL System) Protocol. Alterations are denoted in italics. Section 4B was followed (Pretreatment of paraffin-embedded tissues). Adapted from https://www.promega.ca/-/media/files/resources/protocols/technical- bulletins/0/deadendfluorometric-tunel-system-protocol.pdf.

Before beginning:

- *Set water-bath to 37°C.*
- *Keep methanol-free formaldehyde in PBS out of fridge*
- *Prepare 100%, 95%, 85%, 70%, 50% Ethanol, 0.85% NaCl, 20µg/ml Proteinase K solution, and 2x SSC solution*

1. Deparaffinize tissue sections (attached to microscope slides) by immersing slides in fresh xylene in a Coplin jar for 5 minutes at room temperature. Repeat one time for a total of two xylene washes.
1. Wash the samples by immersing the slides in 100% ethanol for 5 minutes at room temperature in a Coplin jar.
2. Rehydrate the samples by sequentially immersing the slides through graded ethanol washes (100%, 95%, 85%, 70%, 50%) for 3 minutes each at room temperature
3. Wash the samples by immersing the slides in 0.85% NaCl for 5 minutes at room temperature
4. Wash the samples by immersing the slides in PBS for 5 minutes at room temperature.
5. Fix the tissue sections by immersing the slides in 4% methanol-free formaldehyde solution in PBS for 20 minutes at room temperature. *Paraformaldehyde was substituted for methanolfree formaldehyde.*
6. Wash the samples by immersing the slides in PBS for 5 minutes at room temperature. Repeat once for a total of two PBS washes.
7. Remove the liquid from the tissue and place the slides on a flat surface. Prepare a 20 µg/ml
8. Proteinase K solution from the reconstituted Proteinase K (10mg/ml; see Section 2) by diluting 1:500 in PBS. Add 100 µl of the 20 µg/ml Proteinase K to each slide to cover the tissue section. Incubate slides for 8–10 minutes at room temperature.
9. Wash the samples by immersing the slides in PBS for 5 minutes at room temperature in a Coplin jar.
10. Fix the tissue sections after washing by immersing the slides in 4% methanol-free formaldehyde solution in PBS for 20 minutes at room temperature.
11. Wash the samples by immersing the slides in PBS for 5 minutes at room temperature.
12. *Added step: Flood the slides with 1% Bovine Serum Albumin (BSA) for 1 hour.*
13. *Added step: Wash the samples by immersing the slides in PBS for 5 minutes at room temperature. Repeat once for a total of two PBS washes.*

    Move onto protocol 4A (beginning with Step 5):

5. Remove excess liquid by tapping the slides. Cover the cells with 100µl of Equilibration Buffer. Equilibrate at room temperature for 5–10 minutes.

6. While the cells are equilibrating, thaw the Nucleotide Mix on ice and prepare sufficient rTdT incubation buffer for all experimental and optional positive control reactions according to the below table:

Buffer Component	Component Volume per Standard 50µl Reaction		Number of Reactions (Experimental Reactions + Optional Positive Controls)		Component Volume
Equilibration Buffer	45µl	x	_____	=	_____µl
Nucleotide Mix	5µl	x	_____	=	_____µl
rTdT Enzyme	1µl	x	_____	=	_____µl
	Total rTdT Incubation Buffer Volume			=	_____µl

   - Keep the Nucleotide Mix and rTdT incubation buffer solution on ice, protected from light.

7. Blot around the equilibrated areas with tissue paper to remove most of the 100 µl of
8. Equilibration Buffer and add 50 µl of rTdT incubation buffer to the cells on a 5 cm^2 area. Do not allow the cells to dry out.
   a. Avoid exposing the slides to light after completion of Step 7.
9. Cover the cells with Plastic Coverslips to ensure even distribution of the reagent. Place paper towels soaked with water at the bottom of a humidified chamber. Incubate the slides at 37°C for 60 minutes inside the humidified chamber to allow the tailing reaction to occur. Cover the chamber with aluminum foil to protect from direct light.
10. Dilute the 20X SSC 1:10 with deionized water and add enough of the resulting 2X SSC to fill a standard Coplin jar (40 ml). Remove the Plastic Coverslips and terminate the reactions by immersing the slides in 2X SSC in a Coplin jar for 15 minutes at room temperature. Ensure that all salts of the 20X SSC are in solution before diluting (Step 9).

The following steps have been modified as follows:

11. Wash the samples by immersing the slides with 0.1% Triton with 5% BSA for 5 minutes. Repeat this step for a total of 2 washes to remove unincorporated fluorescein-12-dUTP.
12. Wash the samples by immersing the slides in fresh PBS for 5 minutes at room temperature. Repeat this step once for a total of two washes with PBS
13. Using the Vector® TrueVIEW™ Autofluorescence Quenching Kit, for each sample 150 µL of reagent will be required. Prepare the reagent by mixing a ratio of 1:1:1 of Reagents A, B and C.
    a. Add equal volumes of Reagent A and Reagent B in a clean 1.5 mL microcentrifuge tube.
    b. Mix for 10 seconds.
    c. Add Reagent C to the mixture (ensuring a 1:1:1 volume ratio) andmix again for 10 seconds.
14. Drain excess buffer from tissue section.
15. Add Vector TrueVIEW Reagent to cover tissue section completely (~150 µl); and incubate for 2 - 5 minutes.
16. Wash in PBS buffer for 5 minutes.
17. Drain excess buffer from section. Optimal results are obtained if excess buffer is removed around tissue prior to adding mounting medium.
18. Add 1-2 drops of VECTASHIELD® Antifade Mounting Medium with DAPI to the slides
19. Place a glass coverslip on top ensuring that no bubbles form. If desired, coverslips can be sealed around the perimeter with nail polish or a plastic sealant.
20. Allow slides to be stored at 4 °C, protected from light overnight

21. View slides using spinning disk confocal super resolution microscope

Primer Design Parameters

Primers were designed using the online software MethPrimer at https://www.urogene.org/methprimer/

Table 11: Primer Design parameters

	Minimum	Optimal	Maximum
Product Size	70	100	165
Primer Tm	50	55	60
Primer Size	20	25	35
Primer non-CpG 'C's:	2	--	--

Tm = Melting temperature

Plasma Isolation

Blood samples of BAV patients were collected in blood collection tubes and their plasma isolated.

1) Load and balance the blood sample in a centrifuge and run it for 10min at 12 000 RCF at room temperature.
2) After the separation, there will be blood at the bottom, a thin buffy coat in the middle of leukocytes and platelets and plasma at the top.
3) In the fume hood, carefully pipette ONLY the plasma in 2 mL microcentrifuge tubes making sure not to puncture into the buffy coat or the blood layer. Dispose of the vials containing the blood and the buffy coat as biohazard waste
4) Load the microcentrifuge tubes containing the plasma in a centrifuge and spin at 13000 rpm for 16min at 4ºC.
5) In the fume hood, pipette the plasma into fresh 2 mL microcentrifuge tubes avoiding the white pellet at the bottom.
6) Label plasma samples and store in the -80ºC freezer.

Semi-Automated Cell Free DNA Isolation from Patient Plasma

Based on the protocol outlined in the MagNA Pure 24 Total NA Isolation Kit (Roche) for the isolation of double-stranded cell free nucleic acids from 2000 µL of plasma. Adapted from https://lifescience.roche.com/en_ca/products/magna-pure-24-instrument.html#application

Before purifying cell-free nucleic acids:

- Centrifuge the samples for 5 to 10 min at 1000 to 1900 x g. Avoid transferring any of the pellet.
- Avoid introducing foam/bubbles during all pipetting steps.

Protocol	cfNA ds 2000
Proteinase K [µL]	200
CELB [µL]	1750
IPA [µL]	300
cfNA buffer mix (CELB + IPA) [µL]	2050

- In a fresh tube compatible with the MagNA Pure 24 Sample Rack, place the appropriate volume of Proteinase K. Add the sample into the tube containing Proteinase K, mix gently, and incubate at 37°C for 20 min.
- According to the number of samples to be processed, prepare the cfNA buffer mix in bulk by mixing Cell-Free Nucleic Acid Enhancement Buffer (CELB) and isopropanol (IPA) in that order, in an appropriately sized container. The volumes listed in the table are the required amounts for one sample.
- Cap and mix gently by inversion. The solution is stable for a maximum of 2 hours.
- Add the appropriate amount of cfNA buffer mix to each sample (ie: 2000 µL of cfNA buffer mix to 2000 µL of the plasma sample).
- Mix thoroughly by dispensing and aspirating the liquid approximately 8 times to produce a homogeneous mixture.
    - Do not store the lysate.
    - If bubbles form, they may be removed by aspiration into a pipette tip held near the side of the tube just above the surface of the liquid.
    - Alternatively, bubbles may be removed by capping tubes and centrifuging at 2000 x *g* for 1 min.
- Load the tubes onto the sample rack.
- Load the sample rack into the instrument.
- Follow the prompts on the instrument to name each sample and ensure the tubes that will contain the output cfDNA are labelled and placed in the appropriate and corresponding slots.
- Load reagent cartridges and consumables in the appropriate chambers
    - All items loaded to the instrument must be decapped: tubes holding the samples, MGP tubes, internal control tubes, and output consumables.
    - Allow the instrument to scan each area to ensure each item is the in appropriate place prior to starting the automated reaction.

Bisulfite Conversion of Cell-free DNA

Based on the protocol outlined in the EpiTect® Bisulfite Handbook (Qiagen) for the isolation of bisulfite conversion of cfDNA from 20 uL of plasma. Adapted from file:///Users/Ashna/Downloads/HB-0243-002-1090269-HB-EpiTect-Bisulfite-1214-WW%20(2).pdf

Protocol: Sodium Bisulfite Conversion of Unmethylated Cytosines in DNA

DNA amounts of 1 ng – 2 µg in a volume of up to 20 µl can be processed using this standard protocol.

Important points before starting:

- Each aliquot of Bisulfite Mix is sufficient for 8 conversion reactions. If converting fewer than 8 DNA samples, dissolved Bisulfite Mix can be stored at –15 to –30°C for up to 4 weeks without any loss of performance.

- DNA Protect Buffer should turn from green to blue after addition to DNA–Bisulfite Mix (step 2), indicating sufficient mixing and correct pH for the bisulfite conversion reaction. ′ Perform all centrifugation steps at room temperature (15–25°C).

Things to do before starting:

- Add 30 ml ethanol (96–100%) to Buffer BW and store at room temperature (15–25°C). Invert the bottle several times before starting the procedure.
- Add 27 ml ethanol (96–100%) to Buffer BD and store at 2–8°C. Invert the bottle several times before starting the procedure and make sure to close the bottle immediately after use. White precipitates may form in the Buffer BD–ethanol mix after some storage time. These precipitates will not affect the performance of Buffer BD. However, avoid transferring precipitates to the EpiTect spin column.
- Add 310 µl RNase-free water to the lyophilized carrier RNA (310 µg) to obtain a 1 µg/µl solution. Dissolve the carrier RNA thoroughly by vortexing. When processing 48 samples at once, add the complete volume of dissolved carrier RNA to the bottle of Buffer BL, and check the box on the bottle lid label. If processing fewer samples, split the dissolved carrier RNA into conveniently sized aliquots (e.g., 50 µl) and store at –15 to –30°C. Aliquots can be stored for up to 1 year. If fewer than 48 conversions will be performed in a 2-week period, then only make up enough Buffer BL–carrier RNA solution as required (see Table 1, page 17, for example volumes). Carrier RNA enhances binding of DNA to the EpiTect spin-column membrane, especially if there are very few target molecules in the sample. Carrier RNA is not necessary if >100 ng DNA is used.
- Add dissolved carrier RNA to Buffer BL. Calculate the volume of Buffer BL and dissolved carrier RNA required for the number of samples to be processed (see Table 1 for example volumes). If Buffer BL contains precipitates, dissolve by heating (maximum 70°C) with gentle agitation
- Equilibrate samples and buffers to room temperature. ′ Optional: Set a thermomixer, heating block, or heated orbital incubator to 60°C for use in step 1.

Procedure

1. Thaw DNA to be used in the bisulfite reactions. Dissolve the required number of aliquots of Bisulfite Mix by adding 800 µl RNase-free water to each aliquot. Vortex until the Bisulfite Mix is completely dissolved. This can take up to 5 min. Note: If necessary, heat the Bisulfite Mix–RNase-free water solution to 60°C and vortex again. Note: Do not place dissolved Bisulfite Mix on ice.
2. Prepare the bisulfite reactions in 200 µl PCR tubes according to the Table below. Add each component in the order listed. Note: The combined volume of DNA solution and RNase-free water must total 20 µl.

Component	Volume per reaction (µl)
DNA solution (1 ng – 2 µg)	Variable* (maximum 20 µl)
RNase-free water	Variable*
Bisulfite Mix (dissolved), see step 1	85
DNA Protect Buffer	35
Total volume	**140**

* The combined volume of DNA solution and RNase-free water must total 20 µl.

3. Close the PCR tubes and mix the bisulfite reactions thoroughly. Store the tubes at room temperature (15–25°C). Note: DNA Protect Buffer should turn from green to blue after addition to DNA–Bisulfite Mix, indicating sufficient mixing and correct pH for the bisulfite conversion reaction.
4. Perform the bisulfite DNA conversion using a thermal cycler. Program the thermal cycler according to the Table below. The complete cycle should take approximately 5 h. Note: If using a thermal cycler that does not allow you to enter the reaction volume (140 µl), set the instrument to the largest volume setting available.

Step	Time	Temperature
Denaturation	5 min	95°C
Incubation	25 min	60°C
Denaturation	5 min	95°C
Incubation	85 min (1 h 25 min)	60°C
Denaturation	5 min	95°C
Incubation	175 min (2 h 55 min)	60°C
Hold	Indefinite†	20°C

† Converted DNA can be left in the thermal cycler overnight without any loss of performance.

5. Place the PCR tubes containing the bisulfite reactions into the thermal cycler. Start the thermal cycling incubation. IMPORTANT: Since the bisulfite reaction is not overlaid with mineral oil, only thermal cyclers with heated lids are suitable for this procedure. It is important to use PCR tubes that close tightly. Converted DNA can be left in the thermal cycler overnight without any loss of performance. Cleanup of bisulfite converted DNA
6. Once the bisulfite conversion is complete, briefly centrifuge the PCR tubes containing the bisulfite reactions, and then transfer the complete bisulfite reactions to clean 1.5 ml microcentrifuge tubes. Transfer of precipitates in the solution will not affect the performance or yield of the reaction.
7. Add 560 µl freshly prepared Buffer BL containing 10 µg/ml carrier RNA (see Table below to prepare Buffer BL) to each sample. Mix the solutions by vortexing and then centrifuge briefly. Note: Carrier RNA is not necessary when using >100 ng DNA.

Number of samples	1	4	8	16	24	48
Volume of Buffer BL*	620 µl	2.5 ml	5 ml	10 ml	15 ml	31 ml
Volume of carrier RNA solution†	6.2 µl	25 µl	50 µl	100 µl	150 µl	310 µl

* The volumes given contain a 10% surplus for pipetting inaccuracies.

† Resulting in a final concentration of 10 µg/ml carrier RNA in Buffer BL.

8. Place the necessary number of EpiTect spin columns and collection tubes in a suitable rack. Transfer the entire mixture from each tube in step 7 into the corresponding EpiTect spin column.

9. Centrifuge the spin columns at maximum speed for 1 min. Discard the flow-through, and place the spin columns back into the collection tubes.
10. Add 500 µl Buffer BW to each spin column, and centrifuge at maximum speed for 1 min. Discard the flow-through, and place the spin columns back into the collection tubes.
11. Add 500 µl Buffer BD to each spin column, and incubate for 15 min at room temperature (15–25°C). If there are precipitates in Buffer BD, avoid transferring them to the spin columns. IMPORTANT: The bottle containing Buffer BD should be closed immediately after use to avoid acidification from carbon dioxide in the air. Note: It is important to close the lids of the spin columns before incubation.
12. Centrifuge the spin columns at maximum speed for 1 min. Discard the flow-through, and place the spin columns back into the collection tubes.
13. Add 500 µl Buffer BW to each spin column and centrifuge at maximum speed for 1 min. Discard the flow-through and place the spin columns back into the collection tubes.
14. Repeat step 13 once.
15. Place the spin columns into new 2 ml collection tubes, and centrifuge the spin columns at maximum speed for 1 min to remove any residual liquid.
16. Recommended: Place the spin columns with open lids into clean 1.5 ml microcentrifuge tubes (not provided) and incubate the spin columns for 5 min at 56°C in a heating block. This step enables evaporation of any remaining liquid.
17. Place the spin columns into clean 1.5 ml microcentrifuge tubes (not provided). Dispense 20 µl Buffer EB onto the center of each membrane. Elute the purified DNA by centrifugation for 1 min at approximately 15,000 x g (12,000 rpm).
18. To increase the yield of DNA in the eluate, repeat Step 17 once. Note: If the purified DNA is to be stored for up to 24 h, we recommend storage at 2–8°C. For storage longer than 24 h, we recommend storage at –15 to –30°C. At –15 to –30°C, DNA converted and purified using the EpiTect Bisulfite Kit can be stored for at least 3 years* without decrease of quality or conversion.

Polymerase Chain Reaction (PCR)

A master mix with the appropriate volumes of each of the reagents listed below was created to divide the contents equally into each tube and to reduce pipetting errors due to the small volumes required to carry out this reaction.

Contents of each tube:

- 5 µL 5X EpiMark Hot Start Taq Reaction Buffer
- 0.5 µL 10 mM dNTPs
- 0.5 µL 10 µM forward primer
- 0.5 µL 10 µM reverse primer
- 2.0-5.0 µL bisulfite converted cfDNA from HT recipient's plasma
- 0.125 µL EpiMark Hot Start Taq DNA Polymerase
- Required volume of RNAse-free water to reach a total of 25 µL

The following protocol was used for PCR reaction thermocycling:

1) 94°C – 3 minutes
2) 94°C – 45 seconds
3) Variable Tm (55°C – 65 °C) – 45 seconds
4) 68 °C – 1.5 minutes
5) Repeat steps 2-4 40X
6) 68 °C – 10 minutes
7) 4 °C – infinite hold

Gel Electrophoresis

1) Make 3% agarose gel using 1.25 g of agarose and 75 µL of 1% TAE buffer in a 250 mL Erlenmeyer flask and heating it a microwave until boiling and until it is clear
2) Allow it to cool to mildly warm and add 7.5 µL Syber Green (Invitrogen) and pour into the small gel mold with a gel comb
3) Prepare the PCR products by adding 10 µL of the product to a separate 2 mL PCR tube and adding 2 µL of 6X DNA Gel loading dye (Invitrogen)
4) Pull the comb out once gel has completely set
5) Set up gel electrophoresis chamber with the gel and 1% TAE buffer filled till the maximum line
6) Add 10 µL of the prepared PCR products with the 6X DNA Gel loading dye to each well and add a 50 bp DNA GeneRuler ladder (Invitrogen)
7) Run gel at 105 V for around an hour to allow separation of the bands.
8) Use the Bio-Rad ChemiDoc Gel Imaging system to view the bands on the Gel.

II Publicly available datasets

Table 12: Publicly available datasets used for in silico DMR identification

Tissue/cell type	Project	Accession Number
Aorta	Roadmap	GSM983648
Left ventricle	Roadmap	GSM1010978
Thymus	Roadmap	GSM1010979
Ovary	Roadmap	GSM1010980
Adrenal gland	Roadmap	GSM1010981
Adipose tissue	Roadmap	GSM1010983
Gastric	Roadmap	GSM1010984
Psoas muscle	Roadmap	GSM1010986
Right atrium	Roadmap	GSM1010987
Right ventricle	Roadmap	GSM1010988
Sigmoid colon	Roadmap	GSM1010989
Hippocampus	Roadmap	GSM1112838
Breast myoepithelial cells	Roadmap	GSM1127054
Liver	Roadmap	GSM916049
Hippocampus	Roadmap	GSM916050
Sigmoid colon	Roadmap	GSM983645
Small intestine	Roadmap	GSM983646
Lung	Roadmap	GSM983647
Esophagus	Roadmap	GSM983649
Left ventricle	Roadmap	GSM983650
Pancreas	Roadmap	GSM983651
Spleen	Roadmap	GSM983652
CD34	Roadmap	GSM916052
Plasma cell (bone marrow)	Blueprint	EGAX00001128259
Erythroblast (cord)	Blueprint	EGAX00001147730
Inflammatory macrophage (cord)	Blueprint	EGAX00001236255
Neutrophil (cord)	Blueprint	EGAX00001097771
Eosinophil (venous)	Blueprint	EGAX00001097776
Macrophage (venous)	Blueprint	EGAX00001147734

Memory B cell (venous)	Blueprint	EGAX00001345088
Neutrophil (venous)	Blueprint	EGAX00001236260
Neutrophil (venous)	Blueprint	EGAX00001086972
Neutrophil (venous)	Blueprint	EGAX00001223319
Neutrophil (venous)	Blueprint	EGAX00001086971
Regulatory T cell (venous)	Blueprint	EGAX00001340344
CD4+ alpha beta T cell(venous)	Blueprint	EGAX00001236257

III. Bioinformatics

The following are the job scripts utilized for each step of DMR identification.

Converting File Formats (BigWig to Sorted Bedgraph Files)

BigWig to Wig: $ bigWigToWig <file_name.bw> <file_name.wig>
Wig to Bed: $ convert2bed -i wig <file_name.wig> <file_name.bed>
Bed to Bedgraph: $ awk print $1"\t"$2"\t"$3"\t"$5 }' file_name.bed > file_name.bedgraph
Sorted Bedgraph: $ sortBed -i file_name.bedgraph > file_name_sorted.bedgraph

Creating Input Files for Analysis via Metilene
Comparing Aortic Methylomes to Non-Aortic Tissue Methylomes
metilene_input.pl -in1 <comma separated sorted bedgraph files of epigenomes from aortic tissue> -in2 <comma separated sorted bedgraph files of epigenomes from non-aortic tissues> -h1 Aorta -h2 Tissues -out Metilene_Filename.input

Comparing Aortic Methylomes to Hematopoietic Cell Methylomes
metilene_input.pl -in1 <comma separated sorted bedgraph files of epigenomes from aortic tissue> -in2 <comma separated sorted bedgraph files of epigenomes from hematopoietic cells> -h1 Aorta -h2 Cells -out Metilene_Filename.input

Filtering and Sorting DMRs by 10% to Obtain an Output File
Filtering and Sorting DMRs Between Aorta and Non-Aortic Tissues

metilene -M 25 -m 4 -d 0.1 -t 4 -f 1 -a Aorta -b Tissues -X 1 -Y 1 -v 0.7 Metilene_Aorta_Tissues.input > Metilene_Aorta_Tissues.output | sort -V -k1,1 -k2,2n

Filtering and Sorting DMRs Between Aorta and Hematopoietic Cells
metilene -M 25 -m 4 -d 0.1 -t 4 -f 1 -a Aorta -b Cells -X 1 -Y 1 -v 0.7 Metilene_Aorta_Cells.input > Metilene_Aorta_Cells.output | sort -V -k1,1 -k2,2n

Filtering the Output File to Obtain DMRs with a Methylation Difference of 50-90%
Filtering DMRs Between Aorta and Non-Aortic Tissues with a Difference of 50-90%

metilene_output.pl –q Metilene_Aorta_Tissues.output –o Metilene_Aorta_Tissues_Filtered –p 0.05 –d 0.5 –c 4 –l 0 -a Aorta –b Tissues

This will produce a .bedgraph file

It should be noted that only the common DMRs within autosomal chromosomes were considered to avoid variability in dosage depending on the sex of the patient.

Finding overlapping DMRs between the two comparisons: Aorta and Non-Aortic Tissues and Aorta and Hematopoietic Cells

Use bedtools command

bedintersect –a Metilene_Aorta_Tissues.bedgraph –b Metilene_Aorta_Cells.bedgraph

It should be noted that only the common DMRs within autosomal chromosomes were considered to avoid variability in dosage depending on the sex of the patient.

IV Sample Calculations

The Determination of the Concentration of Total cfDNA (copies/mL)
Example: Patient 1006 for DMR Chr 11 (Table 13)

$$(353\ ng/mL)\left(\frac{1\ genome\ copy}{0.00330\ ng}\right) = \ 116490\ copies/mL$$

The Determination of the Concentration of DMRs within Recipients' Plasma (copies/mL)
Example: Patient 1006 for DMR Chr 11 (Table 13)

$$\left(353\frac{ng}{mL}\right)\left(\frac{1\ genome\ copy}{0.00330\ ng}\right)\left(\frac{9\%\ unmethylation}{100}\right) = \ 10484.1\frac{copies}{mL}$$

V. Characteristics of Input Materials from Each Patient for the In Vitro Validation of Aorta-Specific Differentially Methylated Regions

Table 13: The maximal aortic diameter of BAV patients, the total concentration of cfDNA obtained from a blood sample from BAV patients, the concentration of the amplified DMR at Chr 11, and peak molarity of the amplified DMR, which dictated the volume of the amplicon added to the pooled sample for sequencing.

Patient	Max. Aortic Diameter (mm)	Isolated cfDNA (ng/mL)	[Amplified DMR] (ng/µL)	Peak Molarity of DMR (nM)	Volume of Amplicon in pool (µL)
1016	36	353	3.1	33.1	2.68
1006	63	221	2.98	31.8	2.65
1075	43	195	3.14	30.5	1.04
1092	41	193	3.7	41.4	0.85
1127	44	76.7	3.99	43.4	0.70
1142	47	254	3.31	36.4	0.94
1170	39	2480	3.54	38.7	1.88
1173	43	373	5.47	60.6	1.14
1178	45	777	3.72	41.9	1.85
1237	50	109	5.72	61.1	5.04
1267	48	61.6	1.51	16.4	6.45
1277	52	374	4.09	44.7	2.00
1279	50	279	4.81	52.8	1.53
1356	46	557	3.61	40.2	1.88
1360	46	2245	3.34	37.6	2.56
1	52	171	2.33	24.8	8.81
2	45	107	2.79	29.7	3.59
3	47	81.1	2.49	27	11.99
4	49	54.3	1.7	18.4	5.63
5	50	66.1	3.28	35.8	2.77
6	49	56.6	1.25	13.8	5.25
7	43	50.8	1.43	16	17.06
8	46	71.2	0.853	9.55	16.95

Table 14: The maximal aortic diameter of BAV patients, the total concentration of cfDNA obtained from a blood sample from BAV patients, the concentration of the amplified DMR at Chr 18, and peak molarity of the amplified DMR, which dictated the volume of the amplicon added to the pooled sample for sequencing.

Patient	Max. Aortic Diameter (mm)	Isolated cfDNA (ng/mL)	[Amplified DMR] (ng/µL)	Peak Molarity of DMR (nM)	Volume of Amplicon in pool (µL)
1016	36	353	0.432	5.07	17.50
1006	63	221	0.485	5.69	14.82
1075	43	195	0.16	1.96	-
1092	41	193	0.483	5.89	5.97
1127	44	76.7	0.494	6.08	4.98
1142	47	254	0.229	2.92	-
1170	39	2480	0.324	4.16	17.50
1173	43	373	0.363	4.38	15.78
1178	45	777	0.388	4.44	17.50
1237	50	109	1.58	18.4	16.74
1267	48	61.6	0.716	8.47	12.48
1277	52	374	0.433	5.11	17.50
1279	50	279	0.388	4.62	17.50
1356	46	557	0.366	4.33	-
1360	46	2245	0.687	8.38	11.46
2	45	107	0.52	6.09	17.50
3	47	81.1	2.55	29.8	10.86
4	49	54.3	0.492	5.92	17.50
5	50	66.1	1.17	13.9	7.13
6	49	56.6	0.342	4.14	17.50
7	43	50.8	1.31	15.6	17.50
8	46	71.2	0.786	9.25	17.50

Table 15: The maximal aortic diameter of BAV patients, the total concentration of cfDNA obtained from a blood sample from BAV patients, the concentration of the amplified DMR at Chr 20, and peak molarity of the amplified DMR, which dictated the volume of the amplicon added to the pooled sample for sequencing.

Patient	Max. Aortic Diameter (mm)	Isolated cfDNA (ng/mL)	[Amplified DMR] (ng/µL)	Peak Molarity of DMR (nM)	Volume of Amplicon in pool (µL)
1016	36	353	1.16	12.6	7.04
1006	63	221	0.377	4.82	17.50
1075	43	195	0.168	1.82	-
1092	41	193	0.186	2.01	-
1127	44	76.7	0.163	1.73	-
1142	47	254	0.185	1.95	-
1170	39	2480	0.523	5.53	13.16
1173	43	373	0.373	3.95	-
1178	45	777	0.92	9.91	7.84
1237	50	109	1.61	17.6	17.50
1267	48	61.6	0.562	6.04	17.50
1277	52	374	1.02	10.9	8.20
1279	50	279	1.62	18	4.49
1356	46	557	0.547	5.96	12.71
1360	46	2245	0.877	9.6	10.01
2	45	107	0.856	9.36	23.33
3	47	81.1	1.73	18.6	5.73
4	49	54.3	1.74	18.5	17.50
5	50	66.1	2.04	22.2	4.67
6	49	56.6	0.521	5.66	17.50
7	43	50.8	1.3	14	5.18
8	46	71.2	4.01	42.7	6.39

Table 16: The maximal aortic diameter of BAV patients, the total concentration of cfDNA obtained from a blood sample from BAV patients, the concentration of the amplified DMR at Chr 22, and peak molarity of the amplified DMR, which dictated the volume of the amplicon added to the pooled sample for sequencing.

Patient	Max. Aortic Diameter (mm)	Isolated cfDNA (ng/mL)	[Amplified DMR] (ng/µL)	Peak Molarity of DMR (nM)	Volume of Amplicon in pool (µL)
1016	36	353	0.961	11.8	3.70
1006	63	221	1.72	21.3	7.15
1075	43	195	2.32	28.8	1.50
1092	41	193	1.76	22	1.22
1127	44	76.7	1.93	24.7	1.38
1142	47	254	1.35	17.3	1.38
1170	39	2480	3.99	45.7	4.21
1173	43	373	2.99	35.9	1.51
1178	45	777	4.55	55.5	2.16
1237	50	109	2.2	26.5	5.55
1267	48	61.6	3.57	41	3.99
1277	52	374	1.87	23.5	2.18
1279	50	279	1.15	14.5	3.44
1356	46	557	0.426	5.49	5.23
1360	46	2245	6.34	77.7	17.50
2	45	107	2.48	28.3	2.81
3	47	81.1	3.67	42.2	3.77
4	49	54.3	2.98	34.3	7.67
5	50	66.1	3.65	42.2	3.02
6	49	56.6	1.95	23.2	2.35
7	43	50.8	2.01	23.6	3.12
8	46	71.2	2.33	27.9	11.57